CHARACTERIZATION OF VIBRIO VOPS, AN AMPYLATOR OF RHO GTPASES

APPROVED BY SUPERVISORY COMMITTEE

_____
Kim Orth, Ph. D.

_____
Lora Hooper, Ph. D.

_____
Margaret Phillips, Ph. D.

_____
Vanessa Sperandio, Ph. D.

ACKNOWLEDGMENTS

I would like to acknowledge the many people who have been instrumental in helping me to complete this work. Most of all, I would like to thank my mentor, whose knowledge and guidance made the discovery of AMPylation possible. Her enthusiasm and constant flow of new ideas kept me going, even when nothing seemed work.

I would especially like to thank those who helped me in areas that were unknown to me before I started this research. Drs. Haydn Ball and Yan Li provided the expertise in mass spectrometry that allowed us to identify the modification elicited by VopS. The in-depth bioinformatics analysis provided by Dr. Lisa Kinch has given us much insight into the fascinating new world of Fic domains and their activities.

I would also like to thank the members of my thesis committee, Drs. Vanessa Sperandio, Lora Hooper, and Meg Phillips, who always provided helpful advice and thoughtful discussions. Many people provided reagents, constructs, and lots of helpful advice that were essential to the completion of this project. For this, I especially thank Dr. Neal Alto, Dr. Paul Sternweis, and Anthony Orvedahl. Dr. Sternweis deserves another thanks for coming up with the creative name of AMPylation!

Many thanks to all of the former and current members of the Orth lab who provided suggestions when I needed them and just listened when I needed that instead. I will always be grateful that I worked in an environment where my lab mates were always so willing to lend a helping hand. A special thanks goes out to Dara Burdette and Yi-Heng Hao, who I have worked closely with on several projects in the Orth lab. It has been fun working with you both to figure out the kinks in two different uncharacterized

systems, *V. parahaemolyticus* and eukaryotic AMPylation. In addition, I would like to thank all of the rotation students that I had to pleasure to mentor. I hope that I managed to teach all of you as much as you taught me.

Lastly, I would like to thank my family. My parents were always there to encourage me when I was frustrated, cheer me up when I was sad, and let me know how proud of me they were. I hope they realize that the lessons I learned from them about kindness, respect, and love were more important than anything I ever learned in graduate school. I would never have gotten this far without them. I love you, Mom and Dad!

CHARACTERIZATION OF VIBRIO VOPS, AN AMPYLATOR OF RHO GTPASES

by

MELANIE LEANN YARBROUGH

DISSERTATION

Presented to the Faculty of the Graduate School of Biomedical Sciences

The University of Texas Southwestern Medical Center at Dallas

In Partial Fulfillment of the Requirements

For the Degree of

DOCTOR OF PHILOSOPHY

The University of Texas Southwestern Medical Center at Dallas

Dallas, Texas

May, 2009

Copyright

by

MELANIE YARBROUGH, 2009

All Rights Reserved

CHARACTERIZATION OF VIBRIO VOPS, AN AMPYLATOR OF RHO GTPASES

MELANIE LEANN YARBROUGH, Ph. D.

The University of Texas Southwestern Medical Center at Dallas, 2009

KIM ORTH, Ph. D.

Vibrio parahaemolyticus is a gram-negative marine bacterium that causes gastroenteritis associated with the consumption of contaminated shellfish. The emergence of pandemic strains of *V. parahaemolyticus* has increased the need for characterization of the virulence factors of this pathogen. Sequencing of the genome of a clinical isolate revealed the presence of two type III secretion systems (T3SSs), one on each chromosome. The T3SS on chromosome one (T3SS1) has been shown to be responsible for cytotoxicity in HeLa cells, and it shares a high degree of homology to the T3SS of the *Yersinia spp*.

Our studies have shown that infection of HeLa cells with a strain of *V. parahaemolyticus* capable of secreting only from T3SS1 indicated that T3SS1 mediates several events during infection including the rapid induction of autophagy, cell rounding, and finally lysis of the cell. Defining the T3SS1-mediated events of infection gives insight into virulence mechanisms of *V. parahaemolyticus* that have not been well characterized and provide a basis for the elucidation of the functions associated with T3SS1 effectors.

One of the T3SS effectors, VopS, contains a Filamentation induced by cAMP (Fic) domain that we have shown is critical for the function of this effector. Our studies have found that VopS inhibits Rho GTPase signaling during infection by directly modifying Rho, Rac, and Cdc42, preventing their interaction with downstream effectors. These observations reveal a unique activity for VopS, which targets a pathway that is critical in the cellular response to *V. parahaemolyticus* infection. In addition, they provide insight into a novel post-translational modification that may expand our knowledge of eukaryotic cell signaling.

Fic domains are found in proteins from several bacterial and eukaryotic species and are recognized by their conserved motif, HPFX(D/E)GNGR. The presence of Fic domains in higher eukaryotes suggested that this modification could be utilized in cell signaling. Our preliminary studies indicated that AMPylation is utilized by eukaryotes. We have shown that a Fic protein from humans, HYPE, possesses auto-AMPylation activity, confirming our hypothesis that these domains are involved in AMPylation. Ongoing and future studies seek to identify the substrates of HYPE activity and identify other components involved in this new layer of eukaryotic cell signaling.

TABLE OF CONTENTS

PUBLICATIONS

Kinch LN, **Yarbrough ML**, Orth K, and Grishin NV. (2009) Fido, a novel AMPylation domain common to fic, doc, and AvrB. Submitted.

Yarbrough ML, Li Y, Kinch LN, Grishin NV, Ball HL, and Orth K. (2009) AMPylation of Rho GTPases by Vibrio VopS disrupts effector binding and downstream signaling. *Science*, 323(5911): 269-72.

Burdette DL*, **Yarbrough ML***, and Orth K. (2009) Not without cause: *Vibrio parahaemolyticus* induces acute autophagy and cell death. *Autophagy*, 5(1): 100-2.

Burdette DL*, **Yarbrough ML***, Orvedahl A, Gilpin CJ, and Orth K. (2008) *Vibrio parahaemolyticus* orchestrates a multifaceted host cell infection by induction of autophagy, cell rounding, and then cell lysis. *PNAS*, 105(34): 12497-502.

Liverman ADB, Cheng H-C, Trosky JT, Leung DW, **Yarbrough ML**, Burdette DL, Rosen MK and Orth K. (2007) Arp2/3 Independent Assembly of Actin by *Vibrio* Type III Effector VopL. *PNAS*, 104(43): 17117-22.

* These authors contributed equally to this work.

LIST OF FIGURES

LIST OF TABLES

LIST OF ABBREVIATIONS

AMP	Adenosine 5'monophosphate
Amp	Ampicillin
ATP	Adenosine triphosphate
BSA	Bovine serum albumin
Cm	Chloramphenicol
DA-Rac	Dominant active Rac
DMEM	Dulbecco's Modified Eagle Medium
DTT	Dithiothreitol
EDTA	Ethylenediaminetetraacetic acid
ER	Endoplasmic reticulum
FBS	Fetal Bovine Serum
Fic	Filamentation induced by cAMP
FPLC	Fast protein liquid chromatography
Gal	Galactose
GAP	GTPase activating protein
GDI	Guanine nucleotide dissociation inhibitor
GDP	Guanosine diphosphate
GEF	Guanine nucleotide exchange factor
Gen	Gentamicin
GFP	Green fluorescent protein
Glu	Glucose
GS	Glutamine synthetase

GST	Glutathione S-transferase
GTP	Guanosine triphosphate
GTPases	Guanosine triphosphatases
hpi	hours post-infection
HPLC	High pressure liquid chromatography
HRP	Horseradish peroxidase
IPTG	Isopropyl-beta-D-thiogalactopyranoside
kDa	Kilodaltons
KP	Kanagawa phenomenon
LB	Luria Bertani
LC	Liquid chromatography
LC3	Microtubule-associated protein 1 light chain 3
LDH	Lactate dehydrogenase
m/z	mass to charge
MAPK	Mitogen-activated protein kinase
Mg^{2+}	Magnesium
MLB	Marine LB
MOI	Multiplicity of infection
MS	Mass spectrometry
NFκB	Nuclear factor kappa B
Ni-NTA	Nickel-nitriloacetic acid matrix
O.D.	Optical density
PAK-PBD	p21-activated kinase protein binding domain

PARP	PolyADP ribose polymerase
PBS	Phosphate-buffered saline
PI	Protease inhibitors
PI3 kinases	Phosphatidylinositol 3-kinases
PMSF	Phenylmethylsulfonylfluoride
SD	Standard deviation
SDS-PAGE	Sodium dodecyl sulfate-polyacrylamide gel electrophoresis
SS	Secondary structure
Stauro	Staurosporine
T3SS	Type III secretion system
T3SS1	T3SS on chromosome 1
T3SS2	T3SS on chromosome 2
TCA	Trichloroacetic acid
TDH	Thermostable direct hemolysin
Tet	Tetracycline
Thr	Threonine
TM	Transmembrane
TPR	Tetratricopeptide repeat
TRH	Thermostable related hemolysin
Vop	*Vibrio* outer protein
Wort	Wortmannin

CHAPTER ONE
Introduction and Literature Review

Vibrio parahaemolyticus, an emerging pathogen

In 1950, a severe outbreak of foodborne illness sickened 272 people and resulted in 20 deaths in Osaka, Japan. Patients presented with gastroenteritis and severe abdominal pain. Autopsies revealed extensive damage to the stomach and other areas of the gastrointestinal tract. The source of the outbreak was traced to a semi-dried fish called shirasu. Although samples of shirasu were heavily contaminated with many species of bacteria, microbiologist Tsunesaburo Fujino isolated two potential culprits by passage through mice. Of these, one was also isolated from stool samples of infected patients and was deemed to be responsible for the outbreak. Fujino named the newly identified pathogen *Pasteurella parahaemolytica* (40). Several years later, it was discovered that this organism was halophilic, which led to the reclassification of the organism to the genus *Vibrio* (43).

V. parahaemolyticus is a gram-negative, rod-shaped bacterium commonly found in marine and estuarine environments (24). Large populations of free-living bacteria have been detected in water samples (7). However, *V. parahaemolyticus* is also found associated with plankton, copepods, and crustaceans, which provide a reservoir for this organism in the environment (7, 22, 46). *V. parahaemolyticus* possesses two distinct kinds of flagellar systems. In liquid environments, *V. parahaemolyticus* is highly motile through the use of a single polar flagellum

(48). Migration across semi-solid surfaces is accomplished by several lateral flagella. This type of motility, called swarming, is thought to enable the bacteria to attach to the surfaces of eukaryotic cells or shellfish and allows *V. parahaemolyticus* to flourish in and adapt to changing environments (9, 84).

Outbreaks of *V. parahaemolyticus* are common in Southeast Asia, where infection is a major health and economic issue. In Japan, infections with this pathogen account for 20-30% of food poisoning cases (4). However, *V. parahaemolyticus* has spread beyond the realm of Southeast Asia. Between 1996 and 1998, the number of cases of infection rose sharply worldwide, which is likely due to the emergence of new pandemic strains, such as the O3:K6 strain, which was isolated from 50-80% of patients in an outbreak in India during this time (66). The O3:K6 strain has now spread throughout the world and has been isolated off the coasts of Europe, Asia, North and South America, and Africa (24).

In the United States, the spread of *V. parahaemolyticus* has become an increasingly important issue, as infections with this pathogen have become the most frequent cause of *Vibrio*-associated gastroenteritis (55). It is estimated to be responsible for about 5,000 cases of gastroenteritis each year in the United States, though problems associated with *V. parahaemolyticus* infections are believed to be largely underdiagnosed and may represent a larger health risk than is currently appreciated (31). Samples of *V. parahaemolyticus* have been isolated from fish farms and throughout all coastal regions of the United States (24, 64). The incidence of infection is associated with water temperatures, with the highest

number of cases reported in summer months (24). The rise in ocean temperatures due to global warming may enable the further spread of this bacterium, which has now been found as far north as the coastal waters of Alaska and Canada (62).

Infection with *V. parahaemolyticus* typically results from consumption of undercooked and contaminated shellfish and most commonly leads to gastroenteritis characterized by acute diarrhea, abdominal cramps, nausea, vomiting, and fever (64). In rare cases, *V. parahaemolyticus* infections that result from contact of a wound with contaminated seawater or seafood can occasionally lead to primary septicemia (64). Although infection is often self-limiting, individuals who are immunocompromised or burdened with preexisting health conditions such as liver disease or diabetes are at high risk for severe complications that can result in death (64).

Virulence factors of *V. parahaemolyticus*

Although it often exists as a commensal organism in the environment, *V. parahaemolyticus* maintains a number of virulence factors in the event of infection of a human host. The most well-characterized virulence factors from this bacterium are the thermostable direct hemolysin (TDH) and the thermostable-related hemolysin (TRH). TDH is a reversible amyloid toxin that causes β-hemolysis on Wagatsuma agar. This is known as the "Kanagawa phenomenon" (KP) and is used as a classical means of identifying virulent strains of *V.*

parahaemolyticus (33). However, there are KP- isolates of *V. parahaemolyticus* that cause disease, so this is not a foolproof means of identification. TDH and TRH are pore-forming toxins that are thought to alter ion flux in intestinal cells, leading to diarrhea (41, 81). These toxins have been associated with activities such as cytotoxicity, hemolysis, and enterotoxicity in several models of infection (81).

TDH and TRH are most often associated with clinical isolates of *V. parahaemolyticus*, with less than 5% of environmental isolates reported possessing these toxins, suggesting their importance in disease and pathogenesis (96). However, infection with Δ*tdh* and Δ*trh* strains of *V. parahaemolyticus* results in rapid and acute cell death in a tissue culture model, suggesting the presence of additional virulence factors (56, 58, 76). The 2003 sequencing of the *V. parahaemolyticus* genome provided a key insight into this cytotoxicity when it revealed the presence of two type III secretion systems (T3SS) (60). Subsequently, it was shown that the cell death observed during infection with a Δ*tdh* strain is associated with the presence of a functional T3SS (76).

The Type III Secretion System

The T3SS is a structure employed by Gram-negative bacteria to deliver proteins, called effectors, directly into the cytosol of host cells during infection (Figure 1) (35). The first 20-30 amino acids of effectors are thought to contain a secretion signal that targets the protein to its specific T3SS. These sequences are

not cleaved upon secretion and so far no general sequence characteristics of a secretion signal have been identified (34). Upon initiation of secretion, effectors are unfolded and secreted in an ATP-dependent manner through a needle-like apparatus that spans the inner and outer membranes of the bacteria and serves as a channel to deliver effectors directly into the host cell cytosol (35). Secretion of effectors requires translocator proteins that are thought to insert into the target cell membrane and form a pore in the membrane of the host cell (34).

Effectors are held quiescent inside the pathogen through lack of an activator or substrate that is present only in the eukaryotic target cell or through the presence of an accessory protein called a chaperone (72, 91). Many, but not all, bacterial effectors are associated with chaperones, which are classified by their low molecular weight, acidic pI, and a predicted amphipathic helix near their C-terminal end (75, 94). They most often bind to a 50-100 amino acid region that follows the secretion signal. Along with keeping effectors quiescent, chaperones are also proposed to maintain effectors in a semi-unfolded, globular state that facilitates rapid unfolding once secretion has been initiated (34).

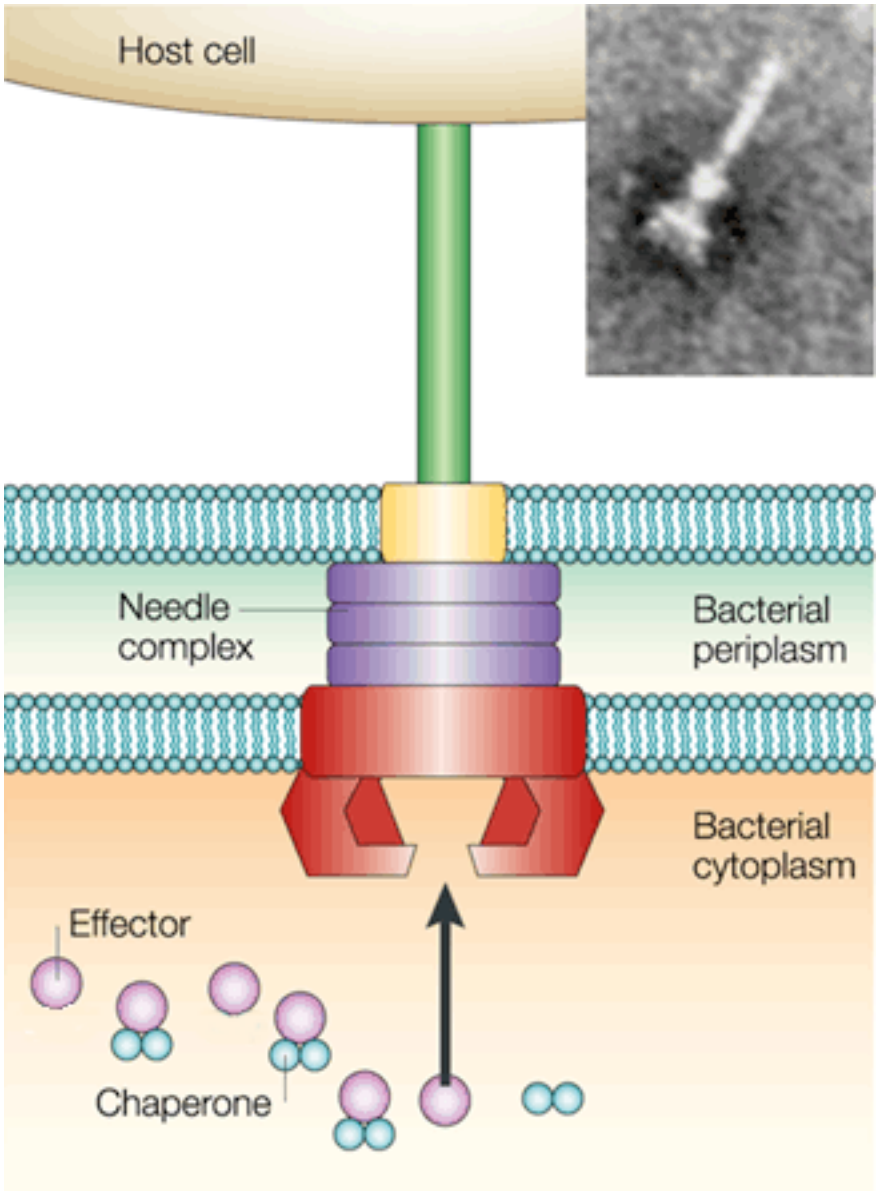

Figure 1. The Type III Secretion System
Electron microscopy images (shown in inset) served as the basis for this schematic of a T3SS. The needle complex is made up of a base with several ring structures that span the inner and outer membranes. A needle-like filament, through which effectors are secreted into the cytosol of the host is shown in green. Inside the bacteria, some effectors (purple) are bound to chaperones (blue) until they are ready to be secreted. Adapted from (86).

Activities of Type III Effector Proteins

Although T3SS machinery is often conserved among gram-negative pathogens, the effectors from each system differ widely in their mechanism of action. However, these effectors, like viral oncoproteins, are commonly characterized as potent factors that often mimic or capture an endogenous eukaryotic activity (72). They target a wide variety of eukaryotic pathways such as those involved in the innate immune response, regulation of host cell architecture, and initiation of cell death (68).

Bacteria utilize type III effectors to avoid clearance by the immune system, escape and spread from the host, or establish a replicative niche inside the cell. One family of effectors, the YopJ family of acetyltransferases, targets the MAPK and NFκB signaling pathways, whose inhibition results in a dampened innate immune response during infection (65, 73, 89). Another common target of bacterial effector proteins are Rho guanosine triphosphatases (GTPases), which regulate the actin cytoskeleton (described below). Inhibition of Rho GTPase signaling by the *Yersinia* effector YopE leads to disruption of the actin cytoskeleton, preventing phagocytic elimination of the bacteria (93). Conversely, the *Salmonella* effector SopE activates Rho GTPases, hijacking the actin cytoskeleton and promoting uptake of this intracellular bacteria (39).

Many other effectors are associated with activation of various cell death pathways (described below). The *Pseudomonas aeruginosa* effector ExoS contributes to the activation of apoptosis, a noninflammatory type of cell death

that requires the activation of caspases (88). Still other effectors target the autophagy pathway, which is a pathway through which cells respond to stress such as nutrient deprivation or infection by sequestration of cytoplasmic contents into double-membraned vesicles that are delivered to the lysosome for degradation (54, 88). To avoid clearance by autophagy, the pathogen *Shigella flexneri* secretes an effector protein called IcsB that masks recognition of the bacterial outer membrane protein, VirG, by the autophagy protein, Atg5 (69). Each pathogen uses its own combination of type III effectors to efficiently attack and evade a host during infection. Regardless of the activity of type III effectors, the utilization of various mechanisms to modulate eukaryotic cell signaling shifts the balance for survival in favor of the invading pathogen.

Features of cell death pathways

Pathogens have been shown to activate a variety of host cell death pathways upon infection. Bacteria may induce death of cells required for immune defense to enable their persistence inside a host. Alternatively, the activation of cell death could allow for the escape and dissemination of the invading bacteria (99). The most commonly described cell death pathways include apoptosis, autophagy, necrosis/oncosis, and pyroptosis. The outcome of the activation of each of the pathways is the death of cells, but the process through which this occurs is different for each. Although some characteristics are shared among

these pathways, each possesses distinct morphological features that are used to distinguish one from the other (Figure 2).

Apoptosis is a noninflammatory type of programmed cell death. It is regulated by a family of proteases called caspases that target and cleave specific proteins resulting in the morphological features of apoptosis (14). Cells undergoing apoptosis exhibit morphologies such as nuclear and cytoplasmic condensation, chromatin cleavage, and cellular blebbing (Figure 2). Remaining condensed cells and cellular fragments are taken up and disposed by phagocytes (47).

Autophagy is a highly regulated process that involves the sequestration of cytoplasmic contents in double-membraned vesicles, called autophagosomes, which are delivered to lysosomes for degradation (54). This pathway is a common target of bacteria and viruses due to its important association as a host defense pathway involved in both innate and adaptive immunity (74). Autophagic cell death is noninflammatory and cells undergoing this process exhibit morphological features such as vacuolization into double-membraned autophagosomes (18) (Figure 2).

Necrosis (or oncosis) is thought of as a passive form of cell death that is unregulated. The process of necrosis, leads to depletion of energy stores and increased membrane permeability, which ultimately results in the death of a cell (59). Unlike apoptosis and autophagy, necrotic cell death is proinflammatory.

Morphological characteristics of necrosis include cellular and organelle swelling and membrane blebbing (59) (Figure 2).

A recently identified type of programmed cell death was termed pyroptosis (29). The hallmark of pyroptosis is that it is dependent upon caspase-1, a caspase not involved in apoptosis. The process of pyroptotic cell death is proinflammatory and leads to membrane breakdown and release of inflammatory cytokines (29) (Figure 2). Previous studies have shown that pyroptosis is activated by infection with bacteria such as *Salmonella* and *Shigella* (15, 82). Bacterial infection often leads to cytotoxicity that can be further characterized by the type of cell death activated during infection. The ability to distinguish between these cell death pathways using their distinct sets of morphological and molecular markers gives critical insight into the targets and pathways that bacteria manipulate during infection.

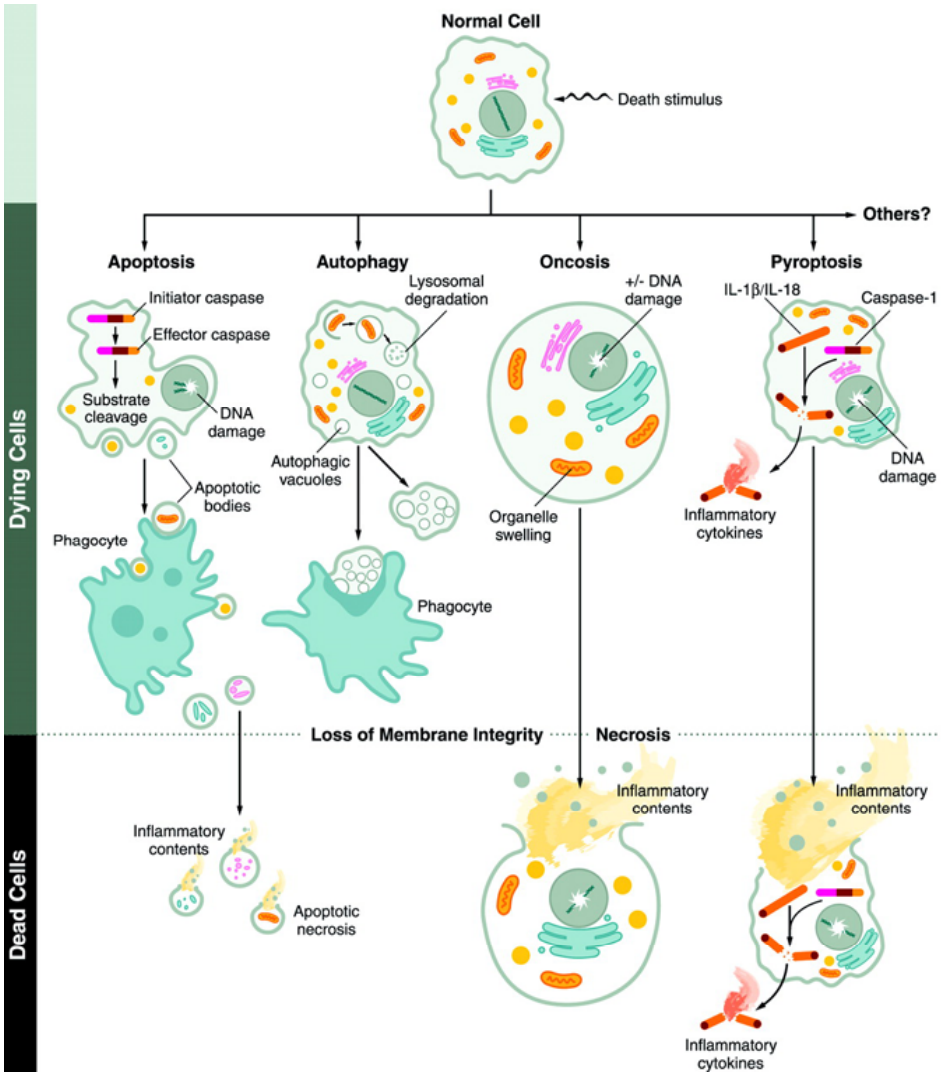

Figure 2. Morphological features of various pathways of cell death.
Upon death-inducing stimuli, cells respond by activating a cell death pathway. Apoptosis is characterized by activation of caspases, which leads to morphological changes such as nuclear and cytoplasmic condensation. During autophagy, cytoplasmic contents are sequestered in autophagic vacuoles that are degraded by lysosomes. The morphological features of necrosis (oncosis) are cell and organelle swelling, followed by the release of proinflammatory contents upon cell death. Pyroptosis is characterized by activation of caspase-1 that results in the processing and release of inflammatory cytokines. In addition to these, there are likely other cell death pathways that remain undiscovered. Figure adapted from (29).

Cytotoxicity of *V. parahaemolyticus* T3SS1

Sequencing of the genome of the RIMD2210633 strain of *V. parahaemolyticus* revealed the presence of two T3SSs. The first T3SS (T3SS1) is encoded on the larger chromosome 1, and the other T3SS (T3SS2) is found on a pathogenicity island on the smaller chromosome 2. T3SS2 is found only in clinical isolates of *V. parahaemolyticus* and is associated with fluid accumulation and enterotoxicity in a rabbit ileal loop model of infection (77). However, mutant strains that are unable to secrete proteins from T3SS2 are cytotoxic to cells, suggesting a role for T3SS1 in virulence (56, 76). Genotyping has shown that all isolates of *V. parahaemolyticus* harbor T3SS1, which resembles the T3SS of *Yersinia* spp. in structure and organization, although there is no similarity between their predicted effectors (60, 77) (Figure 3).

A hypothetical region of genes in the T3SS1 gene cluster that is not found in *Yersinia* spp. is predicted to encode a small number of effectors and their associated chaperones (Figure 3). These effectors, which are encoded by *vp1680*, *vp1683*, and *vp1686*, are named *Vibrio* outer protein Q (VopQ), VopR, and VopS, respectively and have no homology to any proteins of known function. Like previously discovered effectors, they were initially identified by their association with a chaperone (75). Previous studies have shown that VopQ and VopS are secreted in a T3SS1-dependent manner, and they are thought to play a role in cytotoxicity (71). However, the mechanism through which each of these effectors contributes to cytotoxicity is unknown.

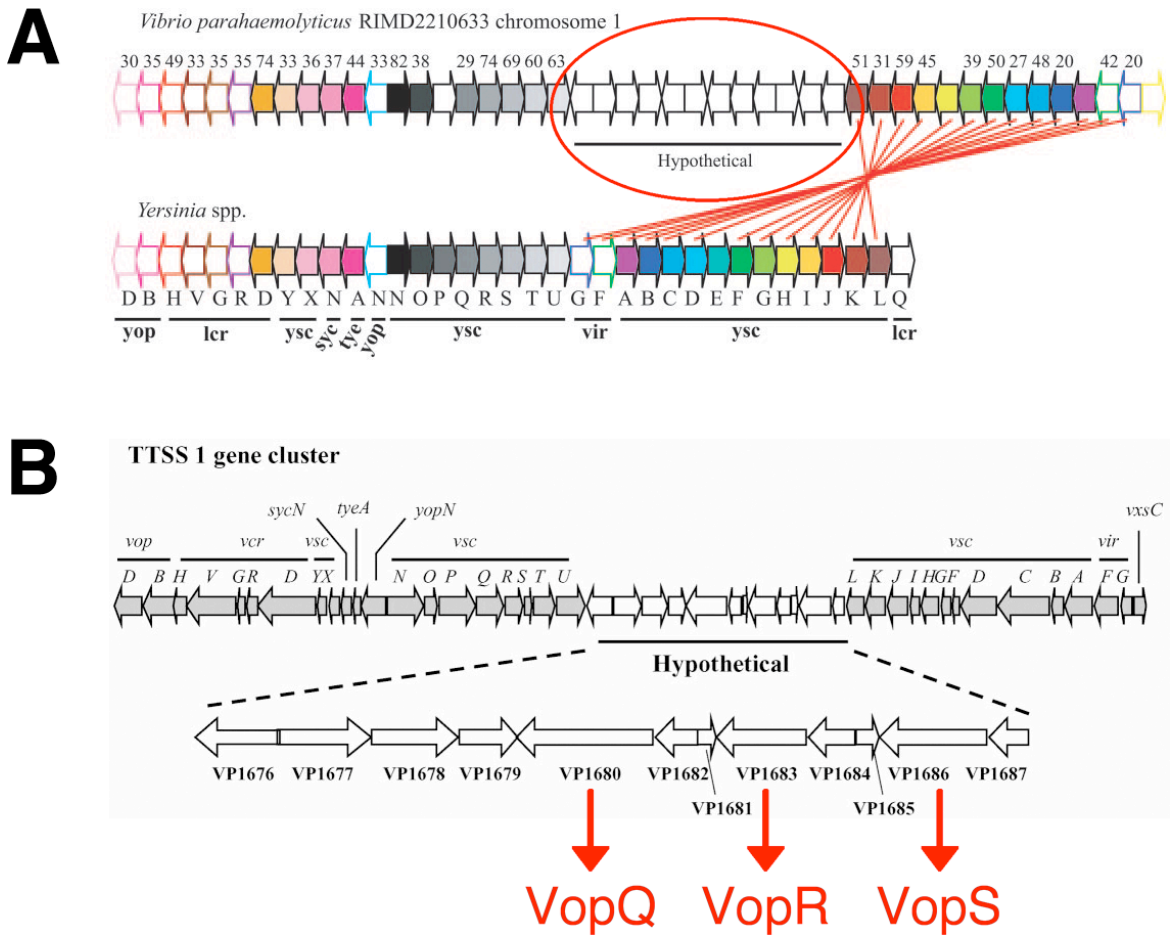

Figure 3. The T3SS1 gene cluster.
The organization of the T3SS1 gene cluster in *V. parahaemolyticus* (top) is similar to that of *Yersinia* spp. (bottom), with the exception of 13 genes that are oriented in the opposite direction (represented by crossed red lines). The numbers above the T3SS1 genes show the percent identity at the amino acid level of the corresponding *Yersinia* T3SS proteins. A region of hypothetical genes not found in *Yersinia* spp. is underlined. (B) A close-up of the T3SS1 hypothetical region of genes shows the association of the genes encoding predicted effector proteins (*vp1680, vp1683,* and *vp1686*) with their corresponding chaperones (*vp1682, vp1684,* and *vp1687*). Protein names of each effector are shown in red. Figure adapted from (71, 77).

The *Vibrio* T3SS1 effector, VopS

VopS is an effector protein that is secreted from *V. parahaemolyticus* in a T3SS1-dependent manner (71). This protein has no homology to any proteins of known function, though a filamentation induced by cAMP (Fic) domain is located in the C-terminus. Although the exact function of this domain is unknown, at least one function is thought to be the regulation of cell division through folate synthesis in *Escherichia coli* (50, 90). A BLAST search reveals that Fic domains are widely distributed through all domains of life, and members of this family are present in many species of bacteria and higher eukaryotes (5). Each domain is recognized by a conserved motif, HPFX(D/E)GNGR. Structures of bacterial Fic domains have been solved, which revealed that these domains are mostly alpha helical in nature, and the residues in the conserved motif are in a loop region that may provide the basis for polar interactions (23) (Figure 4A). A β-hairpin near the Fic motif of one structure is bound to a peptide, placing it within Van der Waals contact of the motif histidine, suggesting that the Fic motif could represent an active site in these proteins (25) (Figure 4B).

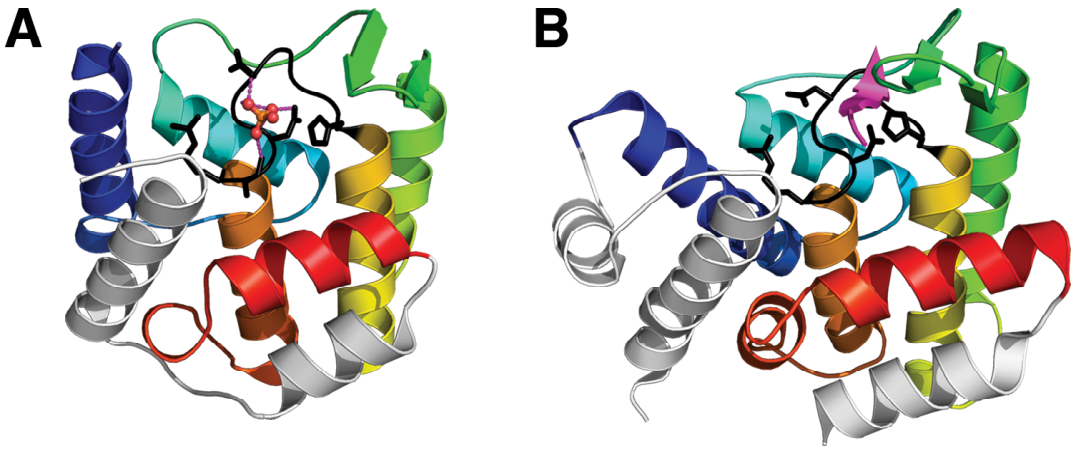

Figure 4. Structures of bacterial Fic domains
(A) Ribbon diagram (modeled from PDB# 2f6s) depicting *Helicobacter pylori* Fic domain structure. Conserved Fic domain secondary structure elements are colored from N to C-terminus in rainbow. Additional secondary structural elements are white. The Fic motif is colored black, with conserved polar residue side chains represented as sticks. Fic motif sidechains E and N provide polar interactions (magenta dashed lines) with phosphate (ball and stick representation). (B) Ribbon diagram (modeled from PDB# 2qc0) depicting the *Shewanella oneidensis* Fic domain structure. Secondary structure elements and Fic motif residues are depicted and colored as in A, with some non-conserved elements omitted. A β-hairpin binds a peptide near the Fic motif His.

Previous reports suggested that VopS induces apoptosis in macrophages during infection (12). Deletion of this effector in a strain of *V. parahaemolyticus* that is functional for secretion only from T3SS1 results in a mutant strain of bacteria that no longer induces apoptosis in macrophages, as measured by Annexin V staining. In the same study, it was reported that VopS interacts with the p65 subunit of NFκB using yeast two-hybrid analysis. Furthermore, gel shifts of the NFκB binding site of the TNF-α promoter using nuclear extracts of

infected cells indicated that nuclear extracts from cells infected with wild-type bacteria showed no NFκB DNA binding, whereas Δ*vopS*-infected nuclear extracts showed binding activity to the TNFα promoter. The authors proposed that VopS induces apoptosis during infection through the mislocalization of p65, thereby preventing this transcriptional regulator from interacting with its cognate promoters and activating pro-survival pathways. This study was limited in that no evidence for interaction of p65 and VopS was presented beyond yeast two-hybrid. In addition, changes in expression of NFκB regulated genes due to the presence or absence of VopS during infection were never addressed. In short, while identifying a potential target of VopS, this study did not clearly define the activity of this effector.

Another study has implicated VopS in the inhibition of Rho GTPases during infection (19). Caselli and colleagues found that during infection with a strain of *V. parahaemolyticus* capable of secreting only from T3SS1, Rho GTPases were no longer activated after one hour of infection. This effect was attributed to VopS, as Rho GTPases remained active throughout the course of infection with a Δ*vopS* mutant strain. Complementation of the mutant restored the GTPase inhibiting effect. However, complementation with VopS lacking its Fic domain did not restore activity, indicating that this domain is important for GTPase inhibition. The authors found that total levels of Rho GTPases remained unchanged during infection, indicating that the stability of these proteins was not affected. While these results clearly associated VopS with the disruption of the

actin cytoskeleton through inhibition of Rho GTPases, many important questions remained unanswered, including the precise identity of the target for VopS and the molecular mechanism this effector employs to inhibit host cell signaling.

Rho GTPases, biological molecular switches

The Rho family of GTPases are members of the Ras superfamily of small G proteins. The most well characterized members of this family are RhoA, RacI, and Cdc42 (42). Rho GTPases act as molecular switches that cycle between an inactive GDP-bound state and an active GTP-bound state. This activity is controlled by a group of proteins that include guanine nucleotide exchange factors (GEFs), GTPase activating proteins (GAPs), and guanine nucleotide dissociation inhibitors (GDIs). GEFs catalyze the exchange GDP for GTP, which causes a conformational change in the GTPase to activate and allow it to interact with its downstream effectors (83). GAPs catalyze the intrinsic hydrolysis of GTP to GDP, returning the GTPases to its inactive confirmation (11). GDIs bind to Rho GTPases in their GDP bound state, blocking spontaneous dissociation of GDP from the GTPase (70) (Figure 5).

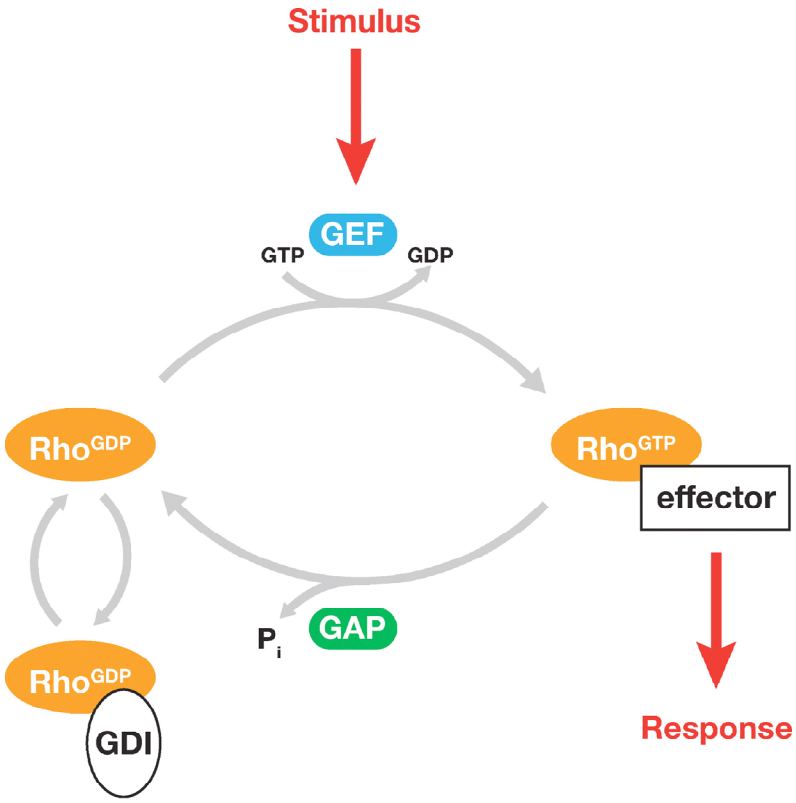

Figure 5. The GTPase cycle.
Rho GTPases act as molecular switches that cycle between an inactive GDP-bound conformation and an active GTP-bound confirmation. Their activity is regulated by many different GEFs, GAPs, and GDIs. Once in their active confirmation, GTPases are able to initiate a response by binding to downstream effector proteins. Adapted from (42).

In the active GTP-bound state, Rho GTPases regulate many essential processes inside the cell such as activation of the NFκB and MAPK pathways, cell migration, cell-cell adhesion, cell polarization, and maintenance of cell shape (42). The most well characterized function of Rho GTPases is regulation of the actin cytoskeleton. Activation of Rho, Rac, or Cdc42 mediates the polymerization and organization of actin. Each Rho GTPase directs the formation of distinct actin structures. Rho activation leads to stress fiber formation, while Rac and Cdc42 form cellular protrusions of lamellipodia, and filopodia, respectively, at the plasma membrane (42). Because of their involvement in so many cellular processes, Rho GTPases are a common target for activation or inhibition by pathogens. Activation of Rho GTPases can promote uptake on intracellular bacteria, while inhibition can lead to a depolymerization of actin that results in collapse of the actin cytoskeleton, cell rounding, and detachment (8).

Aims of this study

The main aim of this thesis project is to elucidate the activity of the *V. parahaemolyticus* effector VopS and characterize its contribution to T3SS1-dependent cytotoxicity during *V. parahaemolyticus* infection. The cytotoxic effects caused by T3SS1 during infection were thought to occur by apoptosis. However, apoptosis is a quiet and controlled form of cell death while *V. parahaemolyticus* infection results in a rapid cytotoxicity uncharacteristic of apoptosis. Thus, many aspects regarding the precise mechanism of T3SS1-

mediated cell death, and the role of T3SS1 effectors in this process, remain incompletely characterized.

The T3SS1 effector, VopS, has been implicated in multiple events during infection. VopS was first suggested to induce apoptosis of macrophages through the inhibition of the NFkB pathway. Additionally, VopS was correlated with the inhibition of Rho GTPases. While both of these pathways are common targets of type III secreted effector proteins, the molecular mechanism of VopS and its precise targets remained completely unknown. Determining the function of this effector will further our limited understanding of the virulence factors of *V. parahaemolyticus* and provide insight into the pathogenic mechanisms of this important emerging pathogen. Furthermore, bacterial effector proteins often mimic or capture an endogenous eukaryotic activity. Therefore, defining the activities of bacterial effectors may uncover critical points in the regulation of eukaryotic pathways, which raises the exciting possibility for new insight into eukaryotic cell signaling.

CHAPTER TWO
Materials & Methods

Cell culture

HeLa cells were cultured in DMEM (Invitrogen) with 10% cosmic calf serum (HyClone). RAW 264.7 macrophages were cultured in DMEM with 10% FBS (HyClone) and 10 mM L-glutamine. The GFP-LC3–stable HeLa cell line was generously provided by Anthony Orvedahl from the laboratory of Beth Levine (UT Southwestern). GFP-LC3 HeLas were cultured in DMEM with 10% FBS (HyClone) and nonessential amino acids (Invitrogen). All cell lines are maintained at 37ºC in 5% CO_2.

Bacterial growth conditions

All bacterial strains used in these studies are listed in Table 1. The *V. parahaemolyticus* POR1, POR2, and POR3 strains were a generous gift of Takeshi Honda and Tetsuya Iida (Osaka University, Japan). These strains were maintained on LB plus 3% NaCl (MLB) at 30ºC. The *Yersinia pseudotuberculosis* YP126 strain was obtained from Jim Bliska (SUNY, Stony Brook, NY). This strain was cultured on LB at 26ºC. The POR3Δ*vopS* strain was grown in MLB and the POR3Δ*vopS* + VopS strain was grown in MLB supplemented with 20μg/ml of tetracycline to maintain the plasmid.

T3SS-inducing conditions

T3SS1 of *V. parahaemolyticus* was induced by growing cultures in LB plus 3% NaCl (MLB) overnight at 30ºC, then diluting the cultures 1:15 into fresh MLB plus 10 mM sodium oxalate and 10 mM $MgCl_2$. Cultures were grown at 37°C for 3 h before infection. To induce the T3SS of YP126, cultures were grown overnight in LB at 26°C. Before infection, the bacteria were diluted 1:50 into LB plus 20 mM sodium oxalate and 20 mM $MgCl_2$. Cultures were incubated with shaking at 26°C for two hours and then shifted to 37°C for one hour (63).

Infections

HeLa cells or RAW 264.7 macrophages were plated at 0.1×10^6 or 0.5×10^6 cells/ml, respectively, in 6-well tissue culture dishes unless otherwise noted one day before infection. For microscopy, cells were plated onto sterile glass coverslips. *V. parahaemolyticus* and *Y. pseudotuberculosis* were added to the cells at a multiplicity of infection (MOI) of 10 and 100, respectively. Cell monolayers and bacteria were centrifuged at 500 × g for 5 min at the onset of each infection.

Transfections

For transfection experiments, HeLa cells were plated on coverslips at a density of 0.2×10^6 cells in 6-well dishes one day before transfection. Cells were transfected using Fugene HD (Roche) transfection agent with 0.5 µg of pSFFV-eGFP and 0.1 µg of pcDNA3-VopS, pcDNA3-VopS-H287A, pcDNA3-VopS-

H348A, pcDNA3-VopS-R356A, pcDNA3-VopSΔ30, or pcDNA3-VopSΔ30-H348A. For transfection of GFP-HYPE fusion, cells were transfected using Fugene HD with 0.5 μg of pSFFV-eGFP, pSFFV-HYPE-eGFP, pSFFV-HYPEΔ47-eGFP, or pSFFV-HYPEΔ99-eGFP. Empty vector was added to each transfection for a total of 2 μg of DNA/well. Eighteen hours after transfection, cells were fixed and stained as described below.

Preparation of Samples for Microscopy

HeLa or RAW 264.7 macrophage cell lines plated on glass coverslips were fixed at the indicated time points in 3.2% paraformaldehyde in 1× PBS for 10 min and permeabilized in 0.1% Triton X-100 in 1× PBS for 5 min at room temperature. Cells were stained for actin with rhodamine-phalloidin (Molecular Probes) and DNA with Hoechst (Sigma) in 1% BSA and 1× PBS for 20 min at room temperature followed by two washes in 1X PBS. Slides were mounted in 10% glycerol plus N-propyl gallate and sealed with clear nail polish.

Visualization of Samples Using Confocal Microscopy

Samples were visualized with a Zeiss LSM 510 scanning confocal microscope. Images were converted by using ImageJ software and Adobe Photoshop.

Caspase 3/7 Activation in Infected Cells

Raw 264.7 macrophages were plated on 100mm dishes at a density of 1 × 10^6 cell/ml. The following day, cells were left untreated, infected with POR3 or YP126 for 2.5 h, or treated with 1 μM staurosporine (Sigma). After 2.5 h, media was removed and cells were collected in 5 ml of PBS-EDTA and spun at 500 × g for 10 minutes at 4ºC. Cells were resuspended in 300 μl of hypotonic cell lysis buffer (25 mM HEPES (pH 7.5), 5 mM $MgCl_2$, 5 mM EDTA, 5 mM DTT, 2 mM PMSF, 10 μg/ml Pepstatin A, 10 μg/ml Leupeptin) and lysed by freeze/thaw for four cycles. Lysate were spun at 16,000 × g for 20 minutes at 4ºC. Protein concentration of cleared lysate was measured by Bradford assay (Biorad). Caspase 3/7 activity of 40 μg of protein was measured by the Caspase-Glo assay (Promega), a luminescent assay that measures caspase 3/7 activity by the production of luciferase. Each sample was measured in triplicate according to the manufacturer's instructions. Results are expressed as relative luciferase units.

PolyADP Ribose Polymerase (PARP) Cleavage Assay

RAW 264.7 macrophages were infected for 1, 2, and 2.5 h with POR3 or YP126 or treated with 1 μM staurosporine for 4 h. Cells were lysed at the indicated time points in PARP sample buffer (62.5 mM Tris-HCl (pH 6.8), 6 M urea, 2% SDS, 5% β-mercaptoethanol, 10% glycerol, and 0.00125% bromophenol blue). Samples were sonicated for 15 s, separated by SDS/PAGE, and

immunoblotted with anti-PARP antibody (Cell Signaling) and anti-aldolase antibody (Santa Cruz Biotechnology) to confirm equal loading.

Measurement of LDH Release During POR3 Infection

RAW264.7 macrophages plated at a density of 2×10^5 cells/ml in 24 well dishes. The following day cells were washed once in PBS and DMEM without serum was added back to each well. Cells were infected in triplicate with POR3 as described over a 4-h time course. Cells were left untreated, infected with YP126 as described, or treated with 1 μM staurosporine in triplicate as controls. Where indicated, the PI3 kinase inhibitor wortmannin (Sigma) was used at 10 μM. At each time point, 125 μl of media was removed in triplicate from each sample and added to a 96-well plate. The plate was spun at 1,000 rpm for 5 minutes and 100 μl of media was removed from each well and put into a new 96-well plate. This plate was stored at 4ºC for the course of the infection. LDH release was measured with a Cytotoxicity Detection kit (Takara) according to the manufacturer's instructions. Results are expressed as cytotoxicity calculated as percent of total lysis of cells lysed in 1% of Triton X-100.

Electron Microscopy

HeLa cells were infected with POR3 as described. After 2 h of infection, cells were fixed in 2.5% glutaraldehyde in 0.1 M sodium cacodylate buffer, followed by 1% osmium tetroxide in 0.1 M sodium cacodylate buffer. After

solvent dehydration, centrifuged pellets of cells were embedded in epoxy resin (EMBED 812, Electron Microscopy Sciences) and polymerized at 60°C. Ultrathin sections were cut at a nominal thickness of 80 nm, picked up on copper grids, and stained with uranyl acetate and lead citrate. Sections were examined at 120 kV with a Tecnai G2 Spirit transmission electron microscope (FEI Company), and images were recorded on a Gatan USC1000 2k CCD camera.

Visualization of GFP-LC3 Punctae Formation

GFP-LC3 HeLa cells were left untreated or infected in the presence or absence of wortmannin (10 μM) for the indicated time points. As a positive control, cells were starved to induce autophagy by incubation of cells in Hank's balanced salt solution (Invitrogen) in the presence of protease inhibitors (10 μg/ml pepstatin A and 10 μg/ml E64-d (Sigma)). For visualization of punctae formation, samples were fixed and stained with Hoechst as described above and punctae were visualized by confocal microscopy.

Monitoring Conversion of LC3-I to LC3-II

GFP-LC3 HeLas were treated as described for visualization of punctae formation. At each time point, samples were harvested for analysis via western blot by the addition of 200 μl of SDS sample buffer. Samples were probed with anti-LC3 antibody (Novus) or anti-GFP antibody (Invitrogen). Relative LC3-II

accumulation was determined by quantitation of band intensity using ImageJ software and calculating the ratio of LC3-II to LC3-I.

Deletion of VopS in POR3 strain

The POR3Δ*vopS* deletion strain was constructed using a method adapted from Datsenko and Wanner (26). VopS and 1kb of upstream and downstream sequence was cloned into the pSP72 vector between two PstI restriction sites. This vector was digested with PstI and ligated into a suicide plasmid, pLafR (kindly provided by Dr. Linda McCarter).

The VopS coding sequence was replaced with a chloramphenicol (Cm) resistance cassette from the pKD3 plasmid. This cassette was amplified by PCR with primers containing 50 bp of sequence flanking vopS. The pLafR plasmid containing VopS with 1000 bp of flanking sequence (Tet^R) was transformed into *E. coli* harboring the lamda red plasmid (Amp^R). The PCR amplified Cm cassette was electroporated into this strain and transformants were selected by growth on LB with Tet and Cm (10 µg/ml and 25 µg/ml, respectively). After recombination, plates were incubated at 37ºC to rid the strain of the temperature sensitive lambda red plasmid. Colonies were screened to verify Tet and Cm resistance and Amp sensitivity. Plasmid DNA of potential positives was prepared and recombination of the Cm cassette was confirmed by sequencing.

The pLafR plasmid containing the resistance cassette in place of VopS was conjugated into POR3 and transconjugants were selected on minimal media

containing 20μg/ml tetracycline (Tet) and 3% NaCl. After passage three times to allow for allelic exchange of the Cm cassette for VopS, the pLafR plasmid was eliminated by conjugation of an incompatible plasmid, pH1JI (gentamicin, Gen^R). Positive deletion strains (Gen^R, Cm^R, Tet^S) were confirmed by PCR and sequencing. The deletion strain was cured of the pH1JI plasmid by successive passage on media without gentamicin at 37ºC.

Reconstitution of VopS in POR3 strain

The POR3Δ*vopS* deletion strain was reconstituted using pLafR encoding *vopS* and 1000bp of upstream sequence to include its endogenous promoter. pLafR-VopS was conjugated into POR3Δ*vopS* and transconjugants were selected with 20μg/ml tetracycline. Reconstitution was confirmed by an in vitro secretion assay.

In vitro Type III Secretion Assay

Overnights of POR3, POR3Δ*vopS*, and POR3Δ*vopS*+VopS were diluted 1:15 in MLB media supplemented with 10mM sodium oxalate and 10mM $MgCl_2$ and cells were grown at 37ºC for 3 hours. Cell culture supernatants from 1 OD equivalent of POR3, POR3Δ*vopS*, and POR3Δ*vopS*+VopS were filtered through a 0.22 μm filter (Millipore) and proteins were precipitated with 10% trichloroacetic acid overnight at 4ºC. Precipitated proteins were spun down for 15 minutes at 14,000 rpm at 4ºC. Pellets were washed twice in acetone and air dried on the

benchtop. Pellets were resuspended in 50 µl of SDS sample buffer and boiled for 5 minutes. Samples were separated on an SDS-PAGE gel and immunoblotted with anti-VopS (peptide antibody generated at UTSW Antibody Core).

Plasmid construction and site-directed mutagenesis

For a list of all of the constructs used in these studies and for details on their construction or source, refer to Tables 2 and 3. The genes that were cloned herein were amplified by PCR using Vent polymerase (New England Biolabs). After amplification, gene products were digested with their respective enzyme (NEB) and ligated into cut vectors using T4 DNA ligase (NEB). Ligations were transformed into *E. coli* (DH5a, Invitrogen). Colonies were grown overnight in the appropriate antibiotic and plasmid DNA was extracted using a miniprep kit (Sigma). Plasmids were screened by digestion and positive clones were confirmed by DNA sequence analysis.

Mutants of VopS and DA-Rac were generated using the Stratagene QuikChangeTM site-directed mutagenesis kit, according to the manufacturer's instructions. Mutants were confirmed by DNA sequence analysis. Refer to Table 3 for details on primers used for mutagenesis.

Expression of VopS in yeast

The BY4741 strain of *Saccharomyces cerevisiae* was transformed with pRS413 empty vector or pRS413 expressing VopS or VopS-H348A and grown on

glucose media. Growth inhibition was assayed by picking one colony from the glucose plate and restreaking the yeast onto galactose media to induce expression from the galactose-inducible promoter of pRS413. To discriminate between growth inhibition and cytotoxicity, yeast from the most heavily streaked area of the galactose plate were restreaked onto glucose media. Under each condition, growth of yeast was assayed after two days at 30ºC.

Yeast Two-Hybrid analysis of VopS binding to chaperone

Various constructs of VopS were clones into the bait plasmid pLexAde, creating a fusion protein with the DNA binding domain of *E. coli* LexA. This plasmid contains the *TRP1* gene so that yeast containing pLexAde are able to grow in media lacking tryptophan. The VopS chaperone, VP1687, was cloned into pVP16 that contains the VP16 activation domain. This plasmid contains an SV40 large T antigen nuclear localization sequence in frame with the coding region of VP16 and the *LEU2* gene that allows the yeast to grow in the absence of leucine. Both plasmids were transformed into to L40 strain of yeast (genotype *Matα his3Δ200 trp1-901 leu2-3,112 ade2 LYS2::lexAop)$_4$-HIS3 URA3::(lexAop)$_8$-lacZ GAL4*) and transformants were selected on media lacking leucine and tryptophan (- LW). The L40 strain contains an integrated HIS3 reporter that is under the control of four LexA operators. Association of the bait with the VP16 activation domain activates transcription of the HIS3 gene so that the yeast are able to grow on media lacking histidine (- WHULK). One colony

from each transformation was streaked onto YCD-WHULK media, and growth on this media was assayed after three days at 30ºC.

Protein expression and purification

pGex-KG-PAK-PBD (kindly provided by Dr. Neal Alto), pGex-Tev-VopSΔ30, pGex-Tev-VopSΔ30-H348A, pET28a-DA-Rac (RacV12), pET28a-DA-Rac-T35A, pET28a-Rac1, and pET28a-RhoA and pGex-KG-Cdc42 (both kindly provided by Dr. Paul Sternweis) were transformed into Rosetta (DE3) cells (Novagen). Single colonies were grown to an OD of 0.6-0.8 and induced with 0.4 mM IPTG for 8-12 hours at room temperature. Cells were harvested and lysed in PBS (pH 8), 1% Triton X-100, 0.1% β-mercaptoethanol (Bio-Rad), and 1 mM phenylmethylsulphonyl fluoride (PMSF, Sigma) using an Emulsiflex C-5 cell homogenizer (Avastin).

His-tagged proteins (DA-Rac, DA-Rac-T35A, Rac1, RhoA, Ran, Rab5a, RasV12, and Arf) were purified using Ni^{2+} affinity purification (Qiagen). GST-tagged proteins (VopSΔ30, VopSΔ30-HA, Cdc42, PAK-PBD, and HYPEΔ47) were purified using glutathione agarose beads (Sigma) and standard GST purification protocol. The GST tag of VopSΔ30 and VopSΔ30-H348A was cleaved by Tev protease overnight at 4ºC. Purified protein was separated from the GST tag over a Superdex 75 gel filtration column using a Pharmacia AKTA FPLC. The GST tag of Cdc42 was cleaved for 3 hours at room temperature using Thrombin CleanCleave kit (Sigma) according to the manufacturer's instructions.

Cleaved Cdc42 was run over a GST column to remove GST. Recombinant His-DA-Rac was sent for mass spectrometric analysis either as a soluble sample (Total MS) or by cutting out bands from a Coomassie Brilliant Blue (Biorad) stained SDS-PAGE gel (LC-MS/MS).

GTPase activation assay in infected cells

HeLa cells were seeded onto 150 mm dishes. Once cells were 80-90% confluent, cells were infected with POR3, POR3Δ*vopS*, or POR3Δ*vopS* + VopS at an MOI of 10 for the indicated time points. At each time point, cells were washed once in PBS and samples were collected by scraping into Mg^{2+} lysis buffer (50mM Tris HCl pH 7.5, 10mM MgCl2, 500mM NaCl, 1% Triton X-100) and immediately snap frozen in liquid nitrogen. Once all samples were collected, samples were incubated at 4ºC with agitation for 15 minutes and genomic DNA was sheared by passing the lysates 4-5 times through a 26-gauge needle. Lysates were cleared by centrifugation at 14,000 rpm for 10 minutes at 4ºC. The supernatant was removed and added to a new tube. Concentration of lysate was determined by Bradford assay (Bio-Rac) and 500µg of cleared lysate was added to 30µg of GST-PAK PBD on glutathione agarose beads in Mg^{2+} lysis buffer. Active Cdc42 was pulled down for one hour at 4ºC after which the beads were spun down and washed three times in Mg^{2+} lysis buffer followed by the addition of 50 µl of SDS sample buffer. As a control, 50 µg of protein from lysate was added to SDS sample buffer to a total volume of 100 µl. Samples of pulldowns

and total cell lysates were separated on SDS-PAGE and immunoblotted with anti-Cdc42 (Cell Signaling). As a loading control, total cell lysates were also immunoblotted with anti-ß-actin (Sigma).

GST-pulldown assays

Proteins that were tested in GST-pulldown assays were *in vitro* translated using the TNT T7 Quick Coupled Transcription/Translation System (Promega) according to the manufacturer's instructions and radiolabeled with ^{35}S-Met (Perkin Elmer). GST-pulldowns were performed with 5 µg of purified GST-labeled proteins on beads and 4 µl of in vitro translated protein in GST pulldown buffer (20 mM HEPES pH 7.4, 50 mM NaCl, 0.1% Triton X-100) in a volume of 100 µl. Samples were rotated for one hour at 4ºC and then washed three times in 750 µl of GST pulldown buffer. SDS sample buffer was added and samples were boiled for 5 minutes, separated by SDS-PAGE and visualized by autoradiography. In some cases ^{35}S-radiolabeled proteins were pre-incubated at 30ºC with the indicated amounts of VopSΔ30 or VopSΔ30-H348A for the indicated time before being pulled down with purified GST-PAK PBD.

GTP Loading Assays

Recombinant DA-Rac expressed alone or coexpressed with VopS was loaded with GTPγ[^{35}S] (Sigma), a radiolabeled, non-hydrolyzable form of GTP.

DA-Rac (0.8 μg) purified from each condition was incubated in GTP loading buffer (50 mM Tris-HCl pH 7.5, 7.5 mM EDTA) containing 50 μM of cold GTPγS (Sigma) mixed 1:10 with radioactive GTPg[^{35}S] for 15 minutes at 30ºC. GTP loading was stabilized with the addition of 50 mM $MgCl_2$. GTP-loaded samples were added to nitrocellulose filters (Whatman) and washed three times in ice-cold buffer containing 20 mM HEPES pH 7.4 and 5 mM $MgCl_2$. Samples were done in triplicate and counts were measured on a scintillation counter for one minute per sample.

In some GST pulldowns, in vitro translated Rho GTPases were loaded with cold GTPγS to facilitate binding. In these samples, 4 μl of in vitro translated protein was loaded with 100 μM of cold GTPγS at 30ºC in GTP loading buffer for 10 minutes. Loading was stabilized with the addition of 30 mM of $MgCl_2$. The entire volume of sample was added to the GST pulldown.

Mass spectrometry

Samples were desalted with C4 Ziptip from Millipore (Billerica, MA). The eluted protein samples were made into a solution that contains 50% acetonitrile and 1% formic acid. The Proxeon nano-tips (Denmark) were used to infuse the samples into a QStar XL Q-TOF mass spectrometer (Applied Biosystems, Framingham, MA). Spectra were acquired with mass range m/z 500-2000. The molecular weights of proteins were calculated with the Baysesian Protein Reconstruct tool of the Analyst QS1.1 software.

Tandem Mass Spectrometry

Ten micrograms of each sample were fractionated by 1D-SDS PAGE and the slices of DA-Rac were treated with DTT and iodoacetamide and were digested with AspN. Samples from the digests were analyzed by nano-LC/MS/MS using a system in which a Dionex LC-Packings HPLC (Sunnyvale, CA) was coupled with a QStar XL mass spectrometer (Applied Biosystems, Framingham, MA). Peptides were first desalted on a 300 µm x 5 mm PepMap C18 trap column with 0.1% formic acid in HPLC grade water at a flow rate of 30 µl/min. After desalting for 5 min, peptides were washed onto a LC-Packings 75µm x 15cm C18 nano column (3 micron, 100A) at a flow rate of 250 nl/min. The composition of mobile phase A is 95:5 water:acetonitrile with 0.2% formic acid. Peptides were eluted with mobile phase B (90% acetonitrile, 0.2% formic acid), increased non-linearly from 3% to 90% in 45 min and maintained at 90% for 10 min. The total run time was 74 min. Mass ranges for the MS survey scan and MS/MS were m/z 300-2000 and m/z 50-2000, respectively. The scan time for MS and MS/MS were 1.0 s and 6.0 s, respectively. The top three multiply charged ions with MS peak intensity greater than 30 counts/scan were chosen for MS/MS fragmentation with a precursor ion dynamic exclusion of 60 s.

In vitro AMPylation assay

For the AMPylation assays using purified recombinant protein, 1 µg of the

Rho GTPase was incubated with 0.6 μg of VopSΔ30 or VopSΔ30-H348A for 10 minutes at 30ºC in 20 mM HEPES buffer containing 300 μM ATP and ^{32}P-α-ATP (2μCi) (Perkin Elmer). Total reaction volume was 20 μl and the final concentration of Rho GTPase was 2 μM and VopS was 40 nM. Rho, Rac and Cdc42 were pre-loaded with GTPgS (Sigma) by incubating in GTP loading buffer (50 mM Tris-HCl pH 7.5, 7.5 mM EDTA) containing 100 μM GTPγS for 15 minutes at 30ºC. GTP loading was stabilized with the addition of 50 mM $MgCl_2$ and 1 μg of GTP-loaded protein was used in each sample. The AMPylation reaction was stopped by the addition of SDS sample buffer. Samples were boiled for 5 minutes, separated by SDS-PAGE, and visualized by autoradiography.

For AMPylation of S100 lysates, 160 μg of lysate was left untreated or boiled for 4 minutes to denature proteins. Lysates were incubated in buffer containing 50 mM Tris-HCl pH 7.5, 20 μM cold ATP, 100 mM NaCl, 0.1 mM EGTA, 2 mM dithiothreitol, 0.01% Brij 35 and 2 mM $MnCl_2$ with ^{32}P-α-labeled ATP in the presence or absence of VopSΔ30 (10 ng), λ-phosphatase (400 units, New England Biolabs), or GST-HYPEΔ47 (100 ng) for 30 minutes at 30ºC. Total reaction volume was 30 μl. λ-phosphatase was added in the last five minutes of incubation. Where indicated, RNase A (Roche) was added at the beginning of the reaction at a final concentration of 0.1 mg/ml. The AMPylation reaction was stopped by the addition of SDS sample buffer. Samples were boiled for 5 minutes, separated by SDS-PAGE, and visualized by autoradiography.

In vitro kinase assay

S100 HeLa cell lysates (160µg) were left untreated or boiled for 4 minutes to denature proteins. Lysates were incubated in buffer containing 20mM HEPES, pH 7.4, 20 µM cold ATP, and 10mM $MgCl_2$ with ^{32}P-γ-labeled ATP in the presence or absence of VopSΔ30 (10 ng) or λ-phosphatase (400 units, New England Biolabs) and 2mM $MnCl_2$ for 30 minutes at 30ºC. λ-phosphatase was added in the last five minutes of incubation. The kinase reaction was stopped by the addition of SDS sample buffer. Samples were boiled for 5 minutes, separated by SDS-PAGE, and visualized by autoradiography.

Lysate preparation for *in vitro* assays

Lysates were prepared based on a previously described protocol. Briefly, HeLa cells for S100 lysates were grown to 90-100% confluency and harvested using PBS + 1mM EDTA. Cells were lysed with an equal volume of HTX lysis buffer (10 mM HEPES, pH 7.4, 10 mM $MgCl_2$, 1 mM $MnCl_2$, 0.5% Triton X-100, 0.1 mM EGTA) containing a protease inhibitor cocktail tablet (Roche) by incubating on ice for 20 minutes. Membrane-free S100 lysates were obtained by performing three consecutive centrifugation steps at 800, 10,000 and 100,000 x *g* and stored at -80°C at a concentration of 10mg/ml.

In vitro AMPylation assay using Biotinylated ATP

Recombinant his-tagged Rac (1 μg) was incubated in the presence or absence of VopSΔ30 (10 ng) with Biotin-11-ATP (Perkin Elmer). Biotin-11-ATP was diluted to a 10X stock at a concentration of 100 μM in 20 mM HEPES, pH 7.5. The reactions proceeded for 15 minutes at 30ºC. Reaction were stopped by the addition of 20 μl of SDS sample buffer and boiled for 5 minutes and 15 μl were loaded onto an SDS-PAGE gel. After transfer, the membrane was blocked overnight at 4ºC in TTBS containing 5% BSA. The membrane was then incubated with Avidin-HRP (eBioscience) at 1:1000 for 1 h at room temperature and developed in ECL plus (GE Healthcare).

Table 1. Bacterial strains used in this study.

Strain	Description	Source
E. coli DH5a	F$^-$ 080d*lacZ* ΔM15 Δ (*lacZYA-argF*)*U169 deoR recA1 endA1 hsdR17*(rK- mK+) *phoA supE44* 1- *thi-1 gyrA96 relA1*	Invitrogen
E. coli BL21(DE3)	F$^-$ *omp*T *hsd*SB(rB–, mB–) *gal dcm* (DE3)	Novagen
E. coli Rosetta (DE3)	F$^-$ *ompT hsdS*$_B$(r_B^- m_B^-) *gal dcm* (DE3) pRARE (Cam^R)	Novagen
E. coli BW26434	Δ(araD-araB)567, Δ(lacA-lacZ)514(::kan), lacIp-4000(lacI^q), λ$^-$, rpoS396(Am), rph-1, Δ(rhaD-rhaB)568, hsdR514	(26)
V. parahaemolyticus POR1	RIMD2210633 Δ*tdhA*, Δ*tdhS*	(76)
POR2	POR1 Δ*vp1662*	(77)
POR3	POR1 Δ*vpa1355*	(77)
POR3Δ*vopS*	POR3 Δ*vopS*	This study
POR3Δ*vopS* + VopS	POR3 Δ*vopS*, pLafR VopS	This study
YP126	Wild type *Y. pseudotuberculosis*, YPIII(pYV$^+$)	(16)

Table 2. Plasmids used in this study.

Plasmid	Description	Source
pcDNA3	Mammalian expression vector; CMV promoter; Amp^R	Invitrogen
pSFFV	Mammalian expression vector, pcDNA3 backbone with SFFV promoter, Amp^R	P.G. Reddy and S. Greenberg, unpublished data
pRS413-gal	Yeast expression; has gal4 promoter cloned between SacI and XbaI of MCS, Amp^R	Yong Wang, UTSW
pLexAde	Yeast two-hybrid bait vector; contains E. coli LexA DNA-binding domain; encodes *TRP1*	(92)
pVP16	Yeast two-hybrid vector; contains VP16 activation domain; encodes *LEU2*	(92)
pGexTev	GST-tag expression vector (pGex4T3) with Tev protease cleavage site between GST and MCS; Amp^R	(21); gift of Yuh Min Chook, UTSW
pET28a	N-terminal His-tag expression vector; Kan^R	Novagen
pSP72	Cloning vector; Amp^R	Promega
pLafR	Broad host range cosmid cloning vector; low-copy; Tet^R	(32)
pDK3	Template for Cm cassette	(26)
pH1JI	Incompatible plasmid with pLafR; Gen^R	(10)
pcDNA3-VopS-flag	Contains 1.1 kB BamHI-XhoI fragment with C-terminal flag tag; Amp^R	This study
pcDNA3-VopS-H287A	pcDNA3-VopSΔ30 with H287A mutation; Amp^R	This study
pcDNA3-VopS-H348A	pcDNA3-VopSΔ30 with H348A mutation; Amp^R	This study
pcDNA3-VopS-R356A	pcDNA3-VopSΔ30 with R356A mutation; Amp^R	This study
pcDNA3-VopSΔ30	Contains 1.0 kB BamHI-XhoI fragment; Amp^R	This study
pcDNA3-VopSΔ30-	pcDNA3-VopSΔ30 with	This study

H348A	H348A mutation; Amp^R	
pSFFV-eGFP	Contains NotI-ApaI eGFP fragment; Amp^R	Dara Burdette, UTSW
pSFFV-HYPE-eGFP	C-terminal fusion of eGFP to HindIII-NotI fragment of HYPE; Amp^R	This study
pSFFV-HYPEΔ47-eGFP	C-terminal fusion of eGFP to HindIII-NotI fragment of HYPEΔ47; Amp^R	This study
pSFFV-HYPEΔ99-eGFP	C-terminal fusion of eGFP to HindIII-NotI fragment of HYPEΔ99; Amp^R	This study
pRS413-VopS	Contains 1.1 kB BamHI-EcoRI VopS fragment with C-terminal flag tag; Amp^R	This study
pRS413-VopS-H348A	pRS413-VopS with H348A mutation; Amp^R	This study
pLexAde-VopS	Contains 1.1 kB EcoRI-SalI VopS fragment; Amp^R	This study
pLexAde-VopSΔFic	Contains 750 bp EcoRI-SalI VopS fragments encoding aa 1-254; Amp^R	This study
pLexAde-VopS-Fic	Contains 400 bp EcoRI-SalI VopS fragment encoding aa 255-387; Amp^R	This study
pLexAde-VopS-H348A	pLexAde-VopS with H348A mutation; Amp^R	This study
pVP16-1687	Contains 430 bp BamHI-NotI VP1687 fragment; Amp^R	This study
pGexTev-VopSΔ30	Contains 1 kB BamHI-XhoI VopSΔ30 fragment with N-terminal GST tag; Amp^R	This study
pGexTev-VopSΔ30-H348A	pGexTev-VopSΔ30 with H348A mutation; Amp^R	This study
pGexTev-HYPEΔ47	Contains 1.2 kB BamHI-NotI fragment of HYPE; Amp^R	This study
pGexKG-PAK-PBD	Contains Cdc42/Rac binding domain (aa 65-136); Amp^R	Gift of N. Alto (UTSW)
pGexKG-Cdc42	N-terminal GST-tagged Cdc42; Amp^R	Gift of P. Sternweis (UTSW)
pET28a-Rac	Contains 0.6 kB BamHI-XhoI Rac fragment with N-terminal His tag; Kan^R	This study

pET28a-RacV12 (DA-Rac)	Contains 0.6 kB BamHI-XhoI RacV12 fragment with N-terminal His tag; Kan^R	This study
pET28a-RacV12-T35A	pET28a-RacV12 with T35A mutation; Kan^R	This study
pET28a-RhoA	Contains N-terminal His tag fusion to RhoA; Kan^R	Gift of N. Alto (UTSW)
pET15b-Ran	Contains N-terminal His tag fusion to Ran; Amp^R	Gift of YM Chook (UTSW)
pET28a-Rab5a	Contains N-terminal His tag fusion to Rab5a; Kan^R	Alicia Farmer, Orth lab rotation student
pET28a-RasV12	Contains N-terminal His tag fusion to RasV12; Kan^R	Alicia Farmer, Orth lab rotation student
pET28a-Arf	Contains N-terminal His tag fusion to Arf; Kan^R	Alicia Farmer, Orth lab rotation student
pSP72-VopS	3.1 kB PstI-PstI fragment containing VopS plus 1 kB of upstream and downstream sequence; Amp^R	This study
pLafR-VopS	Contains 3.1 kB PstI-PstI fragment from pSP72-VopS; Tet^R	This study

Abbreviations: Amp, ampicillin; Kan, kanamycin; Tet, tetracycline; Cm, chloramphenicol; Gen, gentamicin; aa, amino acids

Table 3. List of primers

Primer	Sequence
VopS sequencing primer-5’	5’-CAC GCC GCT GAG CTG AGC-3’
VopS sequencing primer-3’	5’-AGC GTT GAT GAT CCA AGC-3’
VopS—5’ BamHI	5’-ATCG GGATCC ATG ATC AGT TTT GGA AAT GTG-3’
VopS—5’ EcoRI	5’-GTAC GAATTC ATG ATC AGT TTT GGA AAT GTG AG-3’
VopS-Fic—5’ EcoRI	5’-GTAC GAATTC ATG TCA AAA GGG AAC GAT GCG G-3’
VopS—3’ SalI	5’-GTAC GTCGAC TTA TTT GAT ACC TGT AAG GCT AT-3’
VopSΔFic—3’ SalI	5’-GTAC GTCGAC GTT TGA AGC GTT GAT GAT CC-3’
VopS—3’ XhoI (no stop codon)	5’-ATGC CTCGAG TTT GAT ACC GTG AAC GCT AT-3’
VopSΔ30—5’ BamHI	CAGT GGATCC GGT AAG GAA TAT ACG ATC AAT G-3’
VopS—3’ XhoI (w/stop codon)	5’-CAGT CTCGAG TTA TTT GAT ACC GTG AAG GCT-3’
VopS—3’ EcoRI (w/Flag tag)	5’-ATCG GAATTC TTA CTT GTC ATC GTC GTC CTT GTA GTC TTT GAT ACC GTG AAG GCT AT-3’
VopS H348A mutagenesis primer-For	5’-GCT GGT GTG ATT GGT TAT GCC GGC TTT ACC GAT GGC AAC GGA CGC-3’
VopS H348A mutagenesis primer-Rev	5’-GCG TCC GTT GCC ATC GGT AAA GCC GGC ATA ACC AAT CAC ACC AGC-3’
VopS H287A mutagenesis primer-For	5’-ATG GAC AAC CTA AAA GAG TTG GCT GCT CGT TTG GTA CCA AAT GTA-3’
VopS H287A mutagenesis primer-Rev	5’-TAC ATT TGG TAC CAA ACG AGC AGC CAA CTC TTT TAG GTT GTC CAT-3’
VopS R356A mutagenesis primer-For	5’-GGC TTT ACC GAT GGC AAC GGA GCC ATG GGG CGC ATG CTT TAT GCC-3’
VopS R356A mutagenesis primer-Rev	5’-GGC ATA AAG CAT GCG CCC CAT GGC TCC GTT GCC ATC GGT AAA GCC-3’
VopS (pre 1000 bp)—5’ Pst1	5’-ATGC CTGCAG GAC GAA CGT

	CGT CTT AGA C-3’
VopS (post 1000 bp)—3’ PstI	5’-ATGC CTGCAG AGA TTT TTC AAA TTG CCG AGC-3’
VopS (pre 50 bp)—5’ primer for amplification of Cm^R cassette	5’-GCG CGC CAG TGA TGG ATG CTA ACC AAT TCT CTA CAT TAA GGG TGT AAA TC GTG TAG GCT GGA GCT GCT TCG-3’
VopS (post 50 bp)—3’ primer for amplification of Cm^R cassette	5’-AAC ATA CAA ATA CCA ACA CCG AAA ATC ACT GAG TTA TTT CGT GCG CTA AG CAT ATG AAT ATC CTC CTT AG-3’
VP1687—5’ BamHI	5’-ATCG GGATCC TC ATG GCT AAT GGA TTT ATT ACC-3’
VP1687—3’ NotI (w/ stop codon)	5’-ATCGATCG GCGGCCGC TTA CAC CCT TAA TGT AGA GAA-3’
RacI—5’ BamHI	5’-ATCG GGATCC ATG CAG GCC ATC AAG TGT GTG-3’
RacI—3’ XhoI	5’-ACTG CTCGAG TTA CAA CAG CAG GCA TTT TC-3’
RacI T35A mutagenesis primer-For	5’-CCT GGA GAA TAT ATC CCT GCT GTC TTT GAC AAT TAT TCT GCC-3’
RacI T35A mutagenesis primer-Rev	5’-GGC AGA ATA ATT GTC AAA GAC AGC AGG GAT ATA TTC TCC AGG-3’
HYPE sequencing primer-5’	5’-GAC AGC AAA GTG AAG AAG GTC-3’
HYPE sequencing primer-3’	5’-CGT GTT GAT GTA CTT CAT GGC-3’
HYPE—5’ HindIII	5’-ACTG AAGCTT ATG ATG CTC ATA CCA ATG GC-3’
HYPEΔ47—5’ BamHI	5’-ACTC GGATCC GAG GAG CAG TGC TTG GC-3’
HYPEΔ47—5’ HindIII	5’-ACTG AAGCTT ATG GAG GAG CAG TGC TTG GC-3’
HYPEΔ99—5’ HindIII	5’-ACTG AAGCTT ATG CCA GCG GGT AAG TTG GAA G-3’
HYPE—3’NotI (no stop codon)	5’-CTAGCTAG GCGGCCGC GGG CTT CAC AGG AAG CG-3’
HYPE—3’XhoI	5’-ACTG CTCGAG TTA GGG CTT CAC AGG AAG

CHAPTER THREE
T3SS1 of *V. parahaemolyticus* induces a rapid and multifaceted host cell death

INTRODUCTION

Genome sequencing of a clinical isolate of *V. parahaemolyticus* revealed the presence of two T3SSs (60). One of these systems, encoded on chromosome 2, is located within a pathogenicity island and is found only in clinical isolates of *V. parahaemolyticus*. The T3SS encoded on chromosome 1, T3SS1, is homologous to the T3SS of *Yersinia* spp, with the exception of a hypothetical region of genes that is predicted to encode type III effector proteins and their associated chaperones (77).

Previous studies have shown that T3SS2 is associated with enterotoxicity using a rabbit ileal loop model of infection (77). However, infection of HeLa cells with a strain that contains only a functional T3SS1 results in cytotoxicity, suggesting a role for T3SS1 in virulence (56, 77). One study linked T3SS1 cytotoxicity to the induction of apoptosis, which was measured by Annexin V staining and DNA fragmentation analysis (71). However, these studies lacked positive apoptotic controls and the results depicting the inflammatory release of cellular contents contradicted a major characteristic of apoptosis, a noninflammatory type of cell death. Additionally, DNA fragmentation is a characteristic of several types of cell death, including apoptosis, pyroptosis, and in some cases of necrosis (29). Although they cytotoxic effects of T3SS1 during infection are apparent, the mechanism of cell death is not well established.

Our studies reveal that T3SS1 induces several separate but parallel events during *V. parahaemolyticus* infection. First, we observe both microscopically and biochemically that T3SS1 mediates acute activation of autophagy in the cell. Second, we observe T3SS1- dependent manipulation of the actin cytoskeleton that results in cell rounding. Last, the events of infection culminate with lysis of the cell within four hours of infection. These studies highlight a novel paradigm of infection whereby T3SS1 causes a series of events that result in the proinflammatory death of an infected host cell.

RESULTS

V. parahaemolyticus induces T3SS1-dependent cytotoxicity in multiple cell types.

To develop a better understanding of the mechanism of cell death induced by *V. parahaemolyticus*, we infected two cell types, HeLa cells and RAW 264.7 macrophages, with several *V. parahaemolyticus* strains, designated POR1, POR2, and POR3. The parental POR1 strain possesses both T3SSs but lacks genes encoding TDH and TRH. Two isogenic strains derived from the POR1 strain were used to dissect the phenotype caused by each T3SS. The POR2 strain contains a functional mutation in T3SS2, rendering it incapable of secreting effectors from this system. POR3 harbors a functional mutation in T3SS1, making it incapable of secreting from T3SS1 (76) (Figure 6A).

Infection with the POR1 strain induces cell rounding and cytotoxicity in both HeLa cells and RAW 264.7 macrophages (Figure 6B). The strain lacking a

functional T3SS1 (POR2) is unable to induce cell death upon infection, but obvious changes in the actin cytoskeleton are observed (56) (Figure 6B). Infection with a strain lacking a functional T3SS2 (POR3) induces a cytotoxic phenotype similar to that seen in POR1-infected cells (Figure 6B, respectively).

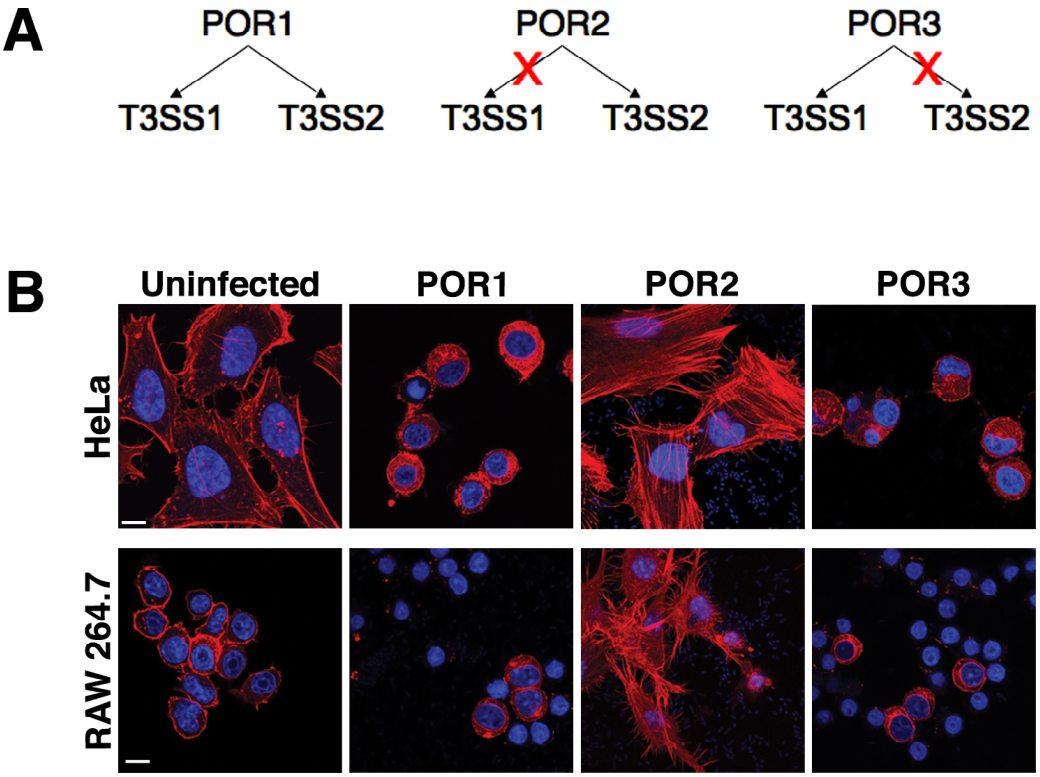

Figure 6. *V. parahaemolyticus*-induced cytotoxicity is dependent upon T3SS1.
(A) Schematic showing the functionality of T3SSs from the *V. parahaemolyticus* strains POR1, POR2, and POR3. (B) HeLa cells or RAW 264.7 macrophages were infected at and MOI of 10 with POR1, POR2, or POR3 for 3 hours and compared to mock infected cells. Nuclei and actin were stained with Hoescht (blue) and rhodamine-phalloidin (red), respectively and cells were visualized by confocal microscopy.

Some T3SSs can be induced in vitro prior to infection by growing the bacteria at a higher temperature and under decreased calcium concentration. These conditions are similar to those used for inducing the T3SS of *Yersinia* spp. (98). To further confirm that these cytotoxic effects were the result of a T3SS, we induced secretion of T3SS1 in vitro prior to infection. Infection of HeLa cells or RAW macrophages with POR3 grown under T3SS-inducing conditions results in an acceleration of the T3SS1-dependent cytotoxic phenotype in which cells are rounded as early as one hour after infection, with only cell fragments observed at three hours after infection (Figure 7). Infection with the uninduced POR3 strain slows the death process, allowing observation of the T3SS1-induced cell death over an extended interval. Under these infection conditions, cells begin to round about two hours after infection and are almost completely dead by four hours post infection (Figure 7). These data support the hypothesis that cytotoxicity is a result of infection with T3SS1. In addition, T3SS1-mediated cell death is rapid, occurring within three hours of infection in multiple types of cells.

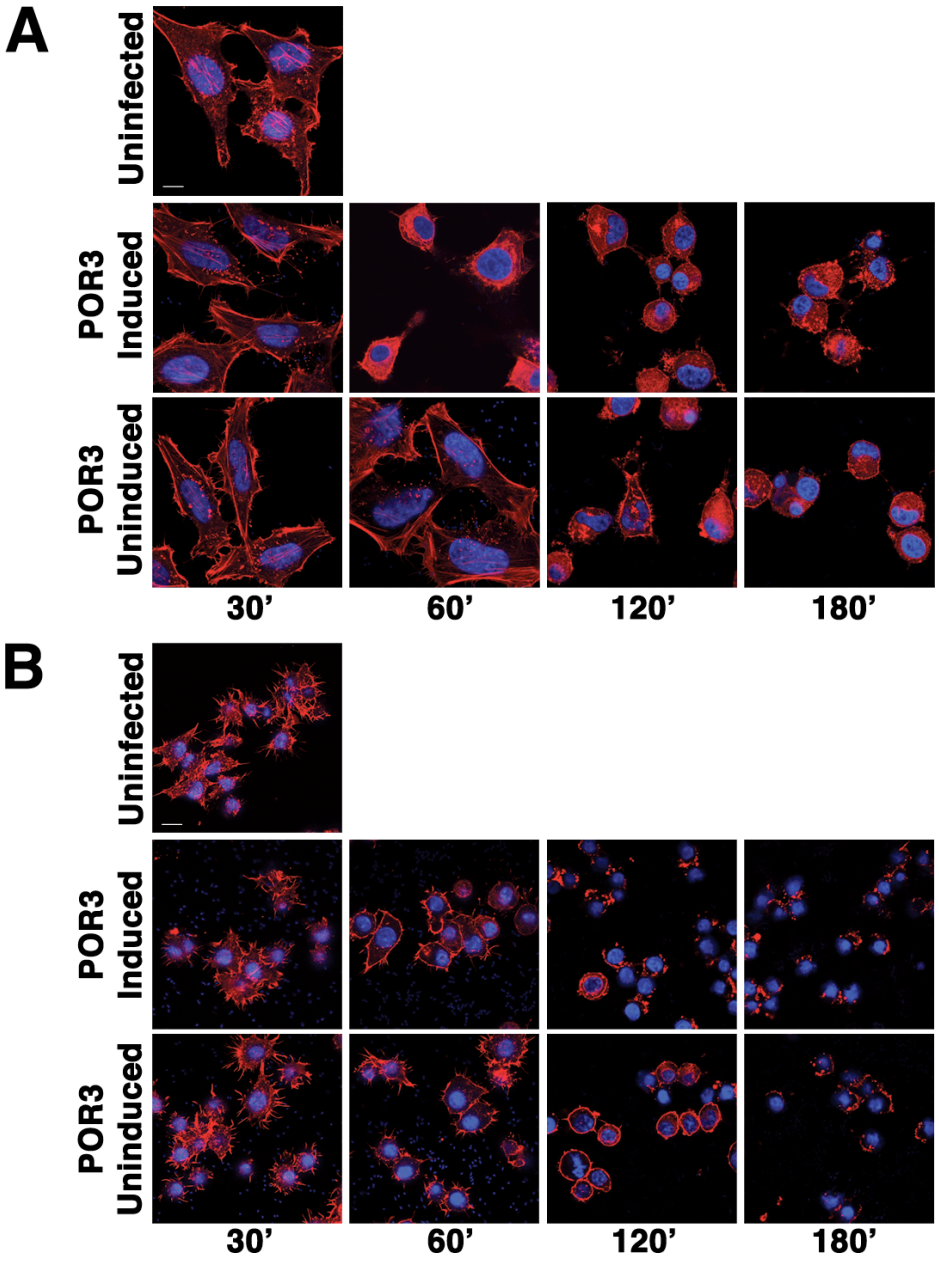

Figure 7. POR3 infection under T3S-inducing conditions accelerates T3SS1-dependent cytotoxicity.
(A) HeLa cells were infected with POR3 grown under T3S-inducing conditions (POR3 Induced) or with POR3 grown overnight at 30ºC (POR3 Uninduced) and compared with the uninfected control. Cells were infected for the indicated time point. At each time point, cells were fixed and stained with Hoechst to visualize nuclei (blue) and rhodamine-phalloidin to visualize actin (red). (B) RAW 264.7 macrophages were infected and visualized as described for HeLa cells in A. Scale bar = 10μm.

T3SS1-induced cytotoxicity is independent of caspase activation.

Previous studies have observed that T3SS1-mediated cell death occurs by apoptosis (12, 71). We also observed that cells infected with the POR3 strain exhibit morphology consistent with apoptotic death, including cell rounding and nuclear shrinkage (88) (Figure 8). This phenotype resembles that seen for cells infected with a wild-type strain of *Yersinia pseudotuberculosis* (YP126), a pathogen that has been well-characterized as inducing apoptosis in infected cells (63) (Figure 8).

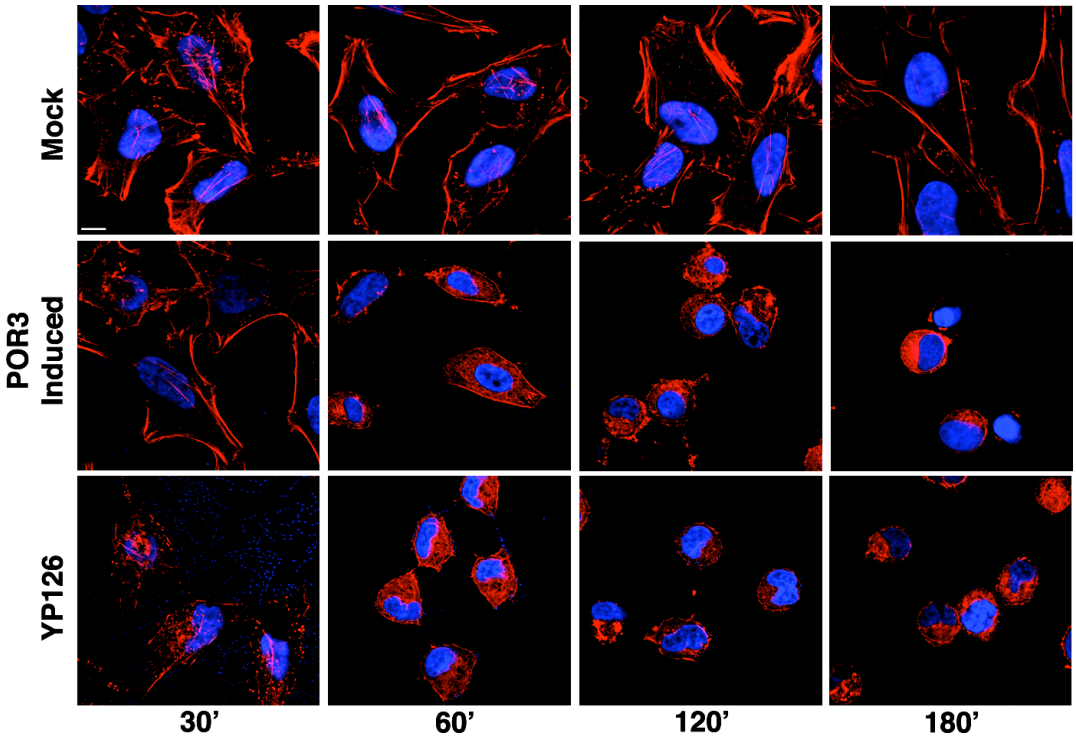

Figure 8. POR3 infection induces a rapid cytotoxicity in HeLa cells that resembles *Yersinia*-induced cytotoxicity.
POR3 and YP126 grown in T3S-inducing conditions were used to infect HeLa cells for the indicated time points. Cells were uninfected (Mock) or were infected with induced POR3 or with YP126. Cells were visualized using confocal microscopy using rhodamine phalloidin to stain actin (red) and Hoechst to stain nuclei (blue). (Scale bar represents 10 µm.)

To test whether *V. parahaemolyticus* induces cell death by apoptosis, we assayed POR3-infected RAW 264.7 macrophages for the activation of caspases. We observed that caspase activity is elevated in cells infected with YP126 or treated with staurosporine, a nonselective protein kinase inhibitor that initiates apoptosis in cells (Figure 9A). However, POR3-infected macrophages do not show any evidence of caspase 3/7 activation (Fig. 9A). In addition, polyADP ribose polymerase (PARP), a downstream target of caspase 3, is cleaved in both staurosporine-treated cells and *Yersinia*-infected cells (Figure 9B, lanes 7–9 and 10–12, respectively) but not in POR3-infected cells (Figure 9B, lanes 4–6). Based on these observations, we conclude that POR3-induced cytotoxicity is independent of apoptotic machinery.

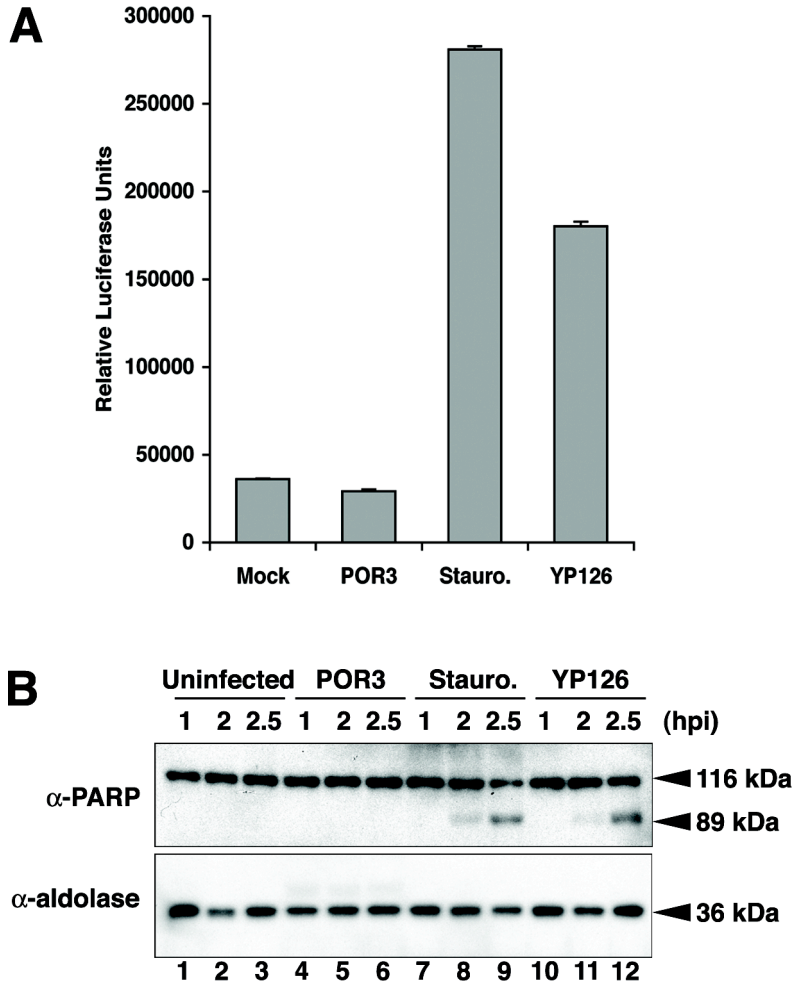

Figure 9. T3SS1-dependent cytotoxicity is not caused by apoptosis.
(A) RAW 264.7 macrophages were infected with POR3 for 2.5 h. Cells were treated with 1 μM staurosporine (Stauro) or infected with YP126 as positive controls. After infection, cells were lysed and normalized for protein content. Caspase 3/7 activation was measured by luminescence with the Caspase-Glo assay. (B) RAW 264.7 macrophages were treated identically as described in A (uninfected, lanes 1–3; POR3, lanes 4–6; Stauro, lanes 7–9; or YP126, lanes 10–12). Cells were lysed at the indicated time points and immunoblotted with anti-PARP antibody or anti-aldolase antibody to confirm equal loading.

POR3-induced cell death is proinflammatory.

While apoptosis is a noninflammatory type of cell death, other forms of cytotoxicity, such as necrosis, are proinflammatory (28). Having ruled out apoptosis as the strategy of T3SS-mediated cell death, we analyzed whether POR3 infection was proinflammatory by measuring the release of cellular contents. In this experiment, the release of the cytoplasmic enzyme lactate dehydrogenase (LDH) is measured by colorimetric assay. During infection of macrophages with the POR3 strain, we observed elevated levels of cytoplasmic LDH released into the media, indicating that the integrity of the host-cell membrane is compromised (Figure 10). Consistent with our microscopic observations over a time-course of infection, the T3SS-induced POR3 strain caused LDH release faster than the uninduced POR3 strain (Figure 10, at 2 and 3 h, respectively). As expected, cells in which apoptotic death was induced by *Yersinia* infection or staurosporine treatment exhibited no increase in LDH release over the course of infection or treatment (Figure 10). In total, these results support the hypothesis that *V. parahaemolyticus* T3SS1-mediated cell death is not caused by apoptosis and that this cytotoxicity is proinflammatory, promoting the lysis of cells within three hours of infection.

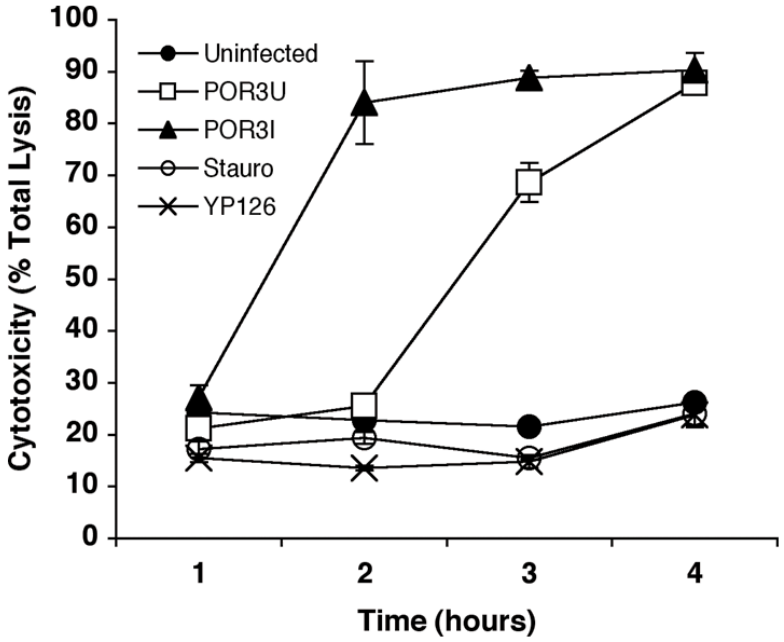

Figure 10. POR3 infection is proinflammatory.
Cytotoxicity of RAW 264.7 macrophages was measured by LDH release. Cells were infected over a time course with POR3 grown in T3S-inducing conditions (POR3I, closed triangle) or in noninducing conditions (POR3U, open square). Cells were left uninfected (closed circle), infected with YP126 (×) or treated with 1μM staurosporine (open circle) as controls. Cytotoxicity was calculated as a percent of total lysis of cells that were lysed in Triton X-100.

V. parahaemolyticus infection rapidly induces T3SS1-dependent autophagy.

To examine the potential role of the autophagy pathway in T3SS1-dependent cytotoxicity, we monitored a marker of autophagic vesicle formation, microtubule-associated protein 1 light chain 3 (LC3), using microscopic and biochemical indicators (44). Induction of autophagy results in incorporation of LC3 into autophagic vesicles, such that when LC3 is fused to green fluorescent protein (GFP), it will form punctae that can be viewed by fluorescence microscopy (44).

For these experiments, we obtained a HeLa cell line that stably expresses GFP-LC3. As a positive control, cells were starved in the presence of protease inhibitors to activate autophagy. Over the course of three hours, GFP-LC3 punctae accumulated slowly in starved cells to levels above those in untreated cells (Figure 11A, G–I and A–C, respectively). By contrast, we observed that the formation of autophagic vesicles in POR3-infected cells was rapid, occurring within one hour after infection and increasing dramatically over the next two hours (Figure 11A, D–F). To confirm that cells infected with the POR3 strain were inducing autophagy, the infected cells were analyzed by electron microscopy. POR3-infected cells contained multiple autophagic vesicles characterized by double or multiple membranes that had engulfed cytoplasm, organelles, membranes, and smaller vesicles (Figure 11B).

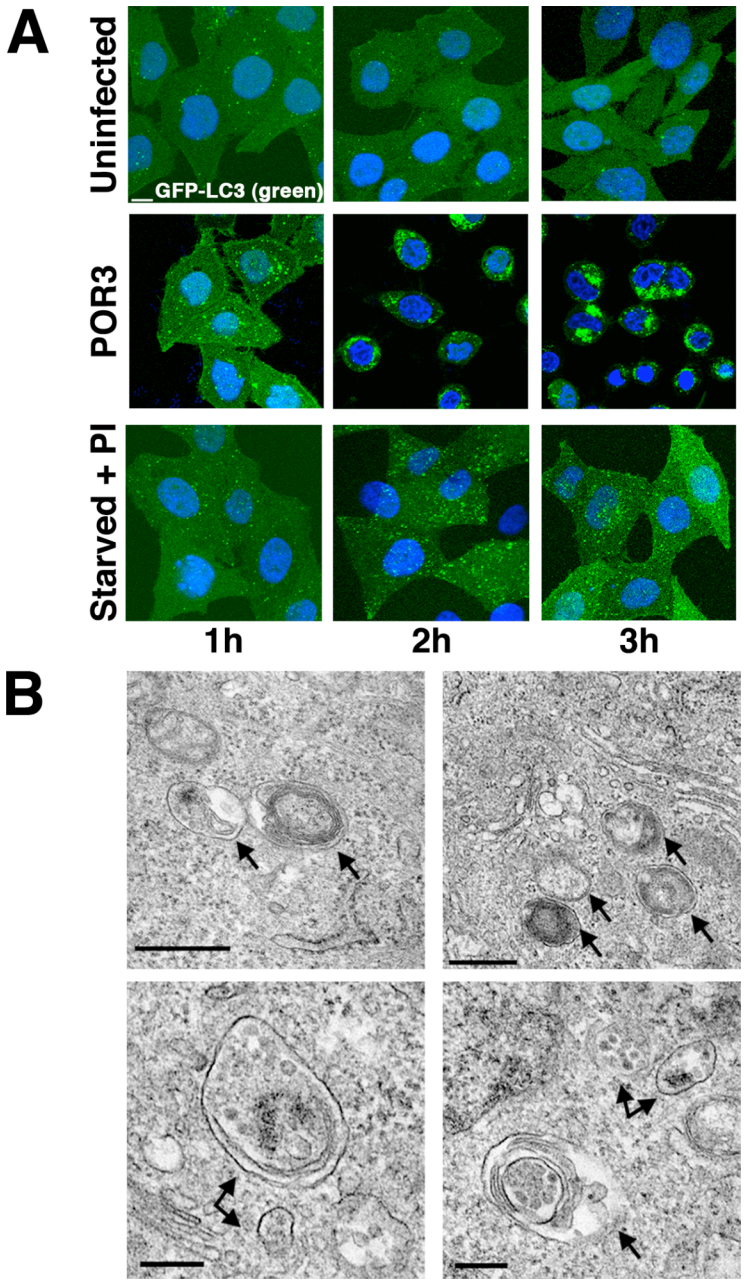

Figure 11. ***V. parahaemolyticus*** **induces autophagy.**
(A) GFP-LC3 HeLa cells were plated on coverslips and left uninfected, infected with POR3, or starved with protease inhibitors (Starved + PI) for 1, 2, and 3 h. Samples were prepared for microscopy at 1-h time points and stained with Hoechst to visualize nuclei (blue). Scale bar = 10 µm. (B-E) HeLa cells were infected with POR3, harvested 2h after infection, and processed for electron microscopy. Arrows designate early autophagosomes. (Scale bars = 0.5 µm in B and C and 0.2 µm in D and E.)

To further test T3SS1-dependent activation of autophagy, we used a biochemical indicator for autophagy that monitors a posttranslational modification of LC3. Cytosolic LC3 (LC3-I) is targeted to newly forming autophagosomes by lipidation with phosphatidylethanolamine via an ubiquitin-like conjugation system, which results in the formation of membrane-associated LC3 (LC3-II) (45, 87). LC3-II migrates more rapidly during SDS/PAGE, allowing its formation to be easily monitored as a marker of autophagy induction.

In a cell line stably expressing GFP-LC3, LC3-II accumulates slowly during amino acid starvation in the presence of lysosomal protease inhibitors (Figure 12A, lanes 7–9, and 10B). In cells infected with the uninduced POR3 strain, GFP-LC3-II accumulates rapidly within one hour and continues to be the dominant form throughout the course of infection (Figure 12A, lanes 4–6, and 12B). These studies parallel the timing of our microscopic observations of punctae formation (Figure 11A) and autophagic vesicle accumulation (Figure 11B).

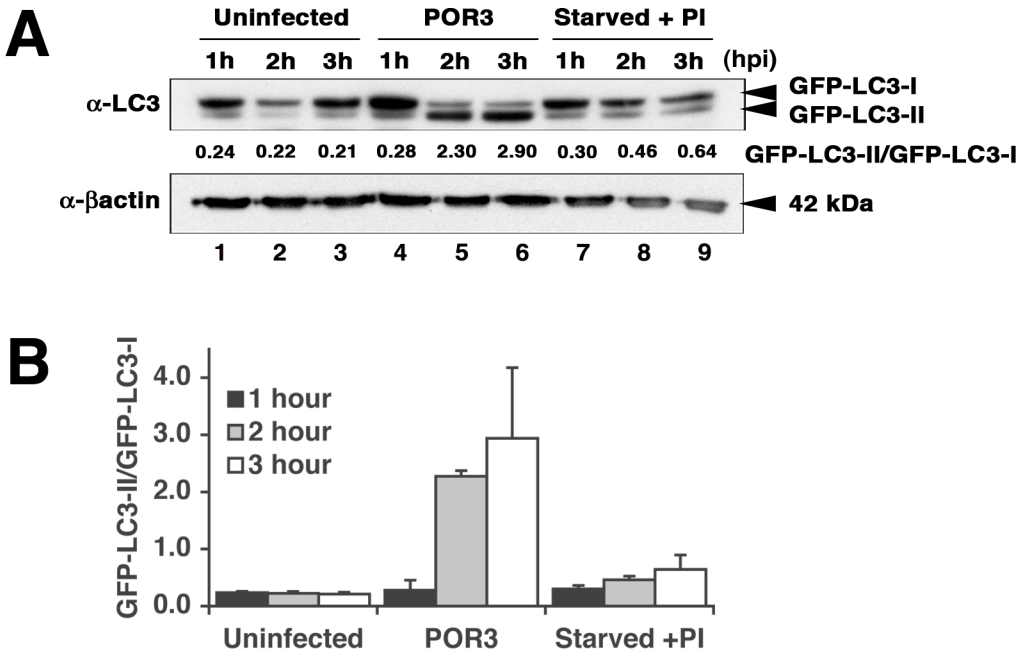

Figure 12. Biochemical observation of POR3-induced autophagy.
(A) GFP-LC3 HeLa cells were left uninfected (lanes 1–3), infected with *V. parahaemolyticus* POR3 (lanes 4–6), or starved with protease inhibitors (Starved + PI) (lanes 7–9) for 1, 2, and 3 h. Samples were immunoblotted using anti-LC3 and anti-β-actin antibodies. (B) Relative LC3-II accumulation was determined as described in Materials and Methods. The data are the means ± SD from three independent experiments.

To test whether autophagy induction is dependent only on T3SS1, we infected HeLa cells stably expressing GFP-LC3 with various T3SS mutants of *V. parahaemolyticus*. Consistent with our hypothesis, only the strains containing a functional T3SS1 (POR1 and POR3) induce conversion of LC3-I to LC3-II, whereas a T3SS1-negative strain (POR2) does not (Figure 13). Our microscopic and biochemical studies support the hypothesis that infection with *V. parahaemolyticus* induces acute and rapid autophagy before the release of cellular contents, because the accumulation of GFP-LC3 punctae (Figure 11A) and the conversion of LC3-I to LC3-II (Figure 12) precede the release of LDH (Figure 10, POR3U).

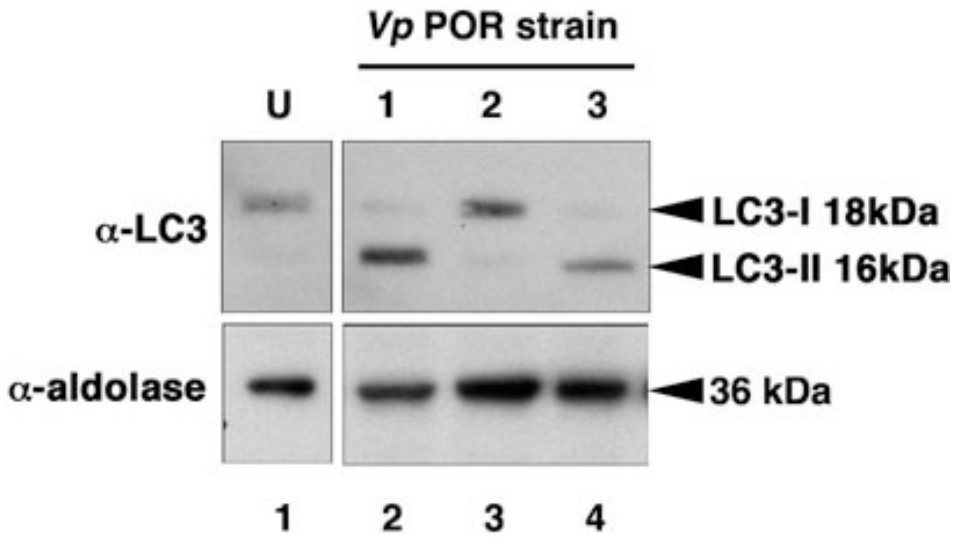

Figure 13. Induction of autophagy is T3SS1-dependent.
HeLa cells were left uninfected (lane 1), or infected with *V. parahaemolyticus* POR1 (lane 2), POR2 (lane 3), or POR3 (lane 4) for 2 h. Samples were immunoblotted with anti-LC3 antibody and probed with anti-aldolase antibody to confirm equal loading.

Inhibitors of PI3 kinase prevent T3SS1-induced autophagy but not cell death.

An early step in the autophagy pathway involves the activation of phosphatidylinositol 3-kinases (PI3 kinases), and treatment of starved cells with PI3 kinase inhibitors prevents autophagy (78). To test whether *V. parahaemolyticus* induces autophagy using known cellular mechanisms, we treated infected cells with the PI3 kinase inhibitor wortmannin (80). Treatment of POR3-infected cells with wortmannin inhibits autophagy, as indicated by a dramatic reduction of GFP-LC3 punctae (Figure 14A). Coincident with the decrease in punctae, we observe a decrease in LC3-II accumulation (Figure 14B, compare lanes 2 and 5, and 14C). Based on these studies, we suspect that acute T3SS1-induced activation of autophagy occurs proximal to, or at the point of, activation of PI3 kinases.

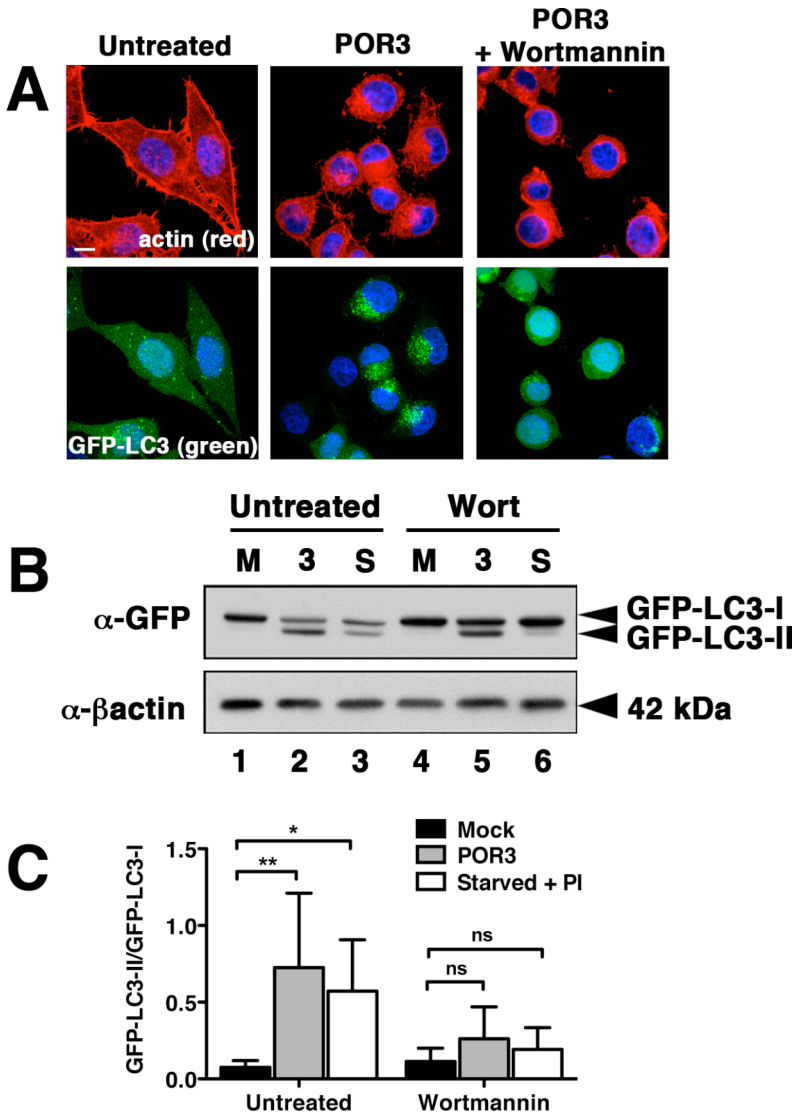

Figure 14. Inhibitors of PI3 kinase prevent *V. parahaemolyticus*–induced autophagy.

(A) GFP-LC3 HeLa cells were untreated or infected with POR3 in the absence (POR3) or presence (POR3 + Wortmannin) of 10 μM wortmannin for 2h. Cells were visualized using confocal microscopy. (Scale bar = 10 μm.) (B) GFP-LC3 HeLa cells were uninfected (M, lanes 1 and 4), infected with *V. parahaemolyticus* POR3 (3, lanes 2 and 5), or starved with protease inhibitors (S, lanes 3 and 6) in the absence (lanes 1–3) or presence (lanes 4–6) of 10 μM wortmannin for 2 h. Samples were immunoblotted with anti-GFP and anti-β-actin antibodies. (C) Relative LC3-II accumulation was determined as described in Materials and Methods. The data are the means ± SD from five independent experiments. *, $P < 0.05$; **, $P < 0.01$; ns, not significant by two-way ANOVA, Bonferroni posttest.

However, we observed that treatment with this PI3 kinase inhibitor did not rescue infected cells from death, as measured by LDH release assay over the course of infection (Figure 15). We hypothesize that this is due to the activities of type III secreted effectors involved in the disruption of other signaling pathways during infection that lead to cell death. For example, effectors that directly cause cell rounding and lysis may not be susceptible to this chemical inhibitor (Figure 14A and 15).

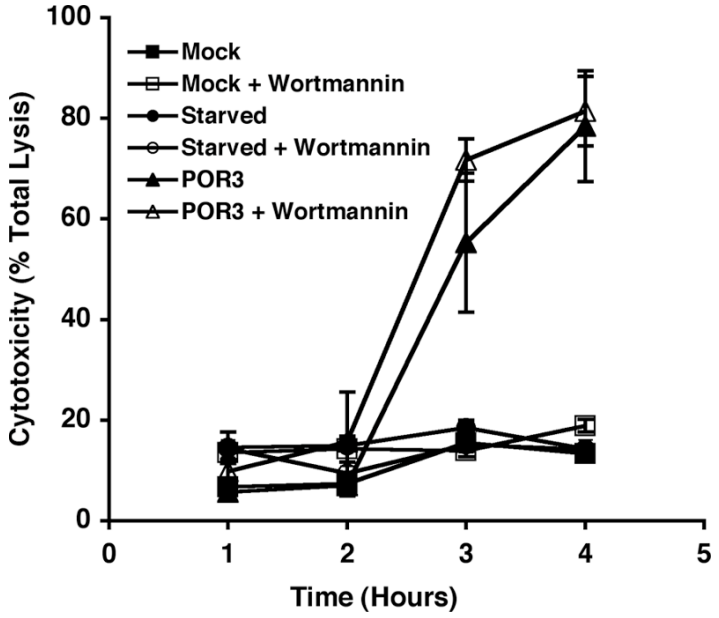

Figure 15. Autophagy inhibition does not prevent POR3-induced cytotoxicity.
Cytotoxicity of uninfected (squares), starved (circles), or POR3-infected (triangles) HeLa cells in the absence (closed symbols) or presence of 10 μM wortmannin (open symbols) was measured over time by LDH release assay. Cytotoxicity was calculated as a percent of total lysis of cells that were lysed in Triton X-100.

DISCUSSION

Pathogens use a wide variety of mechanisms to exploit a host cell during infection. In these studies, we have shown that an extracellular pathogen orchestrates a series of events via a T3SS that culminate in the efficient demise of a host cell. Upon infection, we observed T3SS1-mediated activation of autophagy, both microscopically and biochemically. We then observed a dramatic rounding of the host cell, most likely caused by changes in the cytoskeleton of the infected cell. These events are culminated by the lysis of the host cell two to three hours after infection.

Previously, *V. parahaemolyticus* was reported to kill infected cells by inducing apoptosis (71). Ono and colleagues observed positive Annexin V staining and DNA fragmentation, common markers of apoptosis, in *V. parahaemolyticus*-infected cells after three hours of infection and concluded that cells were dying due to apoptosis. However, using the same strains and conditions, we observed cell lysis via LDH release between two and three hours post-infection. In contrast to this, we observed no LDH release during the activation of apoptosis caused by *Y. pseudotuberculosis* infection or treatment with staurosporine. The cell permeability that occurs during T3SS1-mediated infection could allow Annexin V to access and stain internal phosphatidylserine, thus labeling nonapoptotic cells as apoptotic, which could suggest a possible misinterpretation of results in previous experiments. Consistent with the hypothesis that these infected cells are not dying by apoptosis, we did not observe

activation of caspases or cleavage of the caspase substrate PARP, common markers of apoptosis, during *V. parahaemolyticus* infection.

Rather than induction of apoptosis, we observed the rapid activation of the autophagy pathway. Using common microscopic methods to monitor the induction of autophagy, we observed the incorporation of GFP-LC3 into autophagosomes within one hour of POR3 infection. Consistent with this, our biochemical studies confirm that within two hours of infection with POR3, we observe conversion of LC3-I to LC3-II that occurs upon association of LC3 with the membranes of newly forming phagosomes. These events are specifically mediated by T3SS1, as infection with a strain of *V. parahaemolyticus* lacking a functional T3SS1 (POR2) does not induce the conversion of LC3-I to LC3-II. These results indicate that T3SS1-induced autophagy is robust and rapid when compared to the slower time-course of autophagy activation in our positive control (starved cells).

We investigated the possibility that the induction of autophagy during infection contributed to the lysis of cells that was observed two to three hours after infection. Inhibition of autophagy with the PI3 kinase inhibitor wortmannin prevented the formation of GFP-LC3 punctae and conversion of LC3-I to LC3-II during POR3 infection. However, we observed no change in LDH release in the presence of wortmannin, indicating that the induction of autophagy and the lysis of cells were regulated separately. Our studies reveal an interesting paradigm wherein an extracellular pathogen induces a series of separate but parallel events

during infection, including the rapid induction of autophagy, rounding and detachment of the host cell, and release of cellular contents. While each of these events may be sufficient to cause cytotoxicity on its own, redundant mechanisms such as these ensure the efficacy of infection. This could explain why cytotoxicity still occurred in cells in which autophagy was inhibited during infection. It is likely that the repertoire of T3SS1 effectors coordinately mediated each of these events. Defining the events that occur during *V. parahaemolyticus* infection have provided a starting point for exploring the various molecular targets of T3SS1 effectors, which may provide further insight into this multifaceted host cell death.

CHAPTER FOUR
AMPylation of Rho GTPases by the T3SS1 effector, VopS

INTRODUCTION

T3SS1 of *V. parahaemolyticus* is homologous to the T3SS of *Yersinia* spp., except for a group of hypothetical genes that are not found in *Yersinia* (77) (Figure 3). This region of genes is predicted to encode type III effector proteins based on their association with chaperones (75). One of these effectors, VopS, is predicted to be a 387 amino acid protein with no homology to any proteins of known function. A Fic domain is located at its C-terminus. While the function of this domain is unclear, the Fic domain is genetically correlated with the regulation of cell division in *E. coli* (50, 90). Fic domains are identified by a conserved motif, HPFX(D/E)GNGR.

A previous study implicated VopS in the inhibition of the NFκB pathway (12). This study showed that the N-terminus of VopS binds to the p65 subunit of NFκB through yeast two-hybrid interaction. Furthermore, NFκB, a transcription factor, no longer binds to its cognate promoter in the presence of nuclear extracts from cells infected with wild-type *V. parahaemolyticus*. Deletion of *vopS* from this strain restores NFκB promoter binding. The authors speculate that inhibition of the NFκB pathway at this step will prevent activation of pro-survival genes during infection, thus leading to the induction of T3SS1-induced apoptosis in target cells.

In a later study, Casselli and colleagues connected VopS with the inhibition of Rho GTPases that occurred during infection with *V. parahaemolyticus (19)*. The authors genetically correlated the presence of VopS in a *V. parahaemolyticus* strain with the inhibition of Rho GTPases, as a *vopS* mutant strain no longer prevented activation of Rho, Rac, or Cdc42 during infection. However, no target or mechanism of inhibition by VopS was revealed by these studies.

It was interesting to speculate that VopS was involved in the manipulation of Rho GTPases. This pathway is a common target of bacterial pathogens because of its importance during infection. For instance, the exoenzyme C3 from *Clostridium botulinum* directly modifies Rho by ADP-ribosylation, thereby preventing the GTPase from binding to its downstream effectors (3). *Yersinia* spp. prevent internalization during infection using the T3SS effector, YopE. This effector exhibits unregulated GAP activity towards Rho, Rac, and Cdc42, keeping Rho GTPases in the inactive GDP bound state (93). Lastly, the *Yersinia* effector YpkA contains a domain that mimics GDI activity and prevents nucleotide exchange in Rac and Rho. Alternatively, the *Salmonella* T3SS effector SopE activates Rho GTPases by exhibiting GEF activity, hijacking the actin cytoskeleton to promote uptake of this intracellular bacteria (39). These bacterial pathogens provide many examples of how VopS could inhibit Rho GTPases: by a direct inhibitory modification of Rho GTPases, by mimicking eukaryotic GAP activity, or by acting as a GDI.

Though studies have associated VopS with various activities during infection, the molecular mechanism of this effector remained unknown. Herein, we elucidate the activity of the T3SS1 effector VopS by molecular and biochemical means. First, we observe that VopS is necessary for the efficient killing of host cells during infection and sufficient to cause cytotoxicity on its own. Next, we demonstrate that the Fic domain is critical for the cytotoxic activity displayed by this protein. Lastly, we show that VopS inhibits Rho GTPase signaling by AMPylation of Rho, Rac, and Cdc42, preventing their interaction with downstream effectors. These observations reveal a unique activity for VopS, which targets a pathway that is critical in the response to *V. parahaemolyticus* infection. In addition, they provide insight into a novel post-translational modification that may expand our knowledge of eukaryotic cell signaling.

RESULTS

The N-terminus of VopS is required for chaperone binding.

The T3SS effector VopS is secreted specifically from T3SS1 of *V. parahaemolyticus* (71). Our lab initially identified VopS and other T3SS1 effectors by their association with a chaperone. Chaperones most often bind to the first 100 amino acids of a type III secreted effector (34). We decided to test the ability of various constructs of VopS to bind to its chaperone, VP1687, by

yeast two-hybrid analysis. The interaction of the *Yersinia* effector YopJ with its substrate MEKK was used as a positive control and yeast transformed with lamin and empty vector served as a negative control. While yeast transformed with plasmids containing VopS or various mutants and VP1687 are able to grow on media lacking leucine and tryptophan (-LW), only yeast transformed with wild-type VopS, VopSΔFic, or VopS-H348A and VP1687 are able to grow on media lacking histidine (-WHULK), which indicates a positive interaction by yeast two-hybrid analysis (Figure 16). The results show that the N-terminus of VopS is required for binding for its chaperone, as a VopS construct consisting of only the C-terminal Fic domain is unable to interact with VP1687.

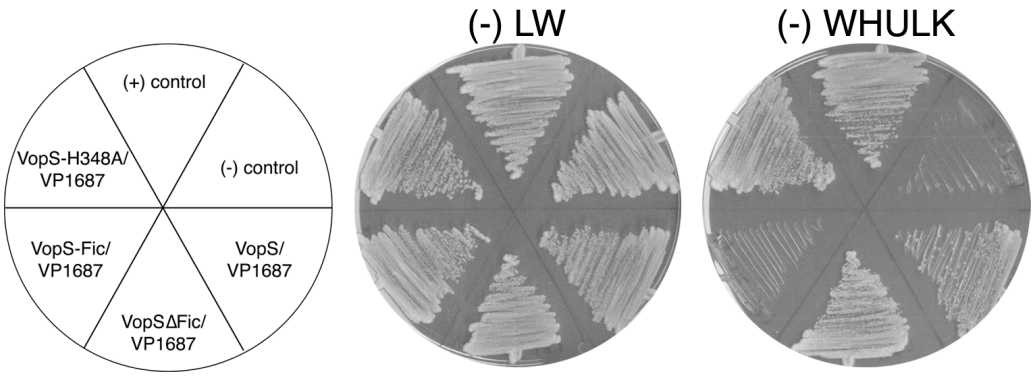

Figure 16. Interaction of VopS with its chaperone, VP1687.
Yeast were cotransformed with pLexAde-VopS or various mutants and pVP16-VP1687 and transformants were grown on media lacking leucine and tryptophan (-LW). Positive interactions by yeast two-hybrid analysis are indicated by the ability of the yeast to grow on media lacking histidine (-WHULK). A known interaction between YopJ and MEKK was used as a positive control while yeast transformed with pLexAde-Lamin and pVP16 empty vector was used as a negative control.

VopS is necessary for efficient killing of host cells.

Infection of HeLa cells with the *V. parahaemolyticus* POR3 strain, which contains a functional T3SS1 and inactivating mutations for both TDHs and T3SS2 results in cell rounding by 2 h after infection and cells that are completely rounded and dying after 3 h (Figure 17A). However, cell rounding is delayed upon infection with a POR3Δ*vopS* strain and does not occur until 3 h post-infection, at which point the cells are rounded and coming off of the plate (Figure 17A). We speculate that the eventual rounding is due to the activities of at least one other type III effector from T3SS1. The *vopS* knockout was complemented by expression of *vopS* under the control of its endogenous promoter on the pLafR plasmid. Complementation was confirmed by in vitro secretion assays with the POR3, POR3Δ*vopS*, and POR3Δ*vopS* + VopS strains (Figure 17B). As expected, infection with the complemented strain restores cell rounding after two hours of infection (Figure 17A).

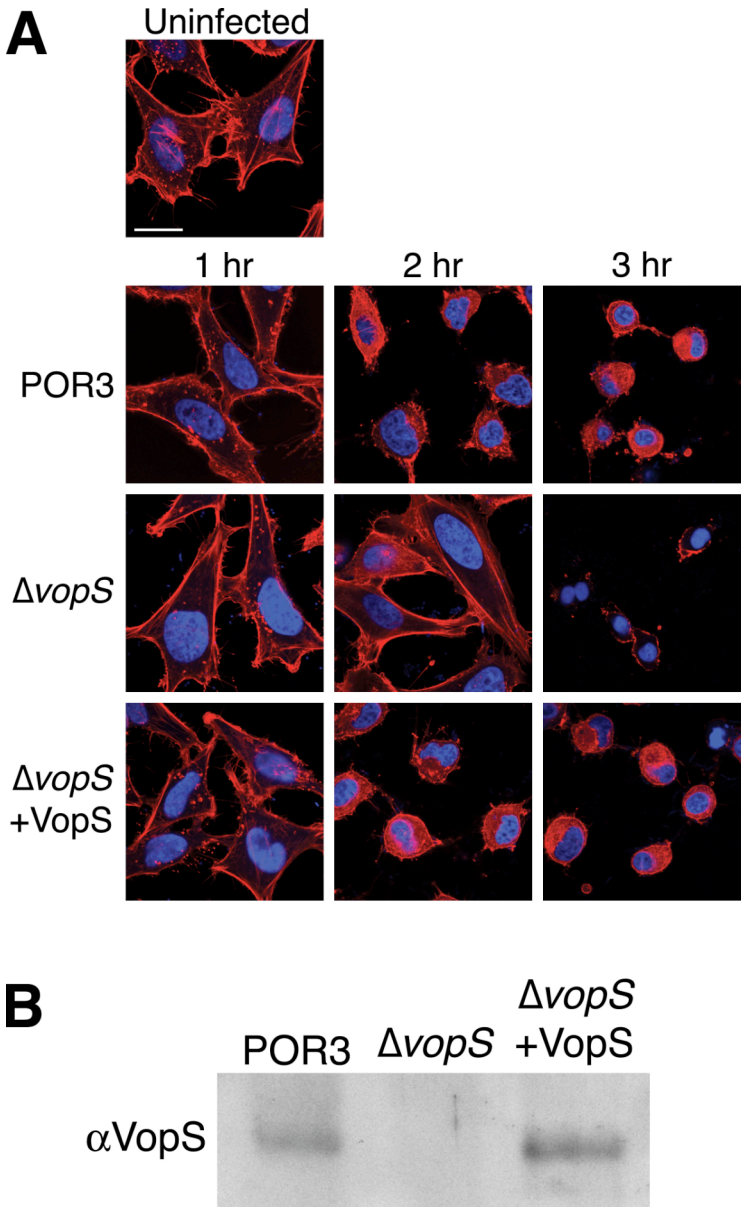

Figure 17. VopS contributes to cell rounding during infection.
(A) HeLa cells infected with POR3, POR3Δ*vopS* (Δ*vopS*), and POR3Δ*vopS*+VopS (Δ*vopS*+VopS) were analyzed over a time course of infection. Cells were stained with Hoechst to visualize nuclei (blue) and rhodamine-phalloidin to visualize the actin cytoskeleton (red). Scale bar represents 10µm. (B) In vitro secretion assay of POR3, POR3Δ*vopS* (Δ*vopS*), and POR3Δ*vopS*+VopS (Δ*vopS*+VopS) strains. Bacteria were induced for type III secretion and cell culture supernatants were collected. Proteins were TCA precipitated, separated by SDS-PAGE and immunoblotted with an antibody to VopS.

VopS is sufficient to cause cytotoxicity

T3SS1 is predicted to harbor several effector proteins. For this reason, attributing an activity to VopS during infection can be challenging. To dissect the function of VopS from other T3SS1 effectors, we transfected HeLa cells with a mammalian expression vector, pcDNA3, encoding a wild-type or one of several mutant versions of VopS and observed cells by confocal microscopy. Expression of full-length VopS induced a severely rounded phenotype in transfected HeLa cells when compared to the vector transfected control (Figure 18A). We mutated several residues in VopS that are conserved among Fic domains to an alanine and tested the activity of these mutants in transfection. Transfection of VopS-H287A or VopS-R356A caused rounding of HeLa cells similar to wild-type VopS (Figure 18A). However, mutation of the conserved histidine in the Fic motif to an alanine (VopS-H348A) completely abrogated the VopS-mediated cell rounding, indicating that this residue is critical for the activity of this effector (Figure 18A).

Type III secreted effector proteins often contain a secretion signal sequence that is located within the first 15 amino acids of the N-terminus (85). We sought to determine whether this signal sequence was required for the activity of VopS. We observed that transfection of VopSΔ30, a mutant deleted for the putative signal sequence, caused rounding of HeLa cells similar to full-length VopS (Figure 18B). As expected, mutation of the conserved Fic motif histidine in this construct (VopSΔ30-H348A) abrogated the actin disruption observed with VopSΔ30 (Figure 18B). Thus, VopS is sufficient to cause cell rounding and

cytotoxicity. This activity is independent of its signal sequence but requires a wild-type Fic domain. Additionally, these results indicate that VopS is cytotoxic to transfected HeLa cells in the absence of stimulation of the NFκB pathway, suggesting that it has targets other than p65 as previously proposed.

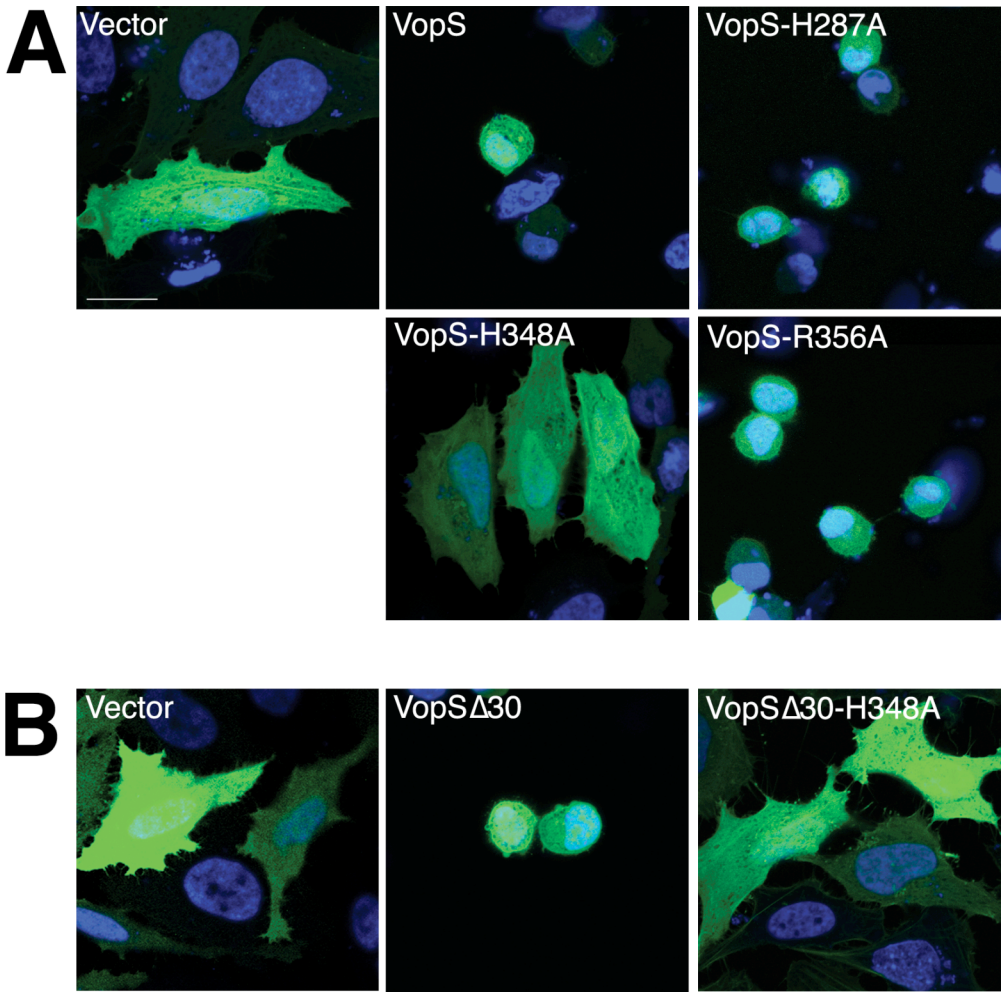

Figure 18. Transfection of VopS causes cell rounding and cytotoxicity.
(A) HeLa cells were transfected with pSFFV-eGFP and pcDNA3 empty vector, pcDNA3-VopS or VopS point mutants. (B) Transfection of HeLas with empty vector or pcDNA3-VopSΔ30 or pcDNA3-VopSΔ30-H348A. Cells were visualized with confocal microscopy for green fluorescent protein (green) to identify transfected cells and Hoechst stain to identify nuclei (blue). Scale bar represents 10 μm.

VopS targets an evolutionarily conserved pathway

Type III secreted effector proteins often target evolutionarily conserved mechanisms (97). To investigate whether VopS is targeting such a pathway, we expressed wild-type VopS or the VopS-H348A mutant under a galactose-inducible promoter in yeast. Initially, yeast cells harboring empty vector, VopS, or VopS-H348A on a plasmid were plated onto glucose, and each of these strains were able to grow on glucose-containing plates (Figure 19A). When yeast were plated onto galactose-containing media, thereby inducing expression of VopS, cells are no longer able to grow (Figure 19B). As expected, yeast expressing empty vector or VopS-H348A are able to grow on galactose media (Figure 19B). To test if VopS is just causing a growth arrest or actually eliciting cytotoxicity in yeast, we replated yeast from the most heavily streaked areas of the galactose plates onto media containing glucose to shut off expression of VopS. Under this condition, we showed that yeast expressing VopS are unable to recover and grow, indicating that VopS is killing yeast (Figure 19C). These observations indicate that VopS is targeting a pathway that is evolutionarily conserved between yeast and mammals. Furthermore, it is interesting to note that there is no homologue for p65 in yeast, supporting the hypothesis that VopS is targeting something besides the NFκB pathway.

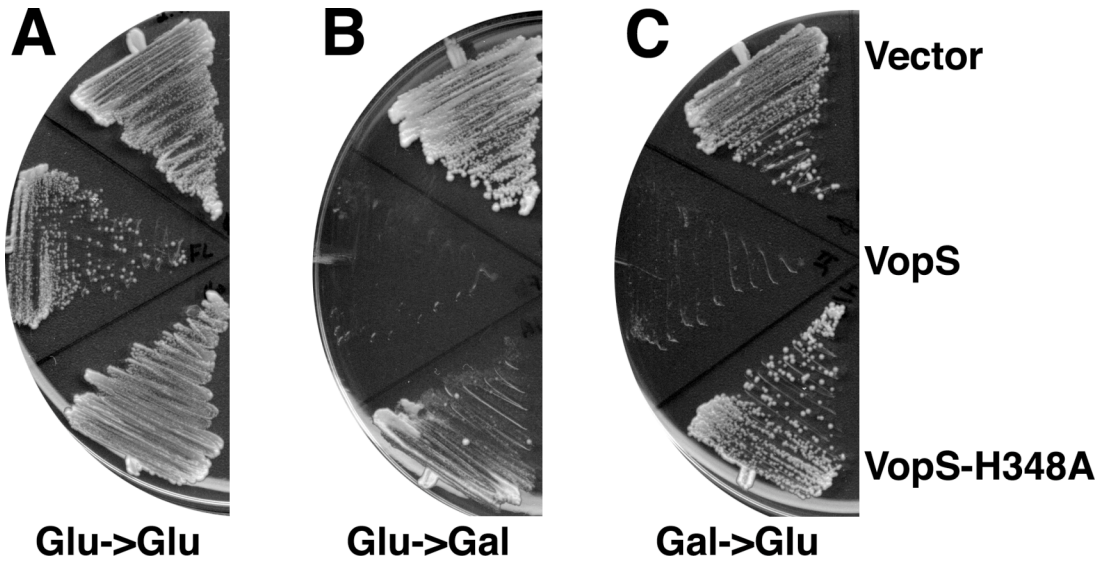

Figure 19. Expression of VopS is cytotoxic to yeast.
(A) A yeast expression plasmid, pRS413, was used to express VopS under a galactose-inducible promoter. Yeast were transformed with vector alone, pRS13-VopS, or pRS413-VopS-H348A and grown on media containing glucose. (B) Colonies were streaked onto galactose-containing media to induce expression of VopS or VopS-H348A. (C) After being plated onto galactose, yeast were picked from the most heavily streaked area and replated onto glucose media.

VopS inhibits Rho GTPase activation

One clue into the activity of VopS comes from evidence that Rho GTPase signaling is inhibited during *V. parahaemolyticus* infection (19). Casselli and colleagues found that Rho GTPases were inactivated after 1 h of infection with *V. parahaemolyticus*, and this activity was correlated with the presence or absence in VopS in the infecting strain. To support and extend their findings, we looked at the activation state of Cdc42 during infection with several strains of *V. parahaemolyticus*. For this experiment, we infected HeLa cells with the POR3,

POR3Δ*vopS*, or POR3Δ*vopS* + VopS strains over a 4 h time course. At each time point, the presence of active GTP-bound Cdc42 was assessed by the ability of Cdc42 to interact with a glutathione S-transferase (GST) fusion of the binding domain of its downstream effector, p21-activated kinase 3 (GST-PAK-PBD). After 1 h of infection of HeLa cells with the POR3 strain, we observed the presence of active Cdc42 (Figure 20, lane 2). Beyond 1 h of infection, the presence of VopS in the POR3 strain was consistent with inactivation of Cdc42, as the population of active GTP-bound Cdc42 was no longer observed (Figure 20, lanes 3-5). In cells infected with a VopS deletion strain (POR3Δ*vopS*), levels of Cdc42 in the active GTP-bound state persisted, but all Cdc42 was eventually inactivated by 4 h, suggesting the presence of another factor contributing to the destabilization of Rho GTPases (Figure 20, lanes 6-9). Reconstitution of the POR3Δ*vopS* strain with wild-type VopS (POR3Δ*vopS* + VopS) restored the loss of active Cdc42 one hour after infection, similar to the POR3 strain (Figure 20, lanes 10-13). During infection with all three strains, the total level of Cdc42 was reduced at later time points of infection, likely due to the lysis of cells that occurs within three hours of infection.

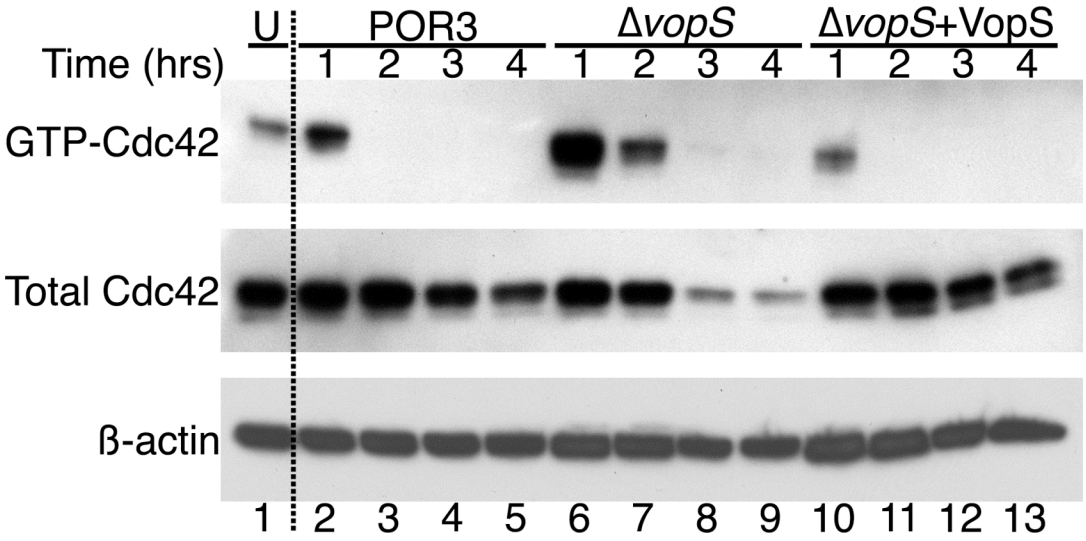

Figure 20. Rho GTPase inhibition is delayed in cells infected with POR3Δ*vopS*.

HeLa cells were left uninfected (U) or infected with POR3, POR3Δ*vopS* (Δ*vopS*), or POR3Δ*vopS*+VopS (Δ*vopS*+VopS) for 4 hours. At each time point, cells were assayed for active GTP-bound Cdc42 by means of GST-PAK PBD pulldown assays followed by immunoblot analysis with antibodies to Cdc42. Western blot for ß-actin was used as a loading control.

VopS binds to active GTP-bound Rac

To begin to understand how VopS inhibits Rho GTPase signaling, we tested whether VopS could interact with Rho GTPases. For this experiment, we produced recombinant GST-tagged VopSΔ30 and VopSΔ30-H348A that lacks the largely hydrophobic secretion signal sequence and tested the ability of each to bind ^{35}S-radiolabeled Rac (^{35}S-Rac) using GST pulldown assays. Although ^{35}S-Rac did not interact with GST-VopSΔ30, it did interact with GST-VopSΔ30-H348A (Figure 21, lanes 4 and 5). In addition, GTP loading of the ^{35}S-Rac increased the amount of ^{35}S-Rac that interacted with recombinant VopSΔ30-H348A (Figure 21, lane 9). This is reminiscent of the conformation-dependent interaction of GTP-bound Rac with its downstream effector p21-activated kinase (PAK) (13). As expected, upon loading of ^{35}S-Rac with GTP, more ^{35}S-Rac interacted with GST-PAK PBD (Figure 21, compare lanes 3 and 7). Many type III effectors use a catalytic mechanism to alter eukaryotic signaling pathways, and in some cases the catalytically inactive form of the effector can act as a substrate trap (1). These results indicate that the VopSΔ30-H348A mutant might act as a trap by binding its substrate, the active GTP-bound Rac, but failing to release a product.

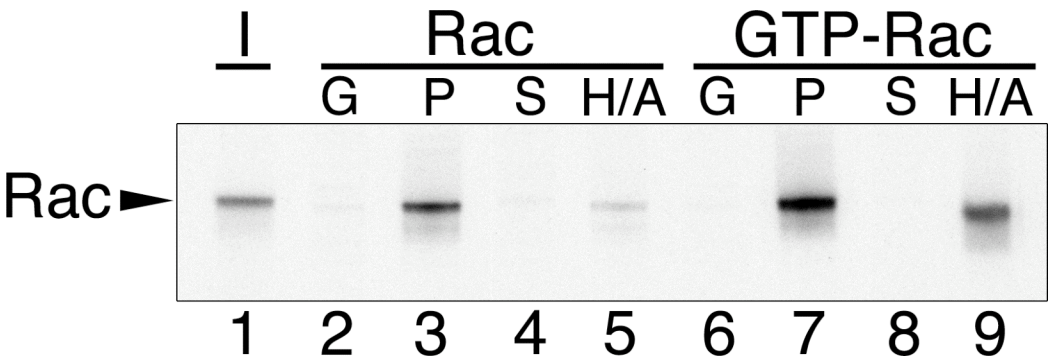

Figure 21. VopS interacts with the Rho GTPase Rac.
GST pulldown of in vitro translated ^{35}S-Rac and GTP-γ-S–loaded ^{35}S-Rac with GST (G), GST-PAK PBD (P), GST-VopSΔ30 (S), or GST-VopSΔ30-H348A (H/A). Samples were separated by SDS-polyacrylamide gel electrophoresis (SDS-PAGE) and analyzed by autoradiography. Input (I) corresponds to 5% of material in pulldown.

VopS inhibits in vitro binding of Rac to its downstream effector, PAK

To further analyze the possibility that GTP-bound Rho GTPases might be substrates for VopS, we produced the ^{35}S-radiolabeled constitutively active form of Rac (^{35}S-DA-Rac). We pre-incubated ^{35}S-DA-Rac with 25 pmol of purified recombinant VopSΔ30 or VopSΔ30-H348A and then tested whether exposure to VopS would abolish the ability of ^{35}S-DA-Rac to interact with its downstream effector, GST-PAK PBD. Surprisingly, ^{35}S-DA-Rac that was pre-incubated with VopSΔ30 was unable to interact with GST-PAK PBD, while ^{35}S-DA-Rac pre-incubated with the mutant VopSΔ30-H348A retained the ability to bind to GST-PAK PBD (Figure 22A), indicating that VopS directly targets Rho GTPases in such a way as to prevent binding to downstream signaling partners.

To test if VopS was utilizing an enzymatic activity, we pre-incubated ^{35}S-DA-Rac with serial 10-fold dilutions of purified recombinant VopSΔ30 (125 to 0.125 pmol) for 15 min and tested whether ^{35}S-DA-Rac could bind to GST-PAK PBD (Figure 22B). Pre-incubation of ^{35}S-DA-Rac with as little as 1.25 pmol of VopSΔ30 prevented the binding of ^{35}S-DA-Rac to GST-PAK PBD (Figure 22B). As expected, the incubation of ^{35}S-DA-Rac with decreasing amounts of VopSΔ30-H348A had no effect on the ability of DA-Rac to bind to GST-PAK PBD (Figure 22B). Next, we pre-incubated ^{35}S-DA-Rac with a limiting amount of VopSΔ30 (0.25 pmol) over the course of one hour. By forty minutes, ^{35}S-DA-Rac no longer interacted with GST-PAK PBD (Figure 22C). Based on the concentration and time dependence of this activity, we hypothesize that VopS uses an enzymatic activity to inhibit the interaction of Rho GTPases with their respective downstream signaling partners.

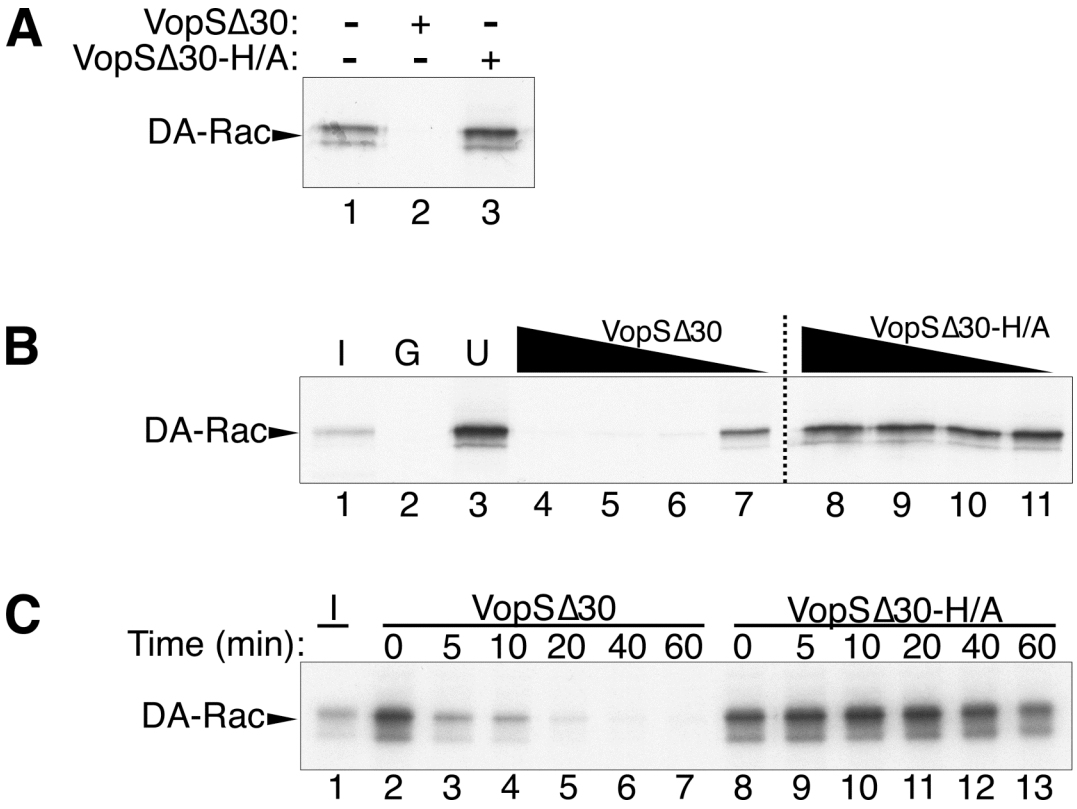

Figure 22. VopS inhibits in vitro binding of the Rho GTPase Rac to its downstream effector PAK.
(A) In vitro translated ^{35}S-DA-Rac was pre-incubated with VopSΔ30 or VopSΔ30-H348A for 15 minutes, followed by a GST pulldown with GST-PAK PBD. (B) In vitro translated ^{35}S-DA-Rac was pre-incubated with decreasing concentrations of VopSΔ30 or VopSΔ30-H348A (125 to 0.125 pmol) for 15 minutes or left untreated (U), followed by a GST pulldown with GST-PAK PBD or GST alone (G). (C) In vitro translated ^{35}S-DA-Rac was pre-incubated over time with 0.25 pmol of VopSΔ30 or VopSΔ30-H348A, followed by a pulldown assay with GST-PAK PBD. Samples were separated by SDS-PAGE and analyzed by autoradiography. Inputs (I) correspond to 5% of material in pulldown.

VopS directly modifies Rho GTPases with adenosine 5'-monophosphate

So far, our results indicate that the interaction of VopS with Rho GTPases prevents them from binding to their downstream effectors. Additionally, we hypothesized that the inhibitory activity VopS exerts on Rho GTPases is catalytic, rather than stoichiometric, suggesting that VopS directly modifies Rho GTPases. In order to test this, we used a bacterial expression system in which His-tagged DA-Rac was expressed alone (DA-Rac) or in the presence of GST-tagged VopSΔ30 (DA-Rac/VopS). His-DA-Rac from both of these conditions was purified by nickel affinity chromatography and run on an SDS-PAGE to check for protein expression (Figure 23A). We observed no difference in the mobility of His-DA Rac that had been expressed alone or in the presence of GST-VopSΔ30.

To further assess whether DA-Rac was altered by co-expression with VopS, we measured the mass of recombinant DA-Rac and DA-Rac/VopS by mass spectrometry. Total mass spectrometry analysis revealed that, although DA-Rac had the expected molecular weight, DA-Rac/VopS had an increase in molecular weight of 329 daltons (Figure 23, compare B and C). As expected, DA-Rac co-expressed with the mutant VopS did not show an increase in molecular weight (data not shown). The increase of 329 daltons is consistent with the mass of adenosine 5'-monophosphate (AMP), indicating that VopS modified Rho GTPases by the addition of a single AMP molecule.

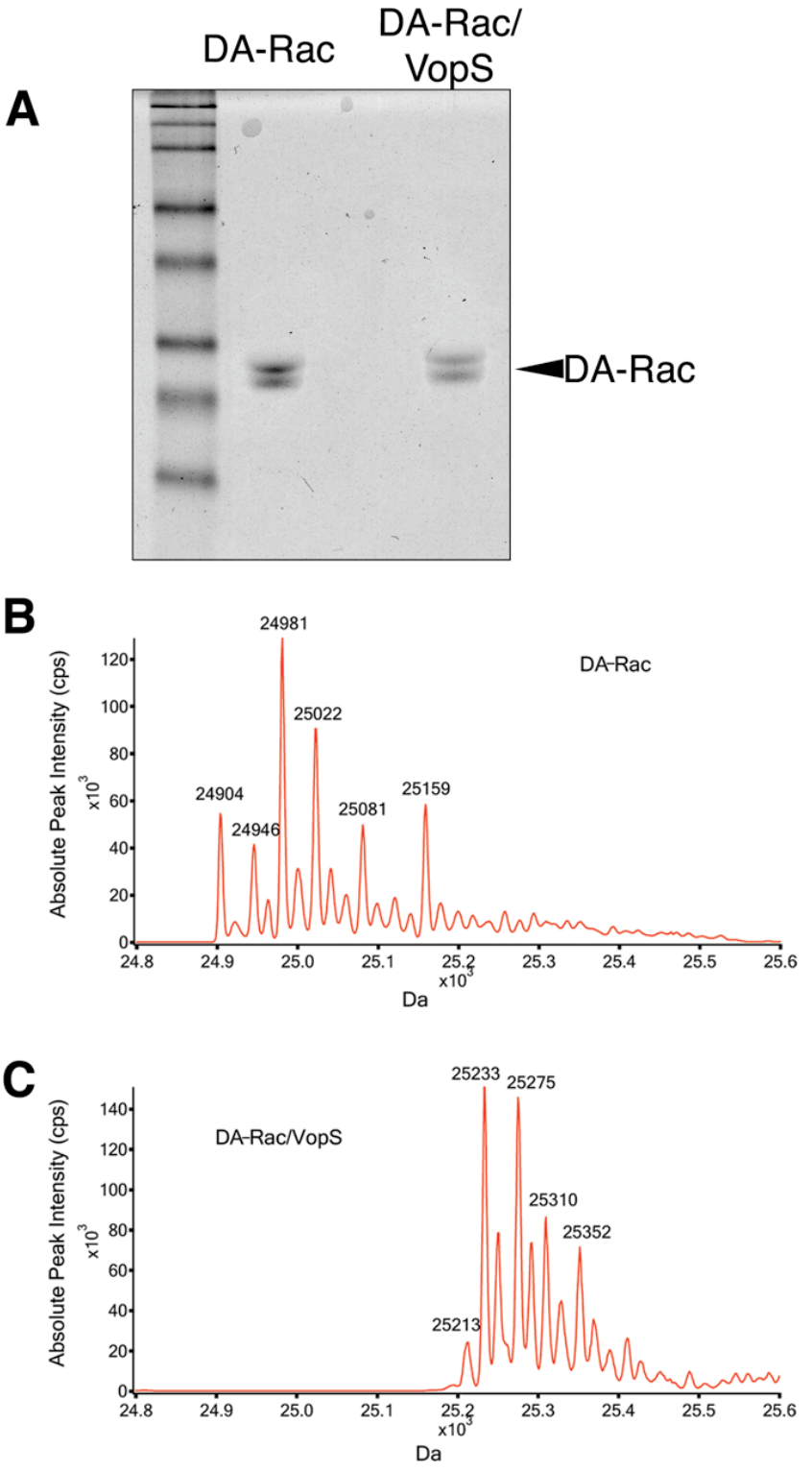
A
DA-Rac
DA-Rac/
VopS
DA-Rac
B
DA-Rac
Absolute Peak Intensity (cps)
x10^3
24981
25022
24904
24946
25081
25159
Da
x10^3
C
DA-Rac/VopS
Absolute Peak Intensity (cps)
x10^3
25233
25275
25310
25352
25213
Da
x10^3

Figure 23. DA-Rac co-expressed with VopS has mass increase of 329 daltons. (A) DA-Rac was expressed in the presence or absence of GST-VopSΔ30. His-DA-Rac was purified by nickel affinity chromatography. Purified protein samples were separated by SDS-PAGE and Coomassie stained to visualize protein. (B) Major peaks found for DA-Rac, 24904, 24946, 24981, 25022 Da, respectively (with ± 2 Da instrumentation error). **(C)** Major peaks found for DA-Rac/VopS, 25233, 25275, 25310, and 25352 Da, have a 329 Da mass increase when compared to major peaks found for DA-Rac.

Rho GTPases are modified on threonine 35 in the switch I region

To identify where this putative covalent modification occurred on Rac, we analyzed tryptic and AspN peptides using liquid chromatography followed by tandem mass spectrometry (LC-MS/MS). When the samples were digested with AspN, peptide A [amino acids 11 to 37, mass-to-charge ratio (m/z) = 1488.7 when z = 2] was observed for DA-Rac (Figure 24A). For DA-Rac/VopS, only the modified form of peptide A was observed [amino acids 11 to 37, with a mass increase of 329.1 daltons, m/z = 1653.3 when z = 2], indicating that all of the DA-Rac coexpressed with VopS was modified with AMP (Figure 24B). Further analysis indicated that Peptide A contained a covalent modification of 329 daltons on threonine 35 (Figure 24C), a highly conserved residue located in the effector loop of the switch I region of Rho GTPases (1, 38) (Figure 24D). Thus, VopS modifies the Rho GTPases with AMP, which prevents Rho GTPases from binding to downstream signaling partners by steric hindrance.

The switch I region of Rho GTPases plays a role in GTP, Mg^{2+}, and effector binding (38). To confirm that VopS was not inhibiting Rho GTPases by

preventing their activation, we looked at the ability of DA-Rac to bind GTP. For this experiment, DA-Rac and DA-Rac/VopS were loaded with ^{35}S-radiolabeled GTP-γ-S, a nonhydrolyzable form of GTP. The amount of GTP loaded was then measured by filter binding assay. Both forms of recombinant DA-Rac retained the ability to be loaded with GTP, eliminating the possibility that VopS modifies the Rho family of proteins to prevent GTP binding (Figure 24E). Thus, we hypothesize that VopS modifies Rho GTPases with AMP, which prevents their interaction with downstream signaling partners through steric hindrance.

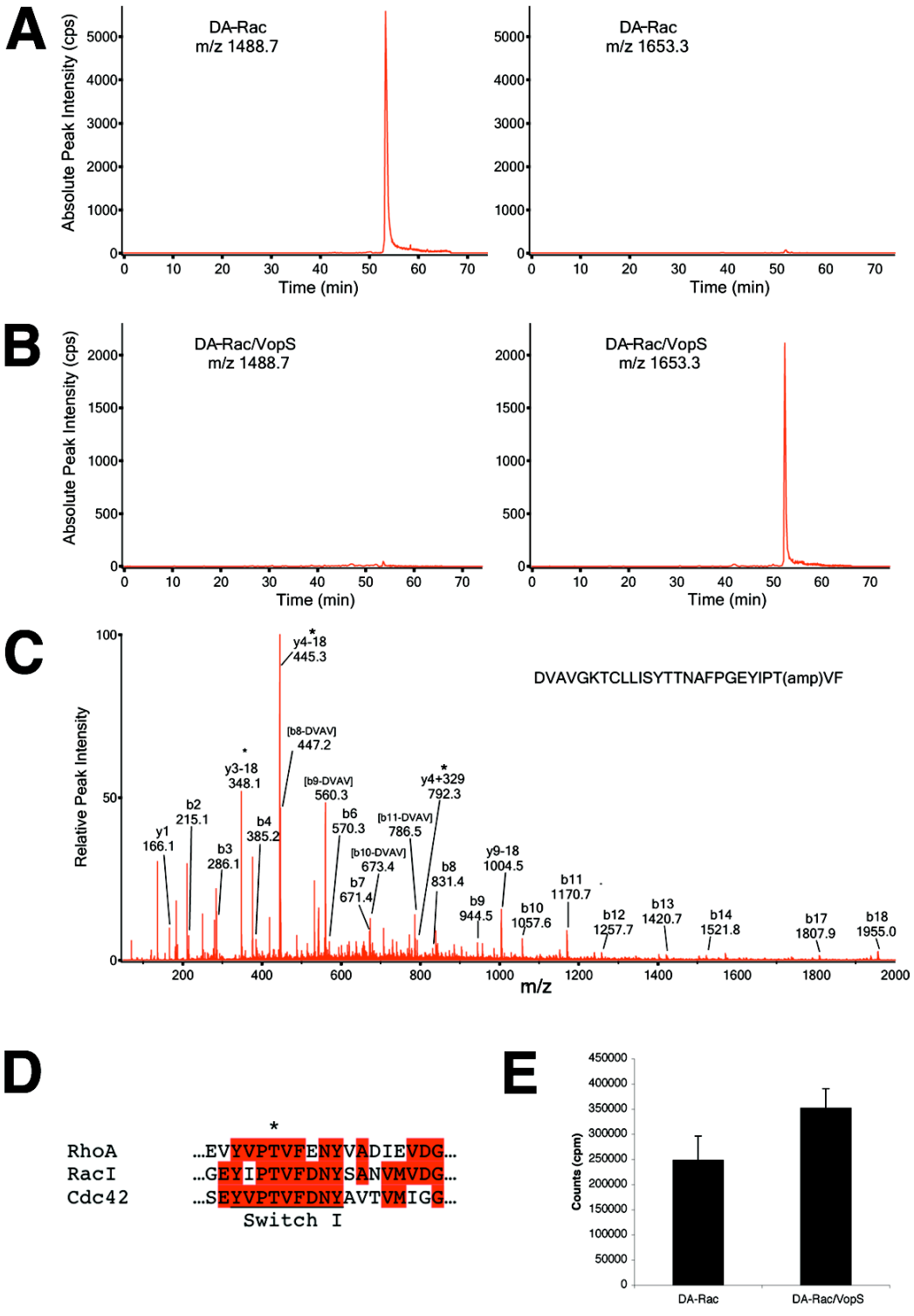
A
DA-Rac
m/z 1488.7
DA-Rac
m/z 1653.3
Absolute Peak Intensity (cps)
Time (min)
B
DA-Rac/VopS
m/z 1488.7
DA-Rac/VopS
m/z 1653.3
C
DVAVGKTCLLISYTTNAFPGEYIPT(amp)VF
Relative Peak Intensity
m/z
y4-18
445.3
[b8-DVAV]
447.2
y3-18
348.1
[b9-DVAV]
560.3
y4+329
792.3
b6
570.3
[b11-DVAV]
786.5
b2
215.1
y1
166.1
b4
385.2
b3
286.1
[b10-DVAV]
673.4
b7
671.4
b8
831.4
y9-18
1004.5
b11
1170.7
b9
944.5
b10
1057.6
b12
1257.7
b13
1420.7
b14
1521.8
b17
1807.9
b18
1955.0
D
RhoA …EVYVPTVFENYVADIEVDG…
RacI …GEYIPTVFDNYSANVMVDG…
Cdc42 …SEYVPTVFDNYAVTVMIGG…
Switch I
E
Counts (cpm)
DA-Rac
DA-Rac/VopS

Figure 24. DA-Rac/VopS is covalently modified on threonine 35.
A and B) Extracted ion chromatogram (XIC) of the wild-type peptide A (m/z = 1488.7) and the modified peptide A (m/z = 1653.3) for DA-Rac (A) and DA-Rac/VopS (B). The XIC indicates the intensity of the ion as a function of time during the LC-MS/MS process. (C) Electrospray ionization MS/MS spectra of modified peptide A. The b and y ions are marked on the MS/MS spectra. Ions corresponding to products of internal fragmentation are marked in brackets. Compared to the MS/MS of the wild-type peptide A (data not shown), two forms of mass shift were detected, either with a mass decrease of 18 daltons or with a mass increase of 329 daltons. Ions with a mass shift are marked with an asterisk. The mass shift started with y3, indicating that the modification site is Thr^{35}. A further cut of peptide A with AspN resulted in an ion corresponding to peptide B (amino acids 32 to 37) with a mass increase of 329 daltons, and the MS/MS spectrum of modified peptide B further confirmed that Thr^{35} is the modification site. (D) Alignment of the effector loop region corresponding to residues 32 to 50 of RhoA and 30 to 48 of RacI and Cdc42. Conserved residues are shown in red and the switch I region is underlined. The asterisk denotes the AMPylated Thr residue. (E) ^{35}S- GTPγS loading of DA-Rac and DA-Rac/VopS. Purified proteins were loaded with radiolabeled GTPγS and subjected to a filter-binding assay. Samples were done in triplicate and counts were measured for one minute per sample on a scintillation counter. The data are the means ± SD from three independent experiments.

VopS uses ATP as a substrate for modification

To test directly whether VopS functions as an enzyme to modify Rho GTPases, we developed an in vitro labeling assay using radiolabeled adenosine triphosphate (ATP). The design of this assay was similar to a kinase assay, except that ^{32}P-α-ATP rather than ^{32}P-γ-ATP is used as a substrate. Incubation of purified recombinant VopSΔ30 with recombinant DA-Rac and ^{32}P-α–labeled ATP resulted in VopS-dependent modification of DA-Rac (Figure 25, lane 2). Mutation of the modified threonine residue to alanine (DA-Rac-T35A) abolished VopSΔ30-dependent modification of DA-Rac, confirming that the AMP

modification is specific for Thr35 (Figure 25, lane3). As expected, DA-Rac incubated with VopS-H348A was not modified (Figure 25, lanes 4-6). These results indicate that VopS utilizes ATP as a substrate to modify Rho GTPases.

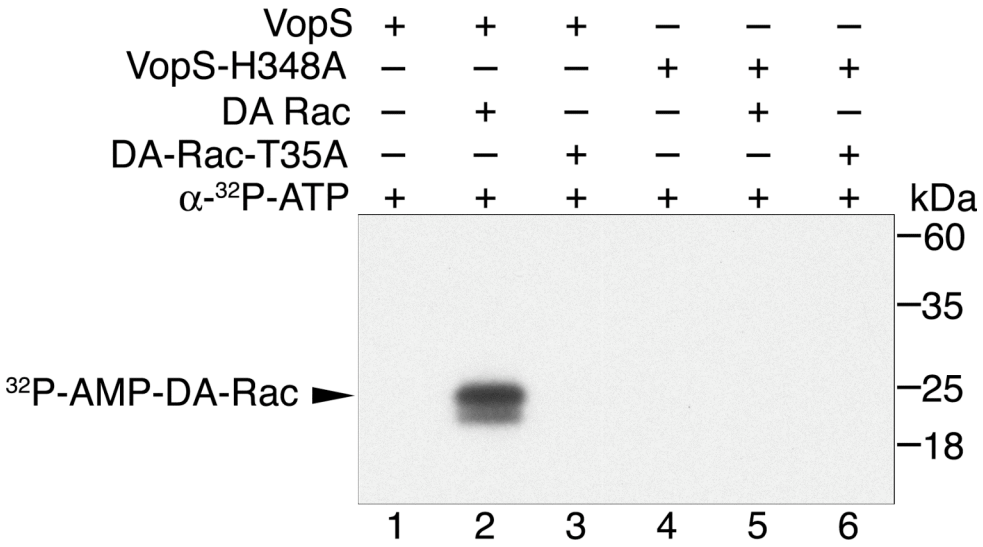

Figure 25. VopS uses ATP to directly modify DA-Rac with AMP.
In vitro assay in which recombinant VopSΔ30 or VopSΔ30-H348A were incubated with or without recombinant DA-Rac or DA-Rac-T35A in the presence of ^{32}P-α–labeled ATP. Samples were separated by SDS-PAGE and analyzed by autoradiography.

In vitro AMPylation of the Rho family of GTPases by VopS

The most well characterized members of the Rho GTPase family are Rho, Rac, and Cdc42. While these proteins are fairly similar, some differences in their structures may affect the ability of VopS to utilize each as a substrate for modification. To confirm that VopS modifies other members of the Rho GTPase family, we repeated the in vitro labeling assay using Rho, Rac, and Cdc42 as substrates. We observed no modification when Rho, Rac, and Cdc42 were incubated with ^{32}P-α-ATP alone (Figure 26, lanes 1-3). However, in the presence of VopS, all of the GTPases were modified with AMP (Figure 26, lanes 4-6). As expected, none of the GTPases were modified by VopS-H348A (Figure 26, lanes 7-9). Thus, VopS modifies Rho GTPases with AMP. We now refer to this activity as AMPylation and the enzyme as an AMPylator. VopS uses the posttranslational modification of AMPylation to block the effector binding site on the switch I region of the GTPase, thereby hindering signaling between Rho GTPases and their downstream effectors.

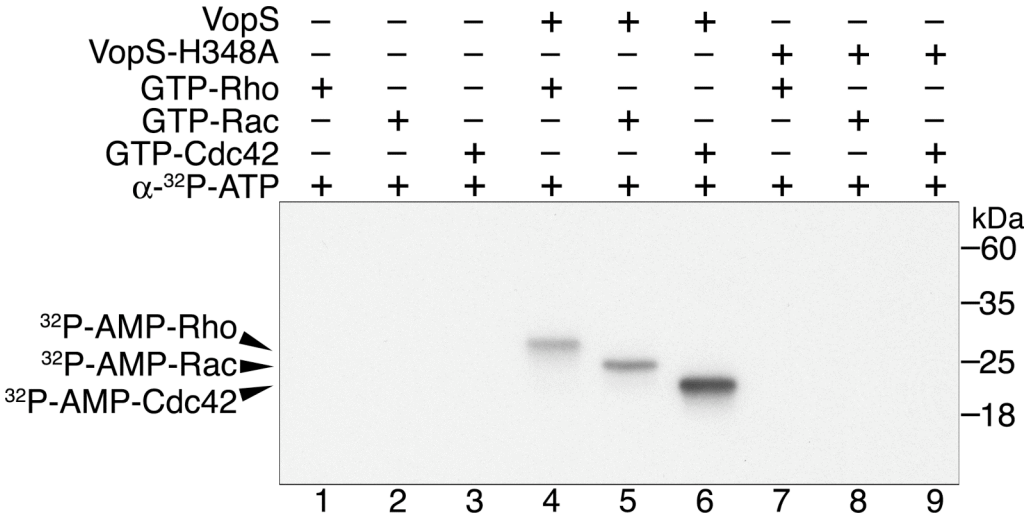

Figure 26. VopS directly modifies Rho, Rac, and Cdc42.
Recombinant VopSΔ30 or VopSΔ30-H348A was incubated with GTP-Rho, GTP-Rac, or GTP-Cdc42 in the presence of ^{32}P-α-labeled ATP. Samples were separated by SDS-PAGE and analyzed by autoradiography.

VopS specifically modifies Rho GTPases.

We tested the ability of VopS to AMPylate other members of the Ras superfamily, including Ran, Rab5a, RasV12, and Arf. Each of these proteins represents a well-characterized member of each of the subfamilies of the Ras superfamily (95). VopS modifies a threonine in the effector-binding loop of Rho GTPases. This threonine is highly conserved among Rho GTPases and other members of the Ras superfamily (Figure 27A). An in vitro AMPylation assay with VopSΔ30 using purified recombinant proteins of the Ras superfamily as substrates shows that only Rac, which was used as a positive control for AMPylation, was labeled with ^{32}P-α-AMP (Figure 27B, lane 4 and 27C, lanes 7 and 11). No other proteins, including Ran, Rab5a, RasV12, and Arf were

modified by VopSΔ30 (Figure 27B, lane 2 and 27C, lanes 2, 5, and 9). These results indicate that VopS specifically modifies the Rho GTPase subfamily of the Ras superfamily. This is likely due to the ability of VopS to recognize Rho GTPases as substrates, as much of the effector-binding domain of members of the Ras superfamily is not conserved.

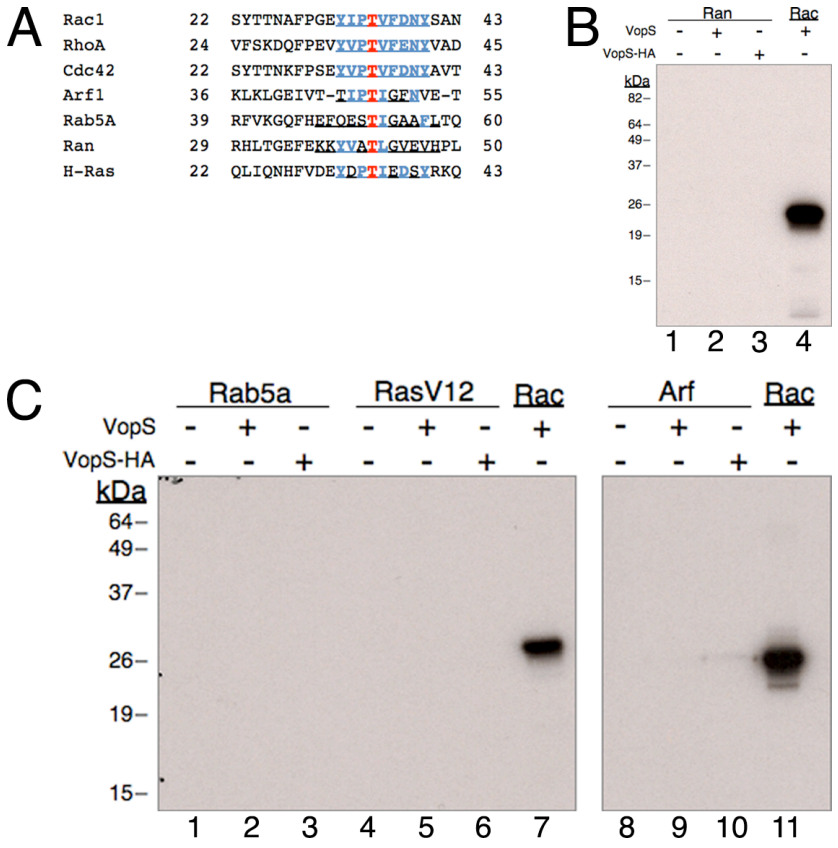

Figure 27. AMPylation of the Ras superfamily by VopS.
(A) Alignment of the core effector-binding domain of Rho GTPases and several representative members of the subfamilies of the Ras superfamily. The highly conserved modified threonine is depicted in red. Other areas of conservation are depicted in blue. Residue numbers are shown on either side of the alignment. (B and C) In vitro AMPylation assay in which VopSΔ30 or VopSΔ30-HA was incubated with Ran, Rab5a, RasV12, or Arf as substrate in the presence of ^{32}P-α-ATP. Samples were separated by SDS-PAGE and analyzed by autoradiography.

DISCUSSION

T3SS1 of *V. parahaemolyticus* induces a multifaceted cell death through the induction of autophagy, disruption of the actin cytoskeleton, and lysis of the cell. This study examined the contribution of one T3SS1 effector to these events. we have shown that the effector VopS from T3SS1 is responsible for the actin cytoskeletal rearrangement observed during infection. Our cell biology studies show that VopS is necessary for the efficient killing of host cells, as cell rounding is delayed in a *vopS* knockout. To look at the effects of VopS without the background of other effectors, we undertook transfection studies of HeLa cells in which we observed that transfection of this effector alone was sufficient to cause cytotoxicity. Additionally, expression of VopS in yeast resulted in the cytotoxicity of cells, indicating that this effector was targeting an evolutionarily conserved mechanism.

A previous study found that infection with *V. parahaemolyticus* resulted in the inhibition of Rho GTPases (19). Microbial genetic studies with deletion strains correlated the effector VopS this inhibition, albeit through an unknown mechanism. We confirmed these studies by showing that deletion of VopS from the POR3 strain delayed cell rounding and inactivation of Cdc42. However, during infection with the POR3Δ*vopS* strain cell rounding and Rho GTPase inactivation eventually occurred, implicating a redundant activity by another effector from T3SS1.

VopSΔ30 was unable to directly interact with the Rho GTPase Rac in a GST pulldown assay. However, Rac interacted with the VopS point mutant (VopSΔ30-H348A). Reminiscent of Rac-binding to its downstream signaling targets such as PAK, GST-VopS-H348A interacted more strongly with the GTP-bound form of Rac. Pre-incubation of VopSΔ30 with Rac renders the GTPase unable to bind to its downstream effector PAK, indicating that the interaction of VopS altered Rac in some way. Bacterial effectors are observed to have very potent activities because only small amounts of protein are secreted by the T3SS, and in many cases, the effectors are likely to utilize an enzymatic mechanism. Thus, we confirmed the concentration and time dependence of the inhibitory activity of VopS.

Our results indicated that VopS was modifying Rac in some way to prevent activation or binding to downstream effectors. To identify this modification, we expressed DA-Rac either alone or in the presence of VopSΔ30 in bacteria. Purified DA-Rac from each condition was analyzed by mass spectrometry. Total mass spectrometry results revealed that DA-Rac that had been coexpressed with VopSΔ30 had an increase in mass of 329 daltons that was consistent with the mass of AMP. Further analysis by LC-MS/MS revealed that this protein was modified with AMP on a threonine residue that is located in the switch I region of Rac, a region that is important for coordination of Mg^{2+} and GTP and effector binding (1, 38). Other bacterial toxins modify this highly conserved residue. For example, the *Clostridium difficile* toxins A and B

covalently modify Rho GTPases by glucosylation of the threonine, resulting in the inability of Rho GTPases to interact with their downstream effectors (2). The AMPylation of threonine 35 does not prevent Rac from binding to GTP. Based on this and the localization of the modification on Rac, we hypothesized that the VopS-mediated addition of a bulky AMP molecule to the effector-binding loop of Rho GTPases prevents their interaction with downstream effectors through steric hindrance. It remains to be shown whether VopS AMPylates Rho, Rac, and Cdc42 and/or exhibits a preference during infection. However, previous results support the hypothesis that VopS modifies all three Rho GTPases during infection (19). Furthermore, the AMPylated threonine is highly conserved throughout Rho GTPases, and all three GTPases were modified by VopS in an in vitro AMPylation assay.

VopS inhibits a pathway that is a common target of many type III effectors during infection. Bacterial effectors block signaling through Rho GTPases for a variety of reasons, including inhibition of phagocytosis and disruption of epithelial membranes. While the outcome of VopS-induced inhibition of Rho GTPases may be similar, the mechanism of inhibition used by VopS is novel, in that the post-translational modification of AMPylation has not previously been seen in eukaryotic cells. However, the covalent addition of AMP to the bacterial protein, glutamine synthetase, has been well documented (17, 20, 30). This modification is autocatalytic and helps regulate the enzymatic activity of glutamine synthetase.

The Fic domain is critical for the activity of VopS. Mutation of the Fic motif histidine completely abrogated cell rounding seen during transfection. In addition, mutation of this residue results in the inability of VopS to modify Rho GTPases with AMP during in vitro assays. Because type III secreted effector proteins often mimic an endogenous eukaryotic activity, it is tempting to suggest that Fic domain-mediated AMPylation could be a modification utilized by eukaryotes. In fact, Fic domain-containing proteins exist in several species of higher eukaryotes (discussed in the next chapter). These studies have revealed the molecular mechanism of the *V. parahaemolyticus* effector VopS. Furthermore, the identification of a novel eukaryotic post-translational modification could lead to the discovery of an uncharacterized component of cell signaling in eukaryotes.

CHAPTER FIVE
The search for eukaryotic AMPylation

INTRODUCTION AND RESULTS

AMPylation is an endogenous eukaryotic activity

We have uncovered the mechanism of a type III secreted effector from *V. parahaemolyticus* that possesses a novel function, the AMPylation of Rho GTPases. This post-translational modification has not previously been found in eukaryotes. However, many characterized bacterial effector proteins act by mimicking the activities of host cells to meet their specific needs (34, 61). AMPylation could be a previously undiscovered modification in eukaryotic cells.

To investigate whether eukaryotes use this post-translational modification, we tested eukaryotic cell lysates for AMPylation activity. We incubated S100 HeLa cell lysate containing cytosolic proteins with ^{32}P-γ-labeled ATP or ^{32}P-α-labeled ATP. Incubation with ^{32}P-γ-labeled ATP predictably revealed many phosphorylated protein substrates (Figure 28A, lane 1). This modification, phosphorylation, was attenuated in the presence of a phosphatase (Figure 28A, lane 4). To test whether the same type of experiment would reveal endogenous AMPylated protein substrates, we incubated S100 lysate with ^{32}P-α–labeled ATP. A number of radiolabeled proteins were observed that were insensitive to phosphatase treatment (Figure 28A, lane 8). The addition of purified recombinant VopSΔ30 to the reaction using ^{32}P-α–labeled ATP, but not ^{32}P-γ–labeled ATP,

specifically increased labeling at the predicted size of the Rho GTPases (Figure 28A, compare lanes 6 and 2). Consistent with this observation, phosphorylation and AMPylation did not occur in the presence of denatured protein (Figure 28A, lanes 3 and 7). Thus, eukaryotic proteins can use ATP to modify proteins by AMPylation. A concern was raised that these bands could represent the incorporation of ATP into RNA molecules. To address this, we co-incubated S100 lysate with ^{32}P-α-ATP and RNase A to rid the lysate of any RNA present. Much of the smearing disappears, indicating that radiolabeled RNA was present on these gels (Figure 28B). However, several bands remain after the treatment of RNase A, suggesting there is endogenous AMPylation of proteins in our cell lysate.

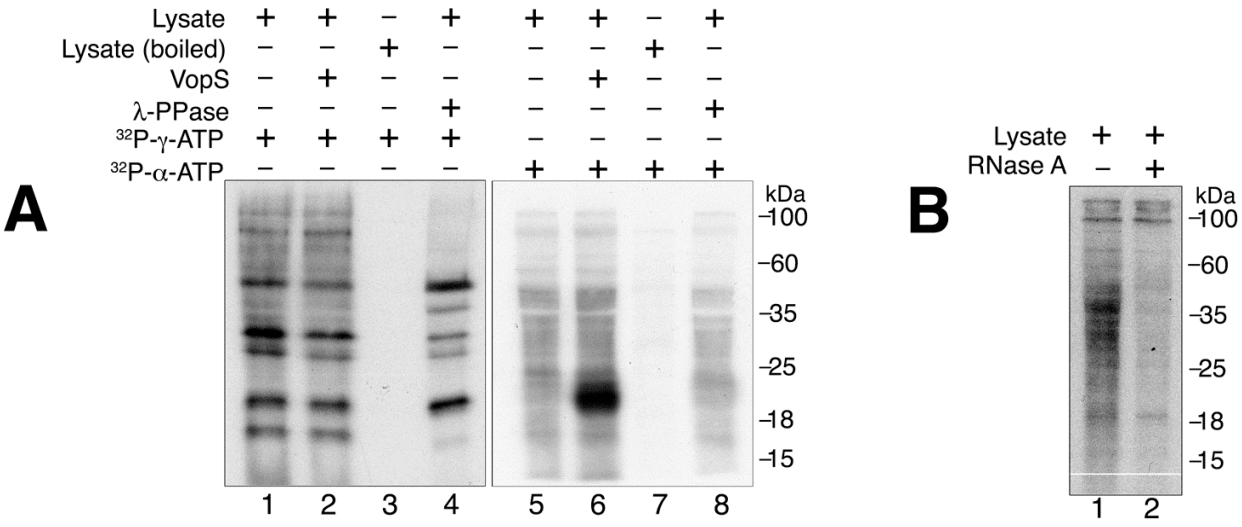

Figure 28. Detection of endogenous eukaryotic AMPylation.
(A) S100 HeLa cell lysates or boiled, denatured S100 HeLa cell lysates were incubated with ^{32}P-γ-ATP or ^{32}P-α-ATP in the presence or absence of VopSΔ30. Samples in lanes 4 and 8 were treated with λ-phosphatase (λ-Ppase) in the last 5 minutes of incubation. (B) S100 HeLa cell lysate was incubated with ^{32}P-α-ATP in the presence or absence of RNase A. Samples were separated by SDS-PAGE and analyzed by autoradiography.

A domain critical for AMPylation activity is present in higher eukaryotes

The bacterial effector VopS contains a C-terminal Fic domain, and mutation of an invariant histidine residue within this domain led to the discovery of the catalytic activity AMPylation. Fic domains are present in proteins from several species of bacteria and higher eukaryotes. An alignment of several Fic domain-containing proteins shows that all contain the conserved motif (HPFx(D/E)GNGR) with no substitutions of the critical histidine (Figure 29).

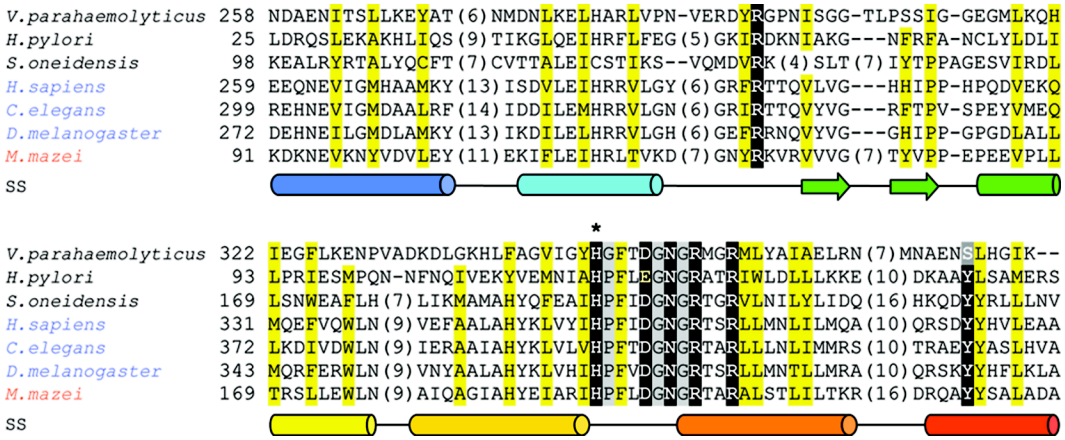

Figure 29. Multiple sequence alignment of VopS with several representative Fic sequences.
Fic sequences are labeled by species and colored by superkingdom: bacteria (black), eukaryote (blue), and archaea (red). Residue positions are highlighted by conservation: hydrophobic (yellow), small (gray), and polar (black). Residue numbers are depicted to the left of the alignment, and omitted residues are in parentheses. Observed secondary structure (SS) elements consistent in all Fic domain structures are indicated below the alignment (cylinder for helix and arrow for strand) and are colored from N to C terminus in rainbow succession. An asterisk above the alignment marks the critical histidine for VopS activity. Alignments refer to the following proteins in the order listed: VopS, GeneInfo Identifier 88192876 (gi|88192876), gi|151567990, gi| 42794620, gi|17544594, gi|24582217, and gi|21228708.

The human protein HYPE is a candidate AMPylator

BLAST searches and sequence alignments have led to the identification of a candidate AMPylator called HYPE from humans based on the presence of a Fic domain. Little is known about the function of HYPE, although it was identified in a yeast two-hybrid screen with Huntingtin, a polyglutamine repeat protein that is responsible for Huntington's disease, (27). Other aspects of the domain architecture of HYPE include the presence of an N-terminal tetratricopeptide repeat (TPR), which are present in a variety of organisms and are likely involved in protein-protein interactions (6). The repeats are followed by the C-terminal Fic domain (Figure 30A). The protein localization program, PSORT, predicts the likely subcellular localization of proteins based on known sorting signals (67). PSORT analysis predicted that HYPE would be localized to the endoplasmic reticulum (ER) or in the extracellular space. Furthermore, PSORT predicted that HYPE has a transmembrane (TM) domain located in the first 50 amino acids of the N-terminus (Figure 30A).

To study the localization of HYPE, we constructed various HYPE and eGFP fusions (Figure 30B). When transfected into HeLa cells, the eGFP vector control is distributed throughout the cell, in both the cytoplasm and the nucleus (Figure 30C). In contrast, full-length GFP-HYPE is localized to the perinuclear region and is excluded from the nucleus (Figure 30C). When cells are transfected with GFP-HYPEΔ47, a truncation mutant that lacks the predicted transmembrane domain, HYPE aggregated into punctae that were located in the cytosol or

possibly trapped in the ER. Transfection of a second truncation mutant that lacks a hydrophobic stretch of amino acids after the transmembrane domain (GFP-HYPEΔ99) shows a diffuse pattern throughout the cell, including the nucleus (Figure 30C). These results support the hypothesis that HYPE contains a sorting and/or retention signal in its first 100 amino acids.

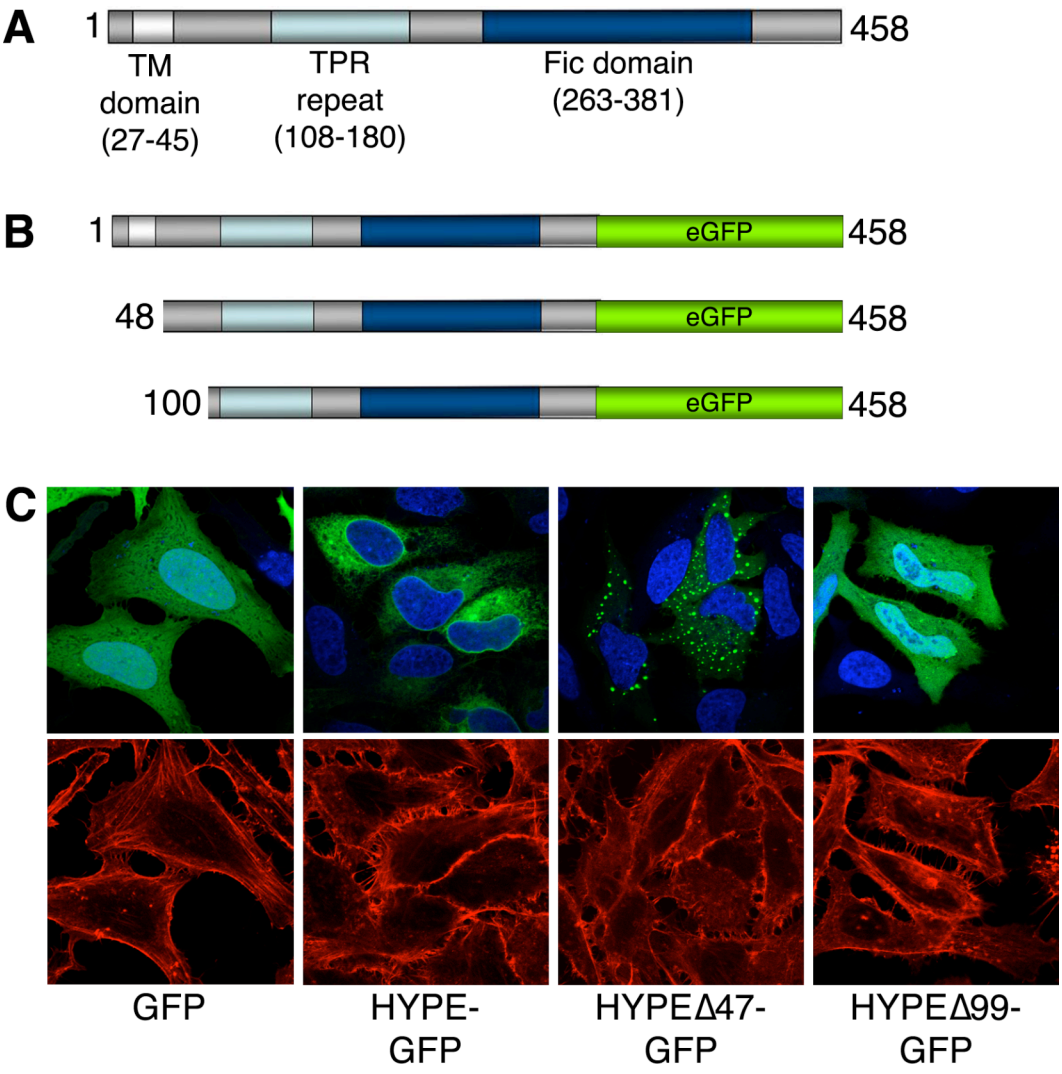

Figure 30. Domain architecture and cellular localization of HYPE.
(A) Schematic of the domain architecture of HYPE. The predicted TM domain is shown is white, the TPR domain in light blue, and the Fic motif in dark blue. Amino acids corresponding to each domain are listed underneath. (B) Schematic of the C-terminal GFP fusions with various constructs of HYPE. (C) Transfection of HeLa cells with GFP alone, HYPE-GFP, HYPEΔ47-GFP, or HYPEΔ99GFP. Transfected cells are shown in green. Cells were stained with Hoechst to visualize nuclei (blue) and rhodamine-phalloidin to visualize actin (red).

AMPylation activity of HYPE

Our in vitro AMPylation assays with S100 HeLa cell lysate revealed the presence of several putative AMPylated proteins. To test if any of these proteins are a substrate for modification by HYPE, we expressed and purified recombinant GST-HPYEΔ47 and incubated it with ^{32}P-α-ATP and S100 HeLa cell lysate. We chose to use the Δ47 form of HYPE to aid in the purification of this protein, as the transmembrane domain is largely hydrophobic and is unlikely to be important for the enzymatic activity of HYPE. As a control in this experiment, we incubated HeLa cell lysate with VopS, which caused specific labeling of Rho GTPases in S100 lysate (Figure 31, lane 3). Upon the addition of HYPEΔ47, no increase in labeling is seen in the bands when compared to the lysate alone control (Figure 31, compare lanes 1 and 2). However, we observed auto-AMPylation of HYPEΔ47, indicating that the activity of this protein is intact (Figure 31, lane 4). Interestingly, no auto-AMPylation occurs in the presence of S100 lysate, suggesting that an inhibitor of AMPylation activity might be present in cell lysate.

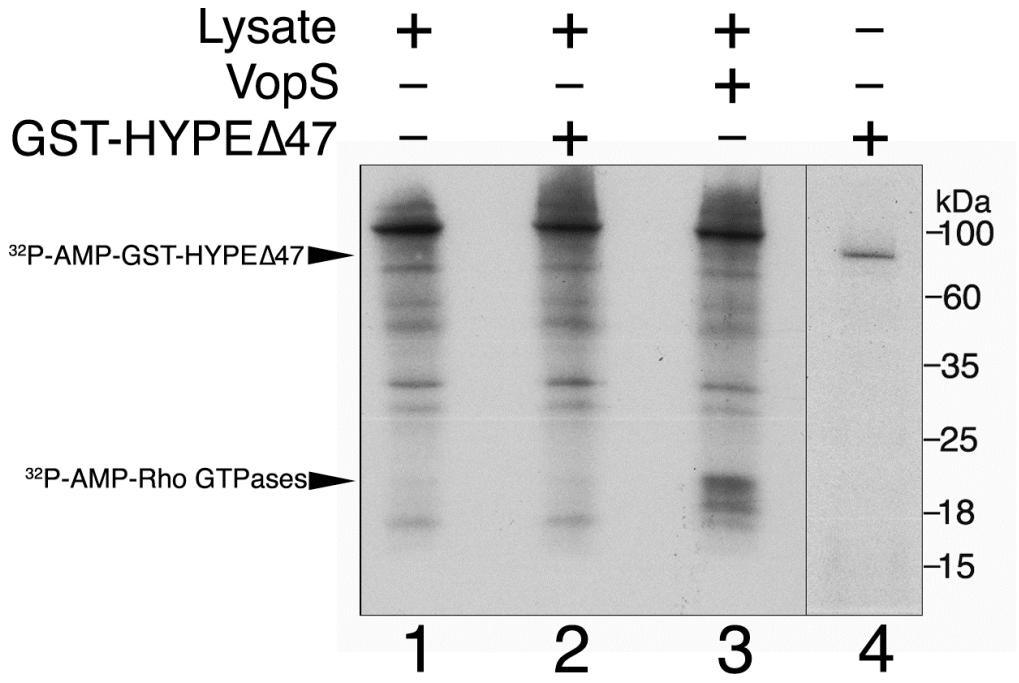

Figure 31. Activity of HYPE in S100 lysate.
In vitro AMPylation assay of S100 lysate alone (lane 1), in the presence of HYPE (lane 3), or in the presence of VopS (lane 3). Auto-AMPylation activity of HYPE was tested by the addition of ^{32}P-α-ATP to recombinant HYPE (lane 4).

DISCUSSION

The identification of AMPylation by a bacterial effector, which often mimic eukaryotic activities, suggested the intriguing possibility that such a mechanism could occur as an undiscovered component of cell signaling. Therefore, we initiated studies that examined AMPylation as an endogenous eukaryotic process. The results provided here support the need for future studies into this exciting new aspect of signal transduction in eukaryotes.

A simple in vitro AMPylation assay was used to look for the modification of eukaryotic proteins. In this experiment, we observed the presence of several radiolabeled bands that were insensitive to RNase A treatment in samples of S100 lysate that were incubated with ^{32}P-α-ATP. These bands represent potential substrates of eukaryotic AMPylation. As of yet, the identities of the substrates are unknown. However, future studies will address their identification through the incorporation of tagged ATP substrates to aid in isolation.

The Fic domain is critical for AMPylation by VopS. Therefore we undertook a bioinformatics approach to identify several Fic domain-containing proteins in higher eukaryotes. Our analysis led to the identification of HYPE, a human protein that contains an N-terminal TPR domain, which is a protein-protein interaction domain that may be involved in substrate recognition, followed by the C-terminal Fic domain. The PSORT program predicted that HYPE localizes to the ER or be secreted to the extracellular space. Localization studies utilizing fusions to GFP revealed that full-length HYPE is perinuclear, suggesting

an association with an organelle such as the ER. Truncation of the predicted transmembrane domain leads to localization of HYPE in punctae that surround the nuclei. This could represent HYPE that is unable to be inserted into its cognate membrane and is therefore trapped in vesicles. Further truncation of a hydrophobic patch of HYPE results in a construct that is diffused throughout the cell upon transfection. These preliminary studies on HYPE localization suggest that HYPE contains a sorting or retention signal peptide between amino acids 47 and 99. Alternatively, the overexpression of a GFP fusion of HYPE could cause aberrant localization of HYPE during transfection. Therefore, future studies will look at the localization of endogenous HYPE using subcellular fractionation.

We hypothesized that HYPE was a good candidate for the AMPylation of proteins in eukaryotic cells. To investigate this, recombinant HYPEΔ47 was incubated in the presence of ^{32}P-α-ATP in the presence or absence of S100 HeLa cell lysate containing cytosolic proteins. While incubation of recombinant protein with ^{32}P-α-ATP indicated that HYPE has auto-AMPylation activity, there was no increase in labeling of proteins upon the addition of HYPE to S100 lysate. This may be due to the GST tag on HYPE preventing it from interacting with substrate. Alternatively, the substrate for HYPE may be present in another fraction of cell lysate, as there are only cytosolic, but no membrane, proteins in the S100 fraction. This possibility is supported by our bioinformatics and GFP-fusion localization data. Another reason for the lack of HYPE activity could be the presence of an inhibitor of AMPylation in cell lysate. This idea is supported by the observation

that the auto-AMPylation of HYPE decreases in the presence of cell lysate when compared to HYPE alone.

Although no endogenous substrate for AMPylation has been identified, the studies presented here are preliminary and much remains to be done. We have shown that eukaryotic proteins can use ATP to modify proteins by AMPylation. Although enzymes, such as the ubiquitin activating enzyme (E1), form AMP-bound covalent enzyme intermediates to drive chemical ligation reactions (37), AMP has not previously been shown to be used as a stable posttranslational modification for a protein. Future studies into AMPylation in eukaryotic cells will increase our understanding of the mechanism behind the modification and the role it plays during signal transduction.

CHAPTER SIX
Discussion and Future Directions

VIRULENCE MECHANISMS OF *V. PARAHAEMOLYTICUS*

More than fifty years ago, an unidentified pathogen sickened almost 300 people in the first of many outbreaks of gastroenteritis. Since then, *V. parahaemolyticus* has emerged as an important public health issue in Southeast Asia. Concerns that this pathogen is extending its reach even farther are increasing as water temperatures rise due to global warming and new pandemic strains emerge. It is clear that a better understanding of the virulence mechanisms of *V. parahaemolyticus* is necessary. Until recently, TDH was the most well characterized virulence factor of *V. parahaemolyticus* although strains lacking TDH were still pathogenic (58, 76). This led to the idea that *V. parahaemolyticus* possessed other virulence mechanisms. In 2003, the genome sequence of a clinical isolate was published, and it revealed the presence of two T3SSs (60). Since then, intense research has focused on characterizing these systems. Tissue culture models of infection linked T3SS1 to cytotoxicity, while a rabbit ileal loop model showed that T3SS2 was responsible for enterotoxicity (77). Subsequent studies have linked T3SS1-dependent cytotoxicity to the activation of apoptosis and the presence of two T3SS1 effectors, though the mechanism of cell death was not well established (12, 71).

In the studies presented herein, we elucidated the mechanism of T3SS1-dependent cytotoxicity and defined the events that occurred during infection. In addition, characterization of VopS, an effector protein from T3SS1, increased our understanding of one of these events, the disruption of the actin cytoskeleton that leads to cell rounding. Discovery of the mechanism of this effector has added to the growing number of ways that bacteria use to usurp host defense mechanisms.

V. parahaemolyticus orchestrates a multifaceted host cell infection

Previous studies on the T3SSs of *V. parahaemolyticus* showed that T3SS1 elicited the cytotoxicity of host cells (77). Our studies have significantly extended this description, and a multifaceted model of *V. parahaemolyticus* infection has emerged that begins with the induction of autophagy, followed by disruption of the actin cytoskeleton, and culminating in the lysis of the cell (Figure 32). Unlike *Yersinia* infection, which causes induction of apoptosis, this mechanism of cell death is proinflammatory. Lysis of the cell results in the release of cytokines that attract innate immune cells such as macrophages. However, our results show that *V. parahaemolyticus* causes death of multiple cell types, including macrophages, so remaining undetected by the immune system may be less important for this pathogen.

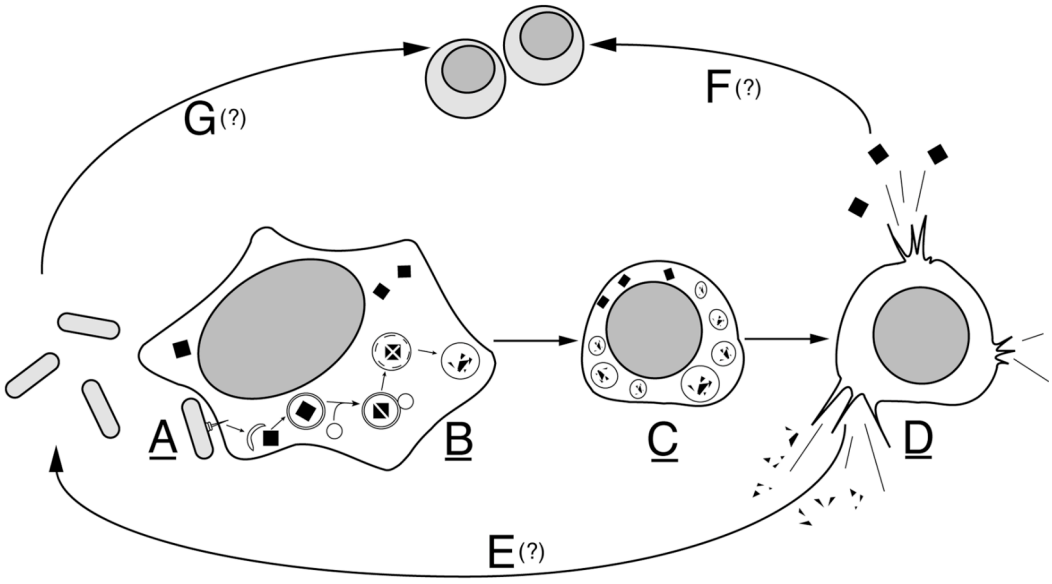

Figure 32. *V. parahaemolyticus* induces a series of events that culminates in the efficient death of host cells.
(A) *V. parahaemolyticus* utilizes a T3SS to inject effectors into a host cell during infection. (B) This results in the rapid induction of autophagy and the formation of autophagosomes. (C) Next, we observe rounding and shrinkage of the infected host cell. (D) This is subsequently followed by cell lysis and release of cellular contents. (E) We hypothesize that lysis will lead to the release of degraded proteins that can be used by the bacteria for nutrients. (F) In addition, the release of inflammatory contents will cause recruitment of innate immune cells, such as macrophages. (G) *V. parahaemolyticus* can also target and kill these immune cells, thereby evading an innate immune response. Underlined letters represent mechanisms that have been experimentally demonstrated herein. Letters with question marks represent events that are hypothesized to occur as a result of these mechanisms.

Our observation of the rapid induction of autophagy during *V. parahaemolyticus* infection presents an interesting paradigm. The importance of autophagy in cellular growth, differentiation, and development is without question, yet its role in cellular death is still being defined. In contrast to

apoptosis, which requires activation of caspases, autophagy is primarily a caspase-independent process that requires a distinct set of autophagy genes (57). Furthermore, some research suggests that these pathways are mutually exclusive or that there is a balance between them. Thus, the decision between apoptosis and autophagy is a critical step in determining cell fate and leads to the question of why an extracellular pathogen such as *V. parahaemolyticus* would want to activate the autophagic machinery.

The autophagy pathway plays roles in both innate and adaptive immunity and as a result is a common target of bacteria and viruses (74). When playing a protective role, autophagy defends against intracellular pathogens such as *Mycobacterium tuberculosis*, *Shigella* spp., and many others (53). A host cell often uses autophagy to prevent the cytoplasmic replication or invasion of intracellular pathogens by engulfing the pathogens in autophagic vesicles and targeting them to lysosomes (52). In addition, one study showed that autophagy might provide defense against a secreted toxin from the noninvasive pathogen *Vibrio cholerae* (36). However, pathogens have evolved ways to usurp this pathway for their own benefit. For example, the intracellular pathogen *Coxiella burnettii* creates a replicative niche within autophagosomes where it can multiply and survive (49). During infection, *Shigella flexneri* disrupts phagocytosis and escapes into the cytosol. The pathogen then avoids clearance by autophagy through the type III secretion of an effector protein that prevents recruitment of a protein necessary for autophagy (69).

So why might *V. parahaemolyticus* induce autophagy at the accelerated rate we observed during the initial stages of infection? One possibility is that *V. parahaemolyticus* may be utilizing autophagy to gain access to essential nutrients. By inducing this pathway, the bacteria force the host cell to do the work for them. The end result is an increased pool of amino acids in a readily usable form. As a gastrointestinal pathogen, these bacteria have evolved mechanisms to rapidly access nutrients before being expelled from the host. In particular, infection with *V. parahaemolyticus* is self-limiting in healthy individuals, thus stressing the need for systems that allow rapid acquisition of essential nutrients.

Another intriguing possibility may be that *V. parahaemolyticus* is inducing autophagy to avoid phagocytosis. In macrophages infected with *V. parahaemolyticus*, we have observed that the bacteria are exclusively extracellular (data not shown). During infection, the cellular machinery required for phagocytosis, including membrane lipids, may be directed inside the cell due to the acute activation of autophagy. We hypothesize that *V. parahaemolyticus* is using T3SS1 to mediate several events during infection to capitalize on the release of nutrients and to defend against phagocytosis by immune cells responding to proinflammatory signals at the site of infection (Figure 32).

The V. parahaemolyticus effector VopS inhibits Rho GTPases

The T3SS1-mediated events that occur during *V. parahaemolyticus* infection are a result of the secretion of several effectors from T3SS1. My studies

have shown that one of these effectors, VopS, contributes to disruption of the actin cytoskeleton through inhibition of Rho GTPases. Infection with the POR3Δ*vopS* strain results in delayed cell rounding during infection, while transfection of wild-type VopS is cytotoxic to HeLa cells. These results indicate that VopS is both necessary and sufficient to cause the death of cells during infection. Mutation of the histidine in the conserved Fic motif completely abrogated the cytotoxic affects of VopS during infection, giving us our first clue that this residue was critical for the activity of the effector.

A previous study linked the presence of VopS during infection with the inactivation of Rho GTPases, although no mechanism for this inhibition was established (19). We have extended these studies to define the molecular mechanism of VopS. Binding studies indicated that VopS directly interacts with the GTP-bound form of the Rho GTPase Rac. This interaction led to the inability of Rac to bind to its downstream effector, PAK. Analysis of the concentration and time-dependence of the VopS/Rac interaction suggested that it was an enzymatic modification, rather than a competitive binding, by VopS that prevented Rac from binding to PAK. Mass spectrometry analysis of Rac co-expressed with VopS in bacteria revealed that Rac had an increase in mass of 329 daltons compared to Rac expressed alone. This mass shift was consistent with the addition of AMP, which LC-MS/MS analysis showed was covalently bound to Rac on threonine 35. This modification occurs in the switch I region of Rac that is involved in the interaction of Rho GTPases to downstream effectors (1, 38).

VopS modification of the switch I region with AMP prevents the effectors from binding to activated GTPases, thereby preventing actin assembly and resulting in cell rounding. We now refer to this activity as AMPylation and the enzyme as an AMPylator.

Both VopS and protein kinases use ATP to modify substrates, but the phosphate attached to the substrate is distinct. Kinases use the γ phosphate of ATP to modify their substrates on tyrosine, threonine, and serine residues, whereas VopS uses the α phosphate linked to adenosine to modify its substrate on a threonine residue. This type of posttranslational modification on eukaryotic proteins has not previously been observed. However, it has been observed for glutamine synthetase (GS), a bacterial protein that is responsible for the synthesis of glutamine from NH_4^+ and glutamate during nitrogen-limited growth (17). GS is located in a key position of nitrogen metabolism and its activity is autocatalytically regulated by modification with AMP. In nitrogen-rich conditions, AMP modification downregulates GS activity, allowing recovery of cellular stores of glutamate (51). In contrast to VopS-mediated AMPylation of Rho GTPases, this covalent modification is reversible and occurs on a tyrosine residue (17, 20). However, the discovery of additional AMPylators or substrates for AMPylation will likely show that this modification also occurs on serine or tyrosine residues.

VopS contains a C-terminal Fic domain, and mutation of an invariant histidine residue within this domain led to the discovery of the catalytic activity of

modifying proteins with AMP. Support for the enzymatic activity of VopS is given by the crystal structures of other bacterial Fic domains. These structures place the conserved polar residues of this motif within a cleft that could represent an active site, with conserved side chains (from E and N) forming polar contacts with a phosphate in one structure (23) (Figure 4). A β hairpin located near the motif binds peptide in another structure, placing a side chain of the peptide within van der Waals contact of the motif histidine (25) (Figure 4). These structures help to envision an active site for VopS that contains the conserved Fic motif with the catalytic histidine residue positioned close enough to its substrate to carry out the chemistry of the reaction.

The characterization of the molecular mechanism of VopS has revealed that this effector targets an old pathway in a new way. Many pathogens such as *Salmonella* spp., *Yersinia* spp., and *Clostridium* spp. inhibit the Rho GTPase family (2). Breakdown of Rho GTPase signaling can result in disruption of the actin cytoskeleton, leading to collapse of the epithelial barrier or prevention of phagocytosis of the bacterium (2). VopS enzymatically modifies Rho GTPases in the highly conserved switch I region with an AMP molecule, preventing their interaction to downstream effectors through steric hindrance. This mechanism could represent a novel function for the Fic domain, a previously uncharacterized domain that is found in a wide variety of organisms.

AMPylation--a novel component of eukaryotic cell signaling

The Fic domain, which contains a conserved HPFx(D/E)GNGR motif, is critical for the AMPylation activity of VopS. The Fic motif is found in proteins from organisms in all domains of life. Although there are no Fic domain-containing proteins in fungi, there are examples in many species of higher eukaryotes. The limited eukaryotic distribution of Fic resembles that of other components of signal transduction machinery and might support a role for AMPylation by eukaryotic Fic domains in signaling (79).

To address the possibility that AMPylation is an endogenous eukaryotic activity, we developed an in vitro assay using ^{32}P-α-ATP to radiolabel proteins. Addition of S100 HeLa cell lysate to the in vitro assay showed several radiolabeled bands representing AMPylated substrates. Addition of VopS to lysate indicated specific labeling at the level of Rho GTPases, confirming that the labeling of AMPylated proteins was possible using our in vitro assay. Our preliminary studies with HYPE, a candidate AMPylator from humans, showed that addition of HYPEΔ47 to lysate in an in vitro assay did not increase labeling of any particular substrate. However, we did observe auto-AMPylation of this protein, indicating that it was active and possessed AMPylation activity. This result is further confirmation that Fic domains are responsible for AMPylation activity.

The discovery of AMPylation of eukaryotic proteins reveals not only a previously uncharacterized component of cell signaling, but also a novel use for

ATP. This activity represents an ideal posttranslational modification in eukaryotic cells because it (i) uses a highly abundant high-energy substrate, ATP; (ii) results in the formation of a reversible phosphodiester bond; (iii) is bulky enough to bind to an adaptor protein and be used in dynamic multidomain signaling complexes; and (iv) alters the activity of the protein it modifies. The identification of the substrates and enzymes involved in eukaryotic AMPylation will undoubtedly add a new layer to the expanding complexity of our information about cellular signal transduction.

FUTURE DIRECTIONS

Assess the contributions of other effectors to the multifaceted mechanism of T3SS1-mediated cell death

We have shown that *V. parahaemolyticus* induces multiple events during infection, including cell rounding and the induction of autophagy. Characterization of VopS showed how this T3SS1 effector leads to the inhibition of Rho GTPases, which contributes to cell rounding. Currently, studies are ongoing to determine the contributions of other T3SS1 effectors during infection. Infections with knockout strains are being analyzed for the induction of autophagy by microscopic and biochemical methods. Additionally, the cytotoxicity of knockout strains will be addressed through LDH release assays and microscopy. Results with the Δ*vopS* knockout strain suggest that there may

be some redundancy between the effectors in the inhibition of Rho GTPases. This is not uncommon, as pathogens often use multiple mechanisms to disrupt the same pathway to ensure inhibition takes place (68). This redundancy could be addressed using transfection studies with individual or combinations of effectors or by secretion of single effectors using a heterologous system such as the *Yersinia* T3SS.

Examine the role of autophagy induction during V. parahaemolyticus infection

T3SS1-mediated infection causes the rapid induction of autophagy. We hypothesize that extracellular bacteria such as *V. parahaemolyticus* may activate this pathway to inhibit phagocytosis or to acquire nutrients in a readily usable form. Studies have been initiated to address the inhibition of phagocytosis using techniques such as electron microscopy of macrophages that were infected with *V. parahaemolyticus* in the presence or absence of inhibitors of autophagy. Comparison of the growth rates of *V. parahaemolyticus* during infection in the presence or absence of the induction of autophagy may shed light on whether the bacteria are acquiring nutrients during infection. Another experiment could assess directly whether the bacteria are taking up nutrients from lysing cells by the incorporation of radiolabeled amino acids into host proteins.

Does AMPylation of Rho, Rac, and Cdc42 occur during V. parahaemolyticus infection?

In vitro assays have shown that VopS mediates the AMPylation of Rho, Rac, and Cdc42. However, these assays were carried out with purified recombinant enzyme and substrate. The next step would be to show that VopS AMPylates Rho GTPases during infection. We and others have indirectly shown that VopS mediates this activity during infection by looking at the ability of Rho GTPases to bind to downstream effectors in infected HeLa cells (19). These results indicated that VopS disrupted the signaling of Rho, Rac, and Cdc42. However, it remains to be shown if these Rho GTPases are modified with AMP during infection. It is likely that VopS utilizes all three of these as substrates for AMPylation, as they are highly conserved in the Switch I region where AMPylation occurs. For this experiment, the modification Rho GTPases during *V. parahaemolyticus* infection could be monitored with a labeled form of ATP, such as ^{32}P-α-ATP, that is readily taken up by a cell. The incorporation of this substrate into Rho GTPases would then be analyzed by pulldown and autoradiography.

Examining the chemistry behind AMPylation

Experiments that tested the concentration and time dependence of VopS supported the idea that this effector possessed an enzymatic activity. However, these experiments did not definitively prove that VopS was an enzyme. Discovery of the catalytic activity of VopS would give insight into the mechanism

of AMPylation, a modification that has never been seen in eukaryotes or on a threonine residue. A quantitative in vitro assay is currently being developed to analyze the kinetics of this modification. This assay uses ^{32}P-α-ATP to measure the transfer of radioactive AMP to the substrate. In addition to enzymatic analysis, crystal structure trials of VopS alone and in complex with Rac have been initiated. A crystal structure of VopS would allow comparisons of this protein with other Fic domain structures. In addition, a depiction of VopS in complex with its substrate will provide further mechanistic insight into the chemistry of AMPylation.

Identification of the enzymes and substrates of eukaryotic AMPylation

Preliminary studies indicate that AMPylation is an endogenous eukaryotic activity. An in vitro AMPylation assay results in the presence of several radiolabeled proteins. Identification of the eukaryotic substrates of AMPylation may provide an idea what pathways are regulated by this mechanism. Development of an antibody that recognizes an AMP modification will help in the identification of these substrates. If this proves difficult, use of another form of ATP, such as biotinylated ATP, will eliminate the need for radioactivity so that substrates can be identified by mass spectrometry. Our preliminary results show that this might be a viable option. An in vitro AMPylation assay using biotinylated ATP with Rac and VopSΔ30 shows that Rac is labeled only in the

presence of VopS (Figure 33). Future studies will test biotinylated ATP as a substrate for eukaryotic AMPylation in HeLa cell lysate.

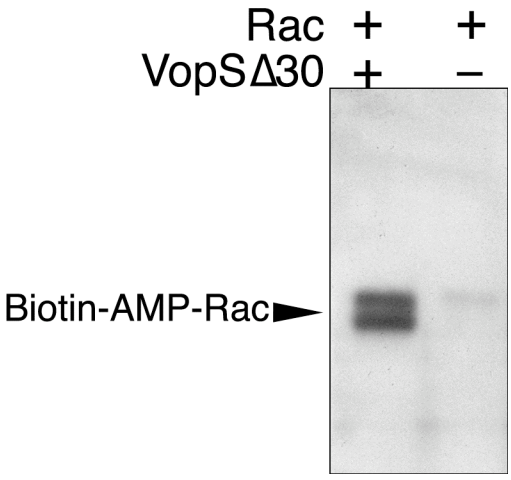

Figure 33. Biotinylated ATP is a substrate for AMPylation.
In vitro assay in which recombinant Rac was incubated in the presence or absence of recombinant VopSΔ30 and biotinylated ATP. Samples were separated by SDS-PAGE and analyzed by western blot with avidin-HRP.

BLAST searches and sequence alignments of Fic domain-containing proteins have led to the identification of several possible candidate AMPylators in higher eukaryotes. Studies have been initiated with the human Fic family protein, HYPE. We have established that this protein has auto-AMPylation activity but have not identified any substrates for this reaction. It is possible that we are missing possible substrates for HYPE in our in vitro AMPylation assay because we are using S100 HeLa cell lysate. This lysate contains only cytoplasmic proteins and lacks membrane-associated and nuclear proteins. Therefore, the use of other fractions of cell lysate may show an activity upon the addition of recombinant HYPE. If this experiment yields no hits, detection of potential HYPE interacting proteins using a yeast two-hybrid screen or GST pulldowns should elicit appealing candidates for the substrates of AMPylation. A mutation of the conserved Fic motif histidine in HYPE could be used to increase the chance of "trapping" a substrate in these binding studies. Potential candidates could then be confirmed as substrates using our in vitro assay with the point mutant as a negative control for AMPylation activity.

Inhibition of AMPylation activity

Our results indicate that the auto-AMPylation activity of HYPE is decreased upon the addition of S100 lysate. This suggests that there is an inhibitor of AMPylation present in the lysate. Furthermore, key components of eukaryotic signaling machinery are often regulated by activities that have

opposing effects, for example phosphorylation by kinases and subsequent dephosporylation by phosphatases. Therefore, it is likely that a mechanism that opposes AMPylation exists in eukaryotes. The AMPylation of proteins results in the formation of a phosphodiester bond, and reversal of this modification is possible through phosphodiesterase activity. Future studies will look at the reversal of AMPylation by phosphodiesterases and will identify these enzymes, which may play an important role in the regulation of AMPylation in eukaryotes.

BIBLIOGRAPHY

1. **Abdul-Manan, N., B. Aghazadeh, G. A. Liu, A. Majumdar, O. Ouerfelli, K. A. Siminovitch, and M. K. Rosen.** 1999. Structure of Cdc42 in complex with the GTPase-binding domain of the 'Wiskott-Aldrich syndrome' protein. Nature **399:**379-383.

2. **Aktories, K., and J. T. Barbieri.** 2005. Bacterial cytotoxins: targeting eukaryotic switches. Nat Rev Microbiol **3:**397-410.

3. **Aktories, K., C. Wilde, and M. Vogelsgesang.** 2004. Rho-modifying C3-like ADP-ribosyltransferases. Rev Physiol Biochem Pharmacol **152:**1-22.

4. **Alam, M. J., K. I. Tomochika, S. I. Miyoshi, and S. Shinoda.** 2002. Environmental investigation of potentially pathogenic Vibrio parahaemolyticus in the Seto-Inland Sea, Japan. FEMS Microbiol Lett **208:**83-87.

5. **Altschul, S. F., W. Gish, W. Miller, E. W. Myers, and D. J. Lipman.** 1990. Basic local alignment search tool. J Mol Biol **215:**403-410.

6. **Andrade, M. A., C. Perez-Iratxeta, and C. P. Ponting.** 2001. Protein repeats: structures, functions, and evolution. J Struct Biol **134:**117-131.

7. **Baffone, W., R. Tarsi, L. Pane, R. Campana, B. Repetto, G. L. Mariottini, and C. Pruzzo.** 2006. Detection of free-living and plankton-bound vibrios in coastal waters of the Adriatic Sea (Italy) and study of their pathogenicity-associated properties. Environ Microbiol **8:**1299-1305.

8. **Barbieri, J. T., M. J. Riese, and K. Aktories.** 2002. Bacterial toxins that modify the actin cytoskeleton. Annu Rev Cell Dev Biol **18:**315-344.

9. **Belas, M. R., and R. R. Colwell.** 1982. Adsorption kinetics of laterally and polarly flagellated Vibrio. J Bacteriol **151:**1568-1580.

10. **Beringer, J. E., J. L. Beynon, A. V. Buchanan-Wollaston, and A. W. B. Johnston.** 1978. Transfer of Drug-resistance Transposon TN5 to Rhizobium. Nature **276:**633-634.

11. **Bernards, A.** 2003. GAPs galore! A survey of putative Ras superfamily GTPase activating proteins in man and Drosophila. Biochim Biophys Acta **1603:**47-82.

12. **Bhattacharjee, R. N., K. S. Park, Y. Kumagai, K. Okada, M. Yamamoto, S. Uematsu, K. Matsui, H. Kumar, T. Kawai, T. Iida, T. Honda, O. Takeuchi, and S. Akira.** 2006. VP1686, a Vibrio type III secretion protein, induces Toll-like receptor-independent apoptosis in macrophage through NF-?B inhibition. Journal of Biological Chemistry **281:**36897-36904.

13. **Bliska, J. B., K. L. Guan, J. E. Dixon, and S. Falkow.** 1991. Tyrosine phosphate hydrolysis of host proteins by an essential Yersinia virulence determinant. Proc Natl Acad Sci U S A **88:**1187-1191.

14. **Boatright, K. M., and G. S. Salvesen.** 2003. Mechanisms of caspase activation. Curr Opin Cell Biol **15:**725-731.

15. **Boise, L. H., and C. M. Collins.** 2001. Salmonella-induced cell death: apoptosis, necrosis or programmed cell death? Trends Microbiol **9:**64-67.

16. **Bolin, I., L. Norlander, and H. Wolf-Watz.** 1982. Temperature-inducible outer membrane protein of Yersinia pseudotuberculosis and Yersinia enterocolitica is associated with the virulence plasmid. Infect Immun **37:**506-512.

17. **Brown, M. S., A. Segal, and E. R. Stadtman.** 1971. Modulation of glutamine synthetase adenylylation and deadenylylation is mediated by metabolic transformation of the P II -regulatory protein. Proc Natl Acad Sci U S A **68:**2949-2953.

18. **Bursch, W.** 2001. The autophagosomal-lysosomal compartment in programmed cell death. Cell Death Differ **8:**569-581.

19. **Casselli, T., T. Lynch, C. M. Southward, B. W. Jones, and R. DeVinney.** 2008. Vibrio parahaemolyticus inhibition of Rho family GTPase activation requires a functional chromosome I type III secretion system. Infect Immun **76:**2202-2211.

20. **Chock, P. B., S. G. Rhee, and E. R. Stadtman.** 1980. Interconvertible enzyme cascades in cellular regulation. Annu Rev Biochem **49:**813-843.

21. **Chook, Y. M., and G. Blobel.** 1999. Structure of the nuclear transport complex karyopherin-beta2-Ran x GppNHp. Nature **399:**230-237.

22. **Covazzi Harriague, A., M. D. Brino, M. Zampini, G. Albertelli, C. Pruzzo, and C. Misic.** 2008. Vibrios in association with sedimentary crustaceans in three beaches of the northern Adriatic Sea (Italy). Mar Pollut Bull **56:**574-579.

23. **Cuff, M. E., X. Xu, H. Zheng, A. Edwards, A. Savchenko, A. Joachimiak, and M. C. f. S. Genomics.** To be published. Structure of cell filamentation protein (Fic) from Helicobacter pylori.

24. **Daniels, N. A., L. MacKinnon, R. Bishop, S. Altekruse, B. Ray, R. M. Hammond, S. Thompson, S. Wilson, N. H. Bean, P. M. Griffin, and L. Slutsker.** 2000. Vibrio parahaemolyticus infections in the United States, 1973-1998. J Infect Dis **181:**1661-1666.

25. **Das, D., S. S. Krishna, D. McMullan, M. D. Miller, Q. Xu, P. Abdubek, C. Acosta, T. Astakhova, H. L. Axelrod, P. Burra, D. Carlton, H. J. Chiu, T. Clayton, M. C. Deller, L. Duan, Y. Elias, M. A. Elsliger, D. Ernst, J. Feuerhelm, A. Grzechnik, S. K. Grzechnik, J. Hale, G. W. Han, L. Jaroszewski, K. K. Jin, H. E. Klock, M. W. Knuth, P. Kozbial, A. Kumar, D. Marciano, A. T. Morse, K. D. Murphy, E. Nigoghossian, L. Okach, S. Oommachen, J. Paulsen, R. Reyes, C. L. Rife, N. Sefcovic, H. Tien, C. B. Trame, C. V. Trout, H. van den Bedem, D. Weekes, A. White, K. O. Hodgson, J. Wooley, A. M. Deacon, A. Godzik, S. A. Lesley, and I. A. Wilson.** 2008. Crystal structure of the Fic (Filamentation induced by cAMP) family protein SO4266 (gi|24375750) from Shewanella oneidensis MR-1 at 1.6 A resolution. Proteins.

26. **Datsenko, K. A., and B. L. Wanner.** 2000. One-step inactivation of chromosomal genes in Escherichia coli K-12 using PCR products. Proc Natl Acad Sci U S A **97:**6640-6645.

27. **Faber, P. W., G. T. Barnes, J. Srinidhi, J. Chen, J. F. Gusella, and M. E. MacDonald.** 1998. Huntingtin interacts with a family of WW domain proteins. Hum Mol Genet **7:**1463-1474.

28. **Festjens, N., T. Vanden Berghe, and P. Vandenabeele.** 2006. Necrosis, a well-orchestrated form of cell demise: signalling cascades, important mediators and concomitant immune response. Biochim Biophys Acta **1757:**1371-1387.

29. **Fink, S. L., and B. T. Cookson.** 2005. Apoptosis, pyroptosis, and necrosis: mechanistic description of dead and dying eukaryotic cells. Infect Immun **73:**1907-1916.

30. **Fisher, S. H.** 1992. Glutamine synthesis in Streptomyces--a review. Gene **115:**13-17.

31. **Food and Drug Administration.** 2001. Draft risk assessment on the public health impact of *Vibrio parahaemolyticus* in raw molluscan shellfish. Online. www.cfsan.fda.gov/~dms/vprisk.html

32. **Friedman, A. M., S. R. Long, S. E. Brown, W. J. Buikema, and F. M. Ausubel.** 1982. Construction of a broad host range cosmid cloning vector and its use in the genetic analysis of Rhizobium mutants. Gene **18:**289-296.

33. **Fukui, T., K. Shiraki, D. Hamada, K. Hara, T. Miyata, S. Fujiwara, K. Mayanagi, K. Yanagihara, T. Iida, E. Fukusaki, T. Imanaka, T. Honda, and I. Yanagihara.** 2005. Thermostable direct hemolysin of Vibrio parahaemolyticus is a bacterial reversible amyloid toxin. Biochemistry **44:**9825-9832.

34. **Galan, J. E., and H. Wolf-Watz.** 2006. Protein delivery into eukaryotic cells by type III secretion machines. Nature **444:**567-573.

35. **Ghosh, P.** 2004. Process of protein transport by the type III secretion system. Microbiol Mol Biol Rev **68:**771-795.

36. **Gutierrez, M. G., H. A. Saka, I. Chinen, F. C. Zoppino, T. Yoshimori, J. L. Bocco, and M. I. Colombo.** 2007. Protective role of autophagy against Vibrio cholerae cytolysin, a pore-forming toxin from V. cholerae. Proc Natl Acad Sci U S A **104:**1829-1834.

37. **Haas, A. L., J. V. Warms, and I. A. Rose.** 1983. Ubiquitin adenylate: structure and role in ubiquitin activation. Biochemistry **22:**4388-4394.

38. **Hakoshima, T., T. Shimizu, and R. Maesaki.** 2003. Structural basis of the Rho GTPase signaling. J Biochem **134:**327-331.

39. **Hardt, W. D., L. M. Chen, K. E. Schuebel, X. R. Bustelo, and J. E. Galan.** 1998. S. typhimurium encodes an activator of Rho GTPases that induces membrane ruffling and nuclear responses in host cells. Cell **93:**815-826.

40. **Honda, T., T. Iida, Y. Akeda, and T. Kodama.** 2008. Sixty years of Vibrio parahaemolyticus research. Microbe **3:**462-466.

41. **Honda, T., Y. Ni, T. Miwatani, T. Adachi, and J. Kim.** 1992. The thermostable direct hemolysin of Vibrio parahaemolyticus is a pore-forming toxin. Can J Microbiol **38:**1175-1180.

42. **Jaffe, A. B., and A. Hall.** 2005. Rho GTPases: biochemistry and biology. Annu Rev Cell Dev Biol **21:**247-269.

43. **Joseph, S. W., R. R. Colwell, and J. B. Kaper.** 1982. Vibrio parahaemolyticus and related halophilic Vibrios. Crit Rev Microbiol **10:**77-124.

44. **Kabeya, Y., N. Mizushima, T. Ueno, A. Yamamoto, T. Kirisako, T. Noda, E. Kominami, Y. Ohsumi, and T. Yoshimori.** 2000. LC3, a mammalian homologue of yeast Apg8p, is localized in autophagosome membranes after processing. EMBO J **19:**5720-5728.

45. **Kabeya, Y., N. Mizushima, A. Yamamoto, S. Oshitani-Okamoto, Y. Ohsumi, and T. Yoshimori.** 2004. LC3, GABARAP and GATE16 localize to autophagosomal membrane depending on form-II formation. J Cell Sci **117:**2805-2812.

46. **Kaneko, T., and R. R. Colwell.** 1975. Adsorption of Vibrio parahaemolyticus onto chitin and copepods. Appl Microbiol **29:**269-274.

47. **Kerr, J. F., A. H. Wyllie, and A. R. Currie.** 1972. Apoptosis: a basic biological phenomenon with wide-ranging implications in tissue kinetics. Br J Cancer **26:**239-257.

48. **Kim, Y. K., and L. L. McCarter.** 2000. Analysis of the polar flagellar gene system of Vibrio parahaemolyticus. J Bacteriol **182:**3693-3704.

49. **Kirkegaard, K., M. P. Taylor, and W. T. Jackson.** 2004. Cellular autophagy: surrender, avoidance and subversion by microorganisms. Nat Rev Microbiol **2:**301-314.

50. **Komano, T., R. Utsumi, and M. Kawamukai.** 1991. Functional analysis of the fic gene involved in regulation of cell division. Res Microbiol **142:**269-277.

51. **Kustu, S., J. Hirschman, D. Burton, J. Jelesko, and J. C. Meeks.** 1984. Covalent modification of bacterial glutamine synthetase: physiological significance. Mol Gen Genet **197:**309-317.

52. **Levine, B., and V. Deretic.** 2007. Unveiling the roles of autophagy in innate and adaptive immunity. Nat Rev Immunol **7:**767-777.

53. **Levine, B., and G. Kroemer.** 2008. Autophagy in the pathogenesis of disease. Cell **132:**27-42.

54. **Levine, B., and J. Yuan.** 2005. Autophagy in cell death: an innocent convict? J Clin Invest **115:**2679-2688.

55. **Levine, W. C., and P. M. Griffin.** 1993. Vibrio infections on the Gulf Coast: results of first year of regional surveillance. Gulf Coast Vibrio Working Group. J Infect Dis **167:**479-483.

56. **Liverman, A. D., H. C. Cheng, J. E. Trosky, D. W. Leung, M. L. Yarbrough, D. L. Burdette, M. K. Rosen, and K. Orth.** 2007. Arp2/3-independent assembly of actin by Vibrio type III effector VopL. Proc Natl Acad Sci U S A **104:**17117-17122.

57. **Lockshin, R. A., and Z. Zakeri.** 2002. Caspase-independent cell deaths. Curr Opin Cell Biol **14:**727-733.

58. **Lynch, T., S. Livingstone, E. Buenaventura, E. Lutter, J. Fedwick, A. G. Buret, D. Graham, and R. DeVinney.** 2005. Vibrio parahaemolyticus disruption of epithelial cell tight junctions occurs independently of toxin production. Infect Immun **73:**1275-1283.

59. **Majno, G., and I. Joris.** 1995. Apoptosis, oncosis, and necrosis. An overview of cell death. Am J Pathol **146:**3-15.

60. **Makino, K., K. Oshima, K. Kurokawa, K. Yokoyama, T. Uda, K. Tagomori, Y. Iijima, M. Najima, M. Nakano, A. Yamashita, Y. Kubota, S. Kimura, T. Yasunaga, T. Honda, H. Shinagawa, M. Hattori, and T. Iida.** 2003. Genome sequence of Vibrio parahaemolyticus: a pathogenic mechanism distinct from that of V cholerae. Lancet **361:**743-749.

61. **Mattoo, S., Y. M. Lee, and J. E. Dixon.** 2007. Interactions of bacterial effector proteins with host proteins. Curr Opin Immunol **19:**392-401.

62. **McLaughlin, J. B., A. DePaola, C. A. Bopp, K. A. Martinek, N. P. Napolilli, C. G. Allison, S. L. Murray, E. C. Thompson, M. M. Bird, and J. P. Middaugh.** 2005. Outbreak of Vibrio parahaemolyticus gastroenteritis associated with Alaskan oysters. N Engl J Med **353:**1463-1470.

63. **Monack, D. M., J. Mecsas, N. Ghori, and S. Falkow.** 1997. Yersinia signals macrophages to undergo apoptosis and YopJ is necessary for this cell death. Proc Natl Acad Sci U S A **94:**10385-10390.

64. **Morris, J. G., Jr., and R. E. Black.** 1985. Cholera and other vibrioses in the United States. N Engl J Med **312:**343-350.

65. **Mukherjee, S., G. Keitany, Y. Li, Y. Wang, H. L. Ball, E. J. Goldsmith, and K. Orth.** 2006. Yersinia YopJ acetylates and inhibits kinase activation by blocking phosphorylation. Science **312:**1211-1214.

66. **Nair, G. B., T. Ramamurthy, S. K. Bhattacharya, B. Dutta, Y. Takeda, and D. A. Sack.** 2007. Global dissemination of Vibrio parahaemolyticus serotype O3:K6 and its serovariants. Clin Microbiol Rev **20:**39-48.

67. **Nakai, K., and P. Horton.** 1999. PSORT: a program for detecting sorting signals in proteins and predicting their subcellular localization. Trends Biochem Sci **24:**34-36.

68. **Navarro, L., N. M. Alto, and J. E. Dixon.** 2005. Functions of the Yersinia effector proteins in inhibiting host immune responses. Curr Opin Microbiol **8:**21-27.

69. **Ogawa, M., T. Yoshimori, T. Suzuki, H. Sagara, N. Mizushima, and C. Sasakawa.** 2005. Escape of intracellular Shigella from autophagy. Science **307:**727-731.

70. **Olofsson, B.** 1999. Rho guanine dissociation inhibitors: pivotal molecules in cellular signalling. Cell Signal **11:**545-554.

71. **Ono, T., K. S. Park, M. Ueta, T. Iida, and T. Honda.** 2006. Identification of proteins secreted via Vibrio parahaemolyticus type III secretion system 1. Infection and Immunity **74:**1032-1042.

72. **Orth, K.** 2007. Versatile Type III Effector Mechanisms can Disrupt Target-Cell Functions. Microbe **2:**183-186.

73. **Orth, K., L. E. Palmer, Z. Q. Bao, S. Stewart, A. E. Rudolph, J. B. Bliska, and J. E. Dixon.** 1999. Inhibition of the mitogen-activated protein kinase kinase superfamily by a Yersinia effector. Science **285:**1920-1923.

74. **Orvedahl, A., and B. Levine.** 2009. Eating the enemy within: autophagy in infectious diseases. Cell Death Differ **16:**57-69.

75. **Panina, E. M., S. Mattoo, N. Griffith, N. A. Kozak, M. H. Yuk, and J. F. Miller.** 2005. A genome-wide screen identifies a Bordetella type III secretion effector and candidate effectors in other species. Mol Microbiol **58:**267-279.

76. **Park, K. S., T. Ono, M. Rokuda, M. H. Jang, T. Iida, and T. Honda.** 2004. Cytotoxicity and Enterotoxicity of the Thermostable Direct

Hemolysin-Deletion Mutants of Vibrio parahaemolyticus. Microbiology and Immunology **48:**313-318.

77. **Park, K. S., T. Ono, M. Rokuda, M. H. Jang, K. Okada, T. Iida, and T. Honda.** 2004. Functional characterization of two type III secretion systems of Vibrio parahaemolyticus. Infection and Immunity **72:**6659-6665.

78. **Petiot, A., E. Ogier-Denis, E. F. Blommaart, A. J. Meijer, and P. Codogno.** 2000. Distinct classes of phosphatidylinositol 3'-kinases are involved in signaling pathways that control macroautophagy in HT-29 cells. J Biol Chem **275:**992-998.

79. **Pires-daSilva, A., and R. J. Sommer.** 2003. The evolution of signalling pathways in animal development. Nat Rev Genet **4:**39-49.

80. **Powis, G., R. Bonjouklian, M. M. Berggren, A. Gallegos, R. Abraham, C. Ashendel, L. Zalkow, W. F. Matter, J. Dodge, G. Grindey, and et al.** 1994. Wortmannin, a potent and selective inhibitor of phosphatidylinositol-3-kinase. Cancer Res **54:**2419-2423.

81. **Raimondi, F., J. P. Kao, C. Fiorentini, A. Fabbri, G. Donelli, N. Gasparini, A. Rubino, and A. Fasano.** 2000. Enterotoxicity and cytotoxicity of Vibrio parahaemolyticus thermostable direct hemolysin in in vitro systems. Infect Immun **68:**3180-3185.

82. **Sansonetti, P. J., A. Phalipon, J. Arondel, K. Thirumalai, S. Banerjee, S. Akira, K. Takeda, and A. Zychlinsky.** 2000. Caspase-1 activation of IL-1beta and IL-18 are essential for Shigella flexneri-induced inflammation. Immunity **12:**581-590.

83. **Schmidt, A., and A. Hall.** 2002. Guanine nucleotide exchange factors for Rho GTPases: turning on the switch. Genes Dev **16:**1587-1609.

84. **Shinoda, S., and K. Okamoto.** 1977. Formation and function of Vibrio parahaemolyticus lateral flagella. J Bacteriol **129:**1266-1271.

85. **Sory, M. P., A. Boland, I. Lambermont, and G. R. Cornelis.** 1995. Identification of the YopE and YopH domains required for secretion and internalization into the cytosol of macrophages, using the cyaA gene fusion approach. Proc Natl Acad Sci U S A **92:**11998-12002.

86. **Stebbins, C. E., and J. E. Galan.** 2003. Priming virulence factors for delivery into the host. Nat Rev Mol Cell Biol **4:**738-743.

87. **Tanida, I., T. Ueno, and E. Kominami.** 2004. LC3 conjugation system in mammalian autophagy. Int J Biochem Cell Biol **36:**2503-2518.

88. **Thorburn, A.** 2008. Apoptosis and autophagy: regulatory connections between two supposedly different processes. Apoptosis **13:**1-9.

89. **Trosky, J. E., Y. Li, S. Mukherjee, G. Keitany, H. Ball, and K. Orth.** 2007. VopA inhibits ATP binding by acetylating the catalytic loop of MAPK kinases. J Biol Chem **282:**34299-34305.

90. **Utsumi, R., Y. Nakamoto, M. Kawamukai, M. Himeno, and T. Komano.** 1982. Involvement of cyclic AMP and its receptor protein in filamentation of an Escherichia coli fic mutant. J Bacteriol **151:**807-812.

91. **Viboud, G. I., and J. B. Bliska.** 2005. Yersinia outer proteins: role in modulation of host cell signaling responses and pathogenesis. Annu Rev Microbiol **59:**69-89.

92. **Vojtek, A. B., and S. M. Hollenberg.** 1995. RAS-RAF INTERACTION - 2-HYBRID ANALYSIS, p. 331-342. Small Gtpases and Their Regulators, Pt A, vol. 255. Academic Press Inc, San Diego.

93. **Von Pawel-Rammingen, U., M. V. Telepnev, G. Schmidt, K. Aktories, H. Wolf-Watz, and R. Rosqvist.** 2000. GAP activity of the Yersinia YopE cytotoxin specifically targets the Rho pathway: a mechanism for disruption of actin microfilament structure. Mol Microbiol **36:**737-748.

94. **Wattiau, P., B. Bernier, P. Deslee, T. Michiels, and G. R. Cornelis.** 1994. Individual chaperones required for Yop secretion by Yersinia. Proc Natl Acad Sci U S A **91:**10493-10497.

95. **Wennerberg, K., K. L. Rossman, and C. J. Der.** 2005. The Ras superfamily at a glance. J Cell Sci **118:**843-846.

96. **Wong, H. C., S. H. Liu, L. W. Ku, I. Y. Lee, T. K. Wang, Y. S. Lee, C. L. Lee, L. P. Kuo, and D. Y. Shih.** 2000. Characterization of Vibrio parahaemolyticus isolates obtained from foodborne illness outbreaks during 1992 through 1995 in Taiwan. J Food Prot **63:**900-906.

97. **Yoon, S., Z. Liu, Y. Eyobo, and K. Orth.** 2003. Yersinia effector YopJ inhibits yeast MAPK signaling pathways by an evolutionarily conserved mechanism. J Biol Chem **278:**2131-2135.

98. **Zhang, Y., A. T. Ting, K. B. Marcu, and J. B. Bliska.** 2005. Inhibition of MAPK and NF-kappa B pathways is necessary for rapid apoptosis in macrophages infected with Yersinia. J Immunol **174:**7939-7949.

99. **Zychlinsky, A., and P. J. Sansonetti.** 1997. Apoptosis as a proinflammatory event: what can we learn from bacteria-induced cell death? Trends Microbiol **5:**201-204.